Hydrodynamic Modeling of the Impact of a Proposed new Coastline Groyne Structure on Floating Debris Pathways at Paget Farm, in Saint Vincent and the Grenadines

Philippe April LeQuéré

Submitted under the supervision of

Dr. Ioan Nistor

Dr. Ronald Townsend

In partial fulfillment of the requirements

for the degree of

Masters of Applied Science in Civil Engineering

Department of Civil Engineering

University of Ottawa

August, 2017

Abstract

To accommodate an increasing number of tourists visiting Bequia, the second largest island of Saint-Vincent and the Grenadines, the local government constructed an airport, through a major coastline land-reclamation project. However, due to the prevailing ocean current patterns in the area, an inlet created on the east side of the new airport is prone to trapping significant amounts of ocean-borne debris. This litter accumulation creates a health risk to local fishermen who clean their daily catch using water from the inlet. It is proposed to install a rubble-mound groyne structure on the eastward side of the new inlet to address this problem. The utilisation of a coastline groyne in this case is somewhat unorthodox, as the latter is normally employed to mitigate against coastal erosion.

The goal of this study is to optimise the groyne design with the assistance of a 3D numerical model. The 'Delft3D' open-source model (WAVE and FLOW modules) was selected to examine the effects of different orientations and lengths of the proposed groyne on the movements of floating debris. Included in the initial phase of the study was a field investigation to collect certain data which were necessary for model calibration and validation. This involves the use of an Acoustic Doppler Current Profiler (ADCP) to measure local shore bathymetry and also current velocities over a range of tidal cycles.

Acknowledgements

The authors wish to thank the following: (1) my supervisors Dr. Ioan Nistor and Dr. Ronald Townsend for the mentoring and support throughout the project with their high expertise in hydrodynamic modeling. It has been an honour to work with such dedicated supervisors, (2) North Grenadines Community Development Inc. and Skylarc Pictures for the collaboration in the funding of the project and accommodation during the field campaigns, (3) Mr. Herman Belmar for assisting with the field work and for facilitating communications with the government of Saint-Vincent and the Grenadines, and (4) Dr. Colin Rennie and Mr. Sean Ferguson for the ADCP training and for lending the equipment necessary for the field campaign.

Table of Content

List of Figures

List of Tables

List of Symbols

Latin characters

A_t : Tide amplitude (m)

C_b: JONSWAP coefficient (m^2s^{-3})

C_D: Drag coefficient

d : Depth (m)

D_{50} : Grain diamater representing the 50th percentile of finer material (mm)

E: Energy density spectrum (W/Hz)

f_u : Coriolis force in the X direction (N)

fv : Coriolis force in the Y direction (N)

F_x: Unbalance of the Reynold's stresses in X direction

F_y: Unbalance of the Reynold's stresses in Y direction

G_{xx}: Conversion term between rectangular and curvilinear co-ordinates in X direction

G_{yy}: Conversion term between rectangular and curvilinear co-ordinates in Y direction

H : The total water depth (m)

H_s : Wave significant height (m)

k: Wave number

M_x: External source contributions or sinks of momentum in X direction

M_y: External source contributions or sinks of momentum in Y direction

n: Manning's coefficient

P_x: Pressure gradient generated by external forces in the X direction (N/m^2)

P_y: Pressure gradient generated by external forces in the Y direction (N/m^2)

q_{in}: Addition of water (l/s)

q_{out}: Sink of water (l/s)

S: Wave's spectral action

s: Sediment at the tip of the groyne

s_o : Longshore sediment transport current

T: Wave period (s)

t: Time (s)

u: Grid's velocity in the X direction (m/s)

u_v: Vertical eddy viscosity term

v: Grid's velocity in the Y direction (m/s)

V_M: Depth-averaged velocity during the field measurement (m/s)

V_w: Wind Speed (m/s)

V_x: Depth-averaged velocity in the X direction (m/s)

V_y: Depth-averaged velocity in the Y direction (m/s)

W: Grid's velocity in the Z direction (m/s)

x, X: First horizontal coordinate (m)

y, Y: Second horizontal coordinate (m)

z, Z: Vertical coordinate (m)

Greek characters

ζ : Free surface elevation above the zero plane (z=0) (m)

θ: Depth-averaged velocity's Nautical direction (clock-wise from the North) during the field measurement (^{o})

κ: Wave Direction (^{o})

ρ: Rock density (kg/m^3)

σ : Ratio between the elevation of a given point and the total water depth (water surface: $\sigma = 0$, bottom: $\sigma = -1$)

Φ: Angular Frequency

Abbreviations

ADCP: Acoustic Doppler Current Profiler

CDB: Caribbean Development Bank

CDRRF: Community Disaster Risk Reduction Fund

GPS: Global Positioning System

HEC-RAS: Hydrologic Engineering Center's River Analysis System

JONSWAP: Joint North Sea Wave Analysis Project

NGCDI: North Grenadines Community Development Inc.

RMSE: Root Mean Square Error

STWAVE: STeady STate WAVE model

SWAN: Simulating WAves Nearshore

UTM: Universal Transverse Mercator coordinate system

WAM: WAve Model

1 Introduction

This study is largely a numerical modeling investigation of the impacts, on local coastal hydrodynamics, of a new rubble-mound groyne that is being proposed for a critical shoreline section of Bequia Island in St. Vincent and the Grenadines. Figure 1.1 illustrates the location of Bequia in the Grenadines section. The city of Port Elizabeth on this 18 square kilometer island is one of the world's most famous stops for yachts and many tourists also visit the island each year to enjoy the beaches and the warm weather. However, as is the case on many of the lesser-known Caribbean Islands, the permanent island population in the rural areas is quite poor and, for the most part, it lives off what the surrounding ocean provides. Consequently, this population is more sensitive to the quality of the environment that they live in.

Figure 1.1: Caribbean Map (C-Change Secretaria (Canada), 2010)

In 1988, a German engineering company, Kocks Consult GbmH and a Netherland's-based contractor, Interbeton/Ham, were hired to begin the construction of an airport in Jetty bay, the

bay in front of the village of Paget Farm on Bequia (Mitchell, 2016). This airport was built by reclaiming land from the ocean. Dredged sand from the ocean next to the site was used for the landing ground. The rock armoring around the reclaimed land was supplied from quarries on the island. This new airport, now called the J.F. Mitchell airport (see Figure 1.2) improves access to the island for tourists.

Figure 1.2: Bird's Eye View of the J.F. Mitchell Airport (Deligny, 2013)

According to the original plan, the reclaimed land was supposed to be detached from shore, such that there would be a channel between the airport and the island. However, at the request of the then Prime Minister Sir James Fitz-Allen Mitchell, the original plan was changed and the airport is now connected to the island. This design modification increased the area of the village by adding some flat ground. There is now a park in that addition of land and a road that gives easy access to the west peninsula of the island. Also, during the construction phase, a small inlet, called the Jeff Gregg inlet, was left open so that the owner of the local bar, situated at the East end of the airport, could haul up his boat right at his bar. This inlet, which is also shown in

Figure 1.2, is now an area where 7 boats are hauled and used by local fishermen. Although the above changes to the original plan were beneficial, some negative impacts were also introduced.

The first negative impact is the ocean-borne litter that now accumulates in the Jeff Gregg inlet. The inlet is open to the east, where the waves and the wind come from. Floating debris is directed into the inlet by the surface current that is created by the wind and the waves. Some sargassum algae are mixed in with the debris. When the debris and the algae find their way into the inlet, they stay there because of the lack of water circulation and they start rotting. There is now permanent "marshy" water in the inlet and it has a very strong smell that spreads through the area. It is also believed that this accumulation of debris is partly the result of some locals throwing their garbage into the inlet. It has been reported that some non-floating debris, such as metal and broken glass, can be found in the inlet. As this area is one of the few protected sections along the coast, the fishermen now 'harbour' their boats in the inlet. Furthermore, as they also clean their fish catches in this polluted water area, this activity poses a serious health risk.

The second negative impact relates to land erosion and fish habitat. Since the airport has been built, the sandy beach in front of the village, where the boats used to be hauled, is now gone and the fish that used to populate the bay have also largely disappeared. A possible reason for the beach erosion is the extensive dredging that was done next to the airport site during its construction. This undoubtedly has reduced the amount of sediment available to maintain the equilibrium of the sediment recycling mechanism. The historical volumes of incoming sediment, which otherwise would have nourished the beach, would have been significantly reduced as a consequence. Over time, this would also adversely affect favourable habitat for attracting marine life. This beach erosion process is now also threatening the main road that follows the island shoreline.

The third impact of the airport is the lack of drainage of rainfall runoff in the village area. Before construction of the new airport, runoff from rainfall used to travel down the mountain slope and drain directly into the ocean. However, following the introduction of the reclaimed 'flat-land' area for the airport, surface drainage in the village has been adversely affected. Consequently, a new drainage system to handle excess rainfall runoff was required to rectify this problem. To this end a new drainage channel, aligned along the boundary between the reclaimed land area and the original coastline, was constructed. However, this new drainage feature did not work as planned.

The flat area of the village is now effectively a swamp, where disease-carrying mosquitos breed. Certain initiatives are presently underway to limit the mosquito population in the village, however their numbers are still high and the source of the problem isn't fixed, (Toy, 2015). Two related critical problem areas were recently identified (Skylarc Pictures Inc., 2015): the elementary school and the cemetery, (see Figure 1.3). As the ditch system of the village is incomplete, excess rainfall runoff continues to flood those areas.

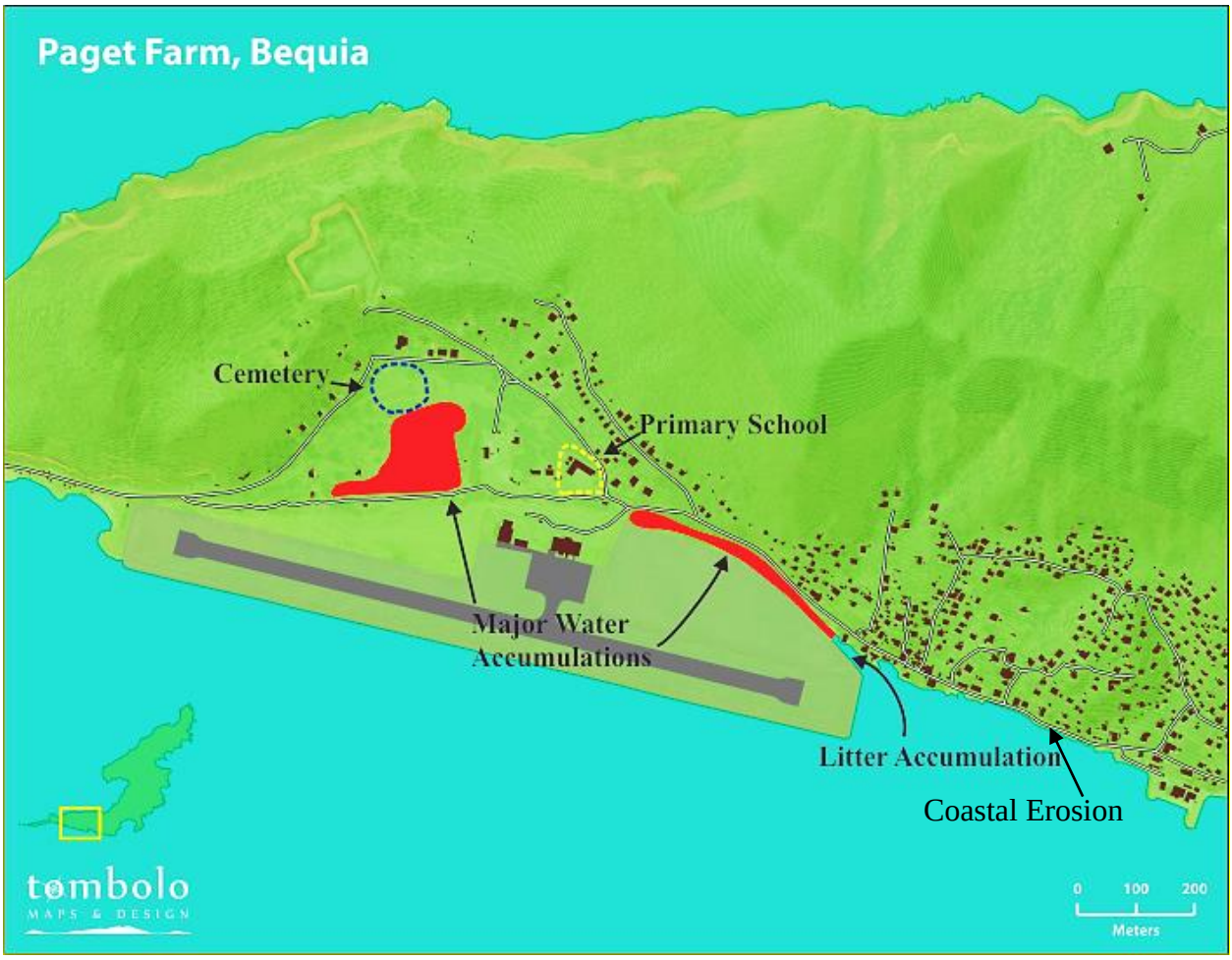

Figure 1.3: Negative Impacts from the Construction of the Airport

These problems need to be quickly remedied for the following reasons: (i) the local shoreline is undergoing significant erosion, and (ii) with the Zika virus spreading rapidly in the nearby islands, there is growing concern for the health of the local population, (CDC, 2016).

In order to obtain the necessary funding for this project, a partnership was created between a local organisation called North Grenadines Community Development Inc. (NGCDI) and the film

production company: Skylarc Pictures. It is hoped that this partnership will assist in obtaining funding through the Community Disaster Risk Reduction Fund (CDRRF), organised by the Caribbean Development Bank (CDB). However, one major constraint of this potential source of capital is the funding 'ceiling' (US$650,000), which is not considered sufficient to address all of the aforementioned problems. A second constraint is the fact that a CDB-funded project must have "community participation" (i.e. the project must involve "local" expertise).

The particular focus of this study is on the previously mentioned problems of ocean-borne litter accumulation. The drainage and coastal erosion problems, described above, will be addressed in a different study. The proposed solution for the problem of litter accumulation is to build a rubble-mound groyne east of the airport. The purpose of the groyne is to redirect the prevalent surface current in this area (and with it the related path of debris) away from inlet entrance and towards the main (bypass) ocean current. It is also well known that groynes have the capacity to accumulate debris on their windward side. (Matthews, 2003) This possible outcome in our case will still need to be tested. Optimizing the design of this structure will require a better understanding of the existing coastal hydrodynamics and related debris movements in the area. This will be accomplished with the aid of a dedicated 3-D mathematical model of the ocean region in question. The model selected for this exercise is the Delft3D numerical model, which is a software that is particularly well-suited for studying complex coastal hydrodynamics. Very little information, relating to shore-region bathymetry as well as local ocean currents and their patterns, is available for this remote region. Accordingly, a field campaign was initiated to gather the necessary information to build and calibrate the model.

1.1 Study Objective

The main objective of this study is to provide design guidance for the proposed rubble mound groyne that will reduce the coastal erosion and litter accumulation at Paget Farm. Different groyne lengths and angles will be tested using Delft3D. The following steps were undertaken to meet the objective of the study:

- Field campaigns were done to assess the problem, collect sand samples and get hydrodynamic data
- Development of a hydrodynamic model using Delft3D
- Calibration of the hydrodynamic model

- Validation of the hydrodynamic model
- Simulation of the different groyne designs under typical hydrodynamic conditions

The chosen numerical model to conduct this study is the open source version Delft3D. The debris pathways along the coast of Paget Farm will be simulated by coupling the FLOW and WAVE modules of Delft3D. The model was calibrated and validated using hydrodynamic data collected during the field campaigns (using an ADCP). This model is employed to monitor the effect of different groyne design on the debris pathways. A final design of groyne will be recommended based on its performance on reducing litter accumulation and reducing coastal erosion.

1.2 Importance and Novelty of the Study

In the past 25 years, multiple attempts by the local community of Paget Farm were done in the past to get the necessary financial support to solve their ongoing problem created by the newly constructed airport with no success. This study will support, using engineering knowledge, their latter attempt to get the necessary financial support needed for the mitigation of the local problems. Being the only hydrodynamic study conducted in the area, it will allow having a better understanding of the coastal processes that generate the debris accumulation and provide guidance for the design of a rubble mound groyne that will reduce this accumulation and slow down the shore erosion. This study will also help for any future funding attempt if the current grant application fails to succeed.

This study provides new data that was never measured in the area. A detailed bathymetric survey along Paget Farm's coast line was successfully done. To complete the absence of water velocity in the area, a point velocity survey was conducted in the area which helped documenting the tide induced current observed in the area.

This tide-induced current generated by tide asymmetry at the boundaries was successfully implemented in Delft3D and calibrated according to the measured velocities. The debris accumulation was monitored in the model by doing small scale tracking of floating debris. Little documentation on this technique used in near-shore wave condition is documented. This thesis provides an example of how this technique can be successfully implemented in a near-shore coastal environment.

1.3 Organization of the Thesis

This thesis is divided in 10 sections:

Section 1 – Introduction: This section presents to the reader a general description of the area of concern as well as a presentation of the numerous problems in Paget Farms. The problem and the solution studied in this thesis is also presented.

Section 2 – Literature Review: The literature review is a general overview of the scientific researches that are related to this thesis, and the weather and sea conditions used in the numerical model

Section 3 – Field Campaigns: Two field campaigns were conducted to get a better understanding of the area and the mechanisms that drive the debris accumulation. Data were collected in the area to gather information on the hydrodynamics, sediment deposits and bathymetry close to Bequia's shore.

Section 4 – Delft3D Model Development: In this section, governing formulas used in Delft3D are described. This section provides a summary of all the tasks done in the construction of the model, including formulation of the boundaries, the grids, the different assumptions employed, calibration of the model, etc.

Section 5 – Modeling of Existing Condition: The existing condition was modeled under three different scenarios to serve as a benchmark to compare the different groyne configurations. This section compiles the debris accumulation observed in the different scenarios.

Section 6 – Proposed Groyne Configurations: A total of six different groyne configurations were tested in this thesis. A description of all the configurations is provided in this section.

Section 7 – Results: The calibrated model is used to assess the performance of the different groyne configurations under the three selected scenarios. Their performance was judged based on their ability to reduce the litter accumulation in the Jeff Greg Inlet

Section 8 – Discussion: A comparison of the performance of the different groynes and the reliability of this study are discussed in this section.

Section 9 – Conclusion and Recommendation: This section of the report compiles the different conclusion from this research and recommendations for similar type researches.

Section 10 – Future Work: This section compiles the future works that the authors regard as important for the advancement of the research in the area to provide a suitable solution.

2 Literature Review

For the completion of a numerical model, it is critical to have a good understanding of the region of interest. However, given that the island of Bequia is very remote, past studies dealing with the coast-line nature of the island are extremely limited. This chapter summarizes the relevant information that was found prior to initiating the two field campaigns described herein. These campaigns were undertaken to gather the data that were necessary for developing the numerical model of the study area. This section includes an overview of the information found regarding:

- The classical use of a Groyne,
- The limits and specifications of a Delft3D model,
- Bottom friction in coastal areas,
- The JONSWAP parameter used in wave models,
- Typical wind, wave and tide condition in the area,
- Bathymetric data in the bay.

2.1 Classic Use of Groyne

Groynes, along with other coastal structures such as breakwaters or seawalls, are typically used to reduce coastal erosion (Harlow, 2013). For beaches with a littoral drift imbalance, a groyne or a series of groynes is the usual methodology employed to deal with the erosion process (I Coghlan, 2013). As indicated in Figure 2.1, these structures act as a physical barrier to the longshore sediment transport current (s_o) and they encourage accretion of material to develop on their windward side. However, on the leeward side, erosion will occur due to the reduction in import of sediments.

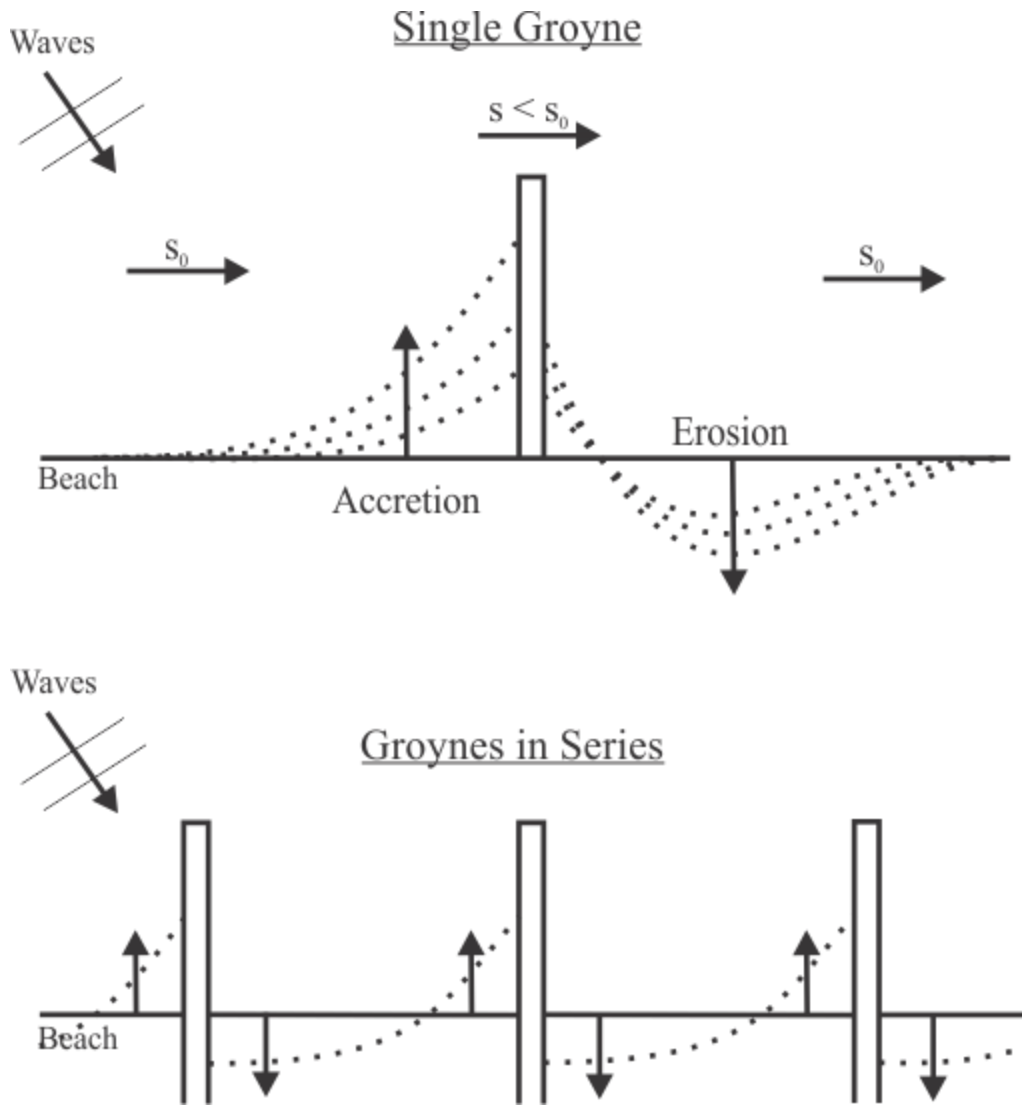

Figure 2.1: Groyne Impact on the Beach Profile (Visser, 2002)(Harlow, 2013)

When comparing the main role of our proposed groyne to the above-mentioned traditional role of coast-line groynes, it is clear that our groyne is to be used in an unconventional way. The principal role of our groyne structure is to re-direct the prevailing coastline current (and hence the pathway of floating debris) away from the entrance to the Jeff Gregg Inlet coastline feature. The aforementioned net reduction of coastline erosion that is normally associated with groynes will be regarded as a secondary benefit in this case.

2.2 Delft3D Numerical Modeling of Coastal Environment

The open source version of the Delft3D numerical model was chosen to gain a better understanding of the hydrodynamic processes that are occurring along the Paget Farm-area

coastline. A good knowledge of its limitations and its capacity to accurately recreate the observed ocean currents is crucial in regards to developing an accurate model. Using its module 'FLOW', Delft3D solves an approximation of the Navier-Stokes equations to simulate the hydrodynamics in a given domain, (Deltares, Delft3D-FLOW, User Manual, 2011). The wave forces in the domain are simulated by solving a SWAN model in the Delft3D module 'WAVE' (Deltares, Delft3D-WAVE , 2011). When the two modules are coupled, they can accurately represent the coastal hydrodynamics of a region.

The SWAN model is an extension of the WAM model (used for waves in deep and intermediate-depth water). It incorporates third-generation formulation (wind generation, whitecapping, triad and quadruplet wave-wave interaction, bottom friction, and depth-induced wave breaking) which makes this wave simulation model accurate in shallow water (N. Booij, 1999). Indeed, good hydrodynamic agreement between field data and Delft3D model, in coastal shallow water under wave condition, has previously been achieved by previous authors (Elias, 1999) (Visser, 2002) (Chatzirodou, 2014). The model can also simulate morphological changes with the MOR module. The changes in morphology due to waves are also accurate. However, the SWAN model fails to accurately simulate the longshore sediment transport (Koen Trouw, 2012). This inaccuracy is not related to an incapacity to properly model the hydrodynamics of the longshore current. Therefore, this limitation should not affect the accuracy of the model to recreate the floating debris pathways.

Given that there is a tide-induced current in the region (See 3.1.4 Tide-Induced Currents), a confirmation that Delft3D is capable of simulating such a phenomenon is necessary. This type of current was described by previous authors (Elias, 1999) (Chatzirodou, 2014). The current decribed in the papers are very similar to the one observed during the field campaign. It changes direction with the reversal of tide and has a high velocity. Some tide-induced currents were documented to have a high enough flow to create erosion, and point velocities measured up to 8 m/s. This type of current can be modeled by imposing the change in water elevation due to tide as a boundary condition and calibrating it by changing the bottom friction. The calibration of the tide effect on water level is typicaly done by comparing the model to offshore tide gauge. The calibration of the model can also be done with velocity measurements using an Acoustic Doppler Current Profiler (Chatzirodou, 2014). The latter option would be more applicable for this study

given that the only tidal gauge that could be used, located 20 km north of Bequia, is reported to be disfucntional (Henson, 2005) (UNFCCC, 2015).

Delft3D also has the capacity of modeling a groyne structure in the modeling domain. This can be done in three different ways:

1. By removing grid cells,
2. By using ‘thin dams’, or
3. By using ‘dry points’ (Visser, 2002).

The first way to model the groyne is by removing cells from the computational grid used in the FLOW and WAVE modules at the location where the groyne is to be installed. As a result, no water exchange will be done with the neighbouring cells, thereby impacting the water velocity surrounding them.

The second way is to define the groyne as a series of ‘thin dams’. These ‘thin dams’ are a barrier that prevents the exchange of water in either the X or Y direction, depending on how the user defines them. The problem with this definition is that it still allows flow in the direction that isn’t blocked at the location of the groyne, which is not a true representation of the fact the circulation will not occur through the groyne in any direction. Therefore, this isn’t the most acceptable way of modeling a groyne.

The third way is to define the grid cells occupied by the groyne as ‘dry points’. These are cells that are defined as being ‘always dry’; therefore they will be excluded from the computation. Given there is no exchange of water through those cells, the velocity around them will be zero. However, since no obstruction is defined in the WAVE module, the wave energy will still propagate through those cells. It is therefore important to also define those cells as ‘obstacles’ in the WAVE module (Koen Trouw, 2012). The definition of one line of ‘obstacle’ along the groyne is sufficient to get realistic hydrodynamic response to the addition of the groyne. In the case of a morphologic simulation, multiple sheets of ‘obstacles’ should be defined in order to surround the cells labelled as ‘dry points’ (see Figure 2.2). Otherwise, a small additional amount of sediment transport could be created on the leeward side of the groyne.

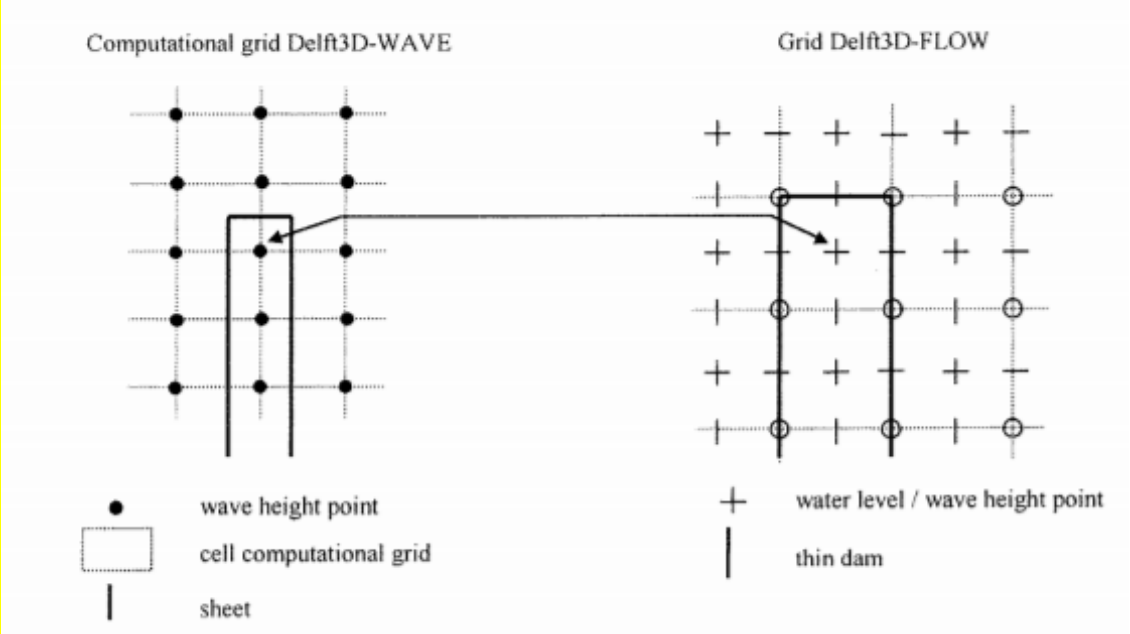

Figure 2.2: Conceptual Representation of a Groyne in Delft3D (Visser, 2002)

2.3 Bottom Friction in the Coastal Area

Bottom friction is a parameter that is often used for calibration in coastal models (Chatzirodou, 2014) (Elias, 1999). Given that this parameter can vary on a wide spectrum of values, knowledge of the type of bottom (and the associated range of roughness) provides a good starting point. When analysing satellite imagery, it can be observed that the sea bed close to the shore is a mix of reefs and sand patches (a condition that was later confirmed in the field campaigns). Drag coefficients (C_D) used in reef circulation models range from 0.02 to 0.1 (J.H. Rosman, 2011). Manning's coefficient (n) ranges from $0.15 < n < 0.25$ (Cialone & McKee Smith, 2007) and was observed to be as low as $n = 0.05$ in Caribbean reefs (Prager, 1991). This wide range of value in the bottom friction coefficient can present a modeling challenge. The ratio between the height of the coral canopy and the water depth seems to be the factor that influences this value (J.H. Rosman, 2011). Given this range, the bottom roughness parameter will require further calibration in the model.

For the rest of the bay, satellite imagery seems to indicate that the bottom material is sand, only. This conclusion was reinforced by dredging activities done in the area (HENDRY, 1997) and was also confirmed during the present field campaign.

Figure 2.3: Dredging Activity in Jetty Bay during the Airport's Construction (Skylarc Pictures inc., 2015)

Manning's coefficient for coastal area with offshore sand is reported to be around n = 0.02 (Cialone & McKee Smith, 2007). An estimation of Manning's coefficient can be calculated for sand bottom using the median diameter obtained from a sieve analysis done on a sand sample (California Departement of Water Resources, 1970). This estimation can then be used as a starting point for the model, as long as it is reasonably close to the proposed value of n = 0.02.

2.4 JONSWAP Bottom Friction

The JONSWAP coefficient (C_b) helps with the formulation of the bottom friction parameter used for energy dissipation in the SWAN model. Two different values were initially proposed for JONSWAP: $C_b = 0.038\ m^2s^{-3}$ for swell condition, and $C_b = 0.067\ m^2s^{-3}$ for fully developed wind-sea condition in shallow water. For many years, these values were taken as default values in SWAN models (Vledder, 2010). Equation 1 models the sink of spectral action due to the bottom roughness where the JONSWAP parameter can be found.

$$S_{ds,b} = -C_b \frac{\Phi^2}{g^2 sinh^2(kd)} E(\Phi, \kappa) \qquad (1)$$

C_b: JONSWAP parameter

Φ: angular frequency

κ: wave direction

g: gravitational acceleration

E: Energy density spectrum

k: wave number

d: water depth

Recently, authors have revisited the validity of those values, especially the one for wind-sea condition (C_b=0.067 m^2s^{-3}), suggesting that other factors, such as the type of bottom, affect the JONSWAP coefficient instead of only the type of waves (Vledder, 2010). When the lower value (C_b=0.038 m^2s^{-3}), originally used only for swell condition, is used to model waves over a sandy bottom, the agreements with field data are very strong. A weaker, but relevant correlation was found for other bottoms (G.Ph Van Vledder, 2009). In the latest version of the SWAN manual, a value as low as C_b=0.019 m^2s^{-3} was recommended for smooth seafloors such as the one found in the Gulf of Mexico (The SWAN team, 2017). Other studies have used a JONSWAP coefficient that varies in the range of $0.04m^2s^{-3} < C_b < 0.06m^2s^{-3}$ to mimic wave's significant height observations over a reef sea bed (Cialone & McKee Smith, 2007). This value of JONSWAP seems to correlate with the Manning's roughness found for the same area. However, the model used for this study was the STWAVE model that uses the same bottom friction dissipation formula as the SWAN model. In summary, values for JONSWAP varying in the range of $0.019m^2s^{-3} < C_b < 0.067\ m^2s^{-3}$ need to be tested in the formulation of a SWAN model.

2.5 Weather Condition

Given that Jetty Bay (the bay area in front of Paget Farm) is not very developed, historical weather data and sea conditions for that bay are not available. As a result, the weather forecasts, sea conditions and statistics presented in this chapter are for Friendship Bay, a bay located 2 kilometer east of Jetty Bay. These bays are presumed to be close enough to have essentially the same weather and sea conditions. This assumption is used for the wind, wave and tide condition subsections.

2.5.1 Wind Condition

Figure 2.4 summarizes the number of days that the wind was blowing within particular speed intervals for every month of the year. These statistics were made using the daily observations between December 2011 and March 2016:

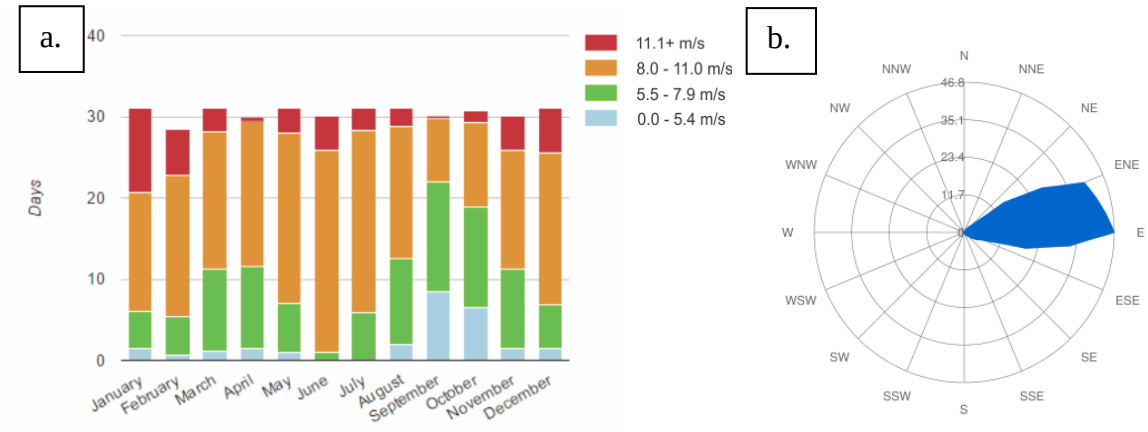

Figure 2.4: Wind Statistics in Friendship Bay (wisuki, 2016)

The typical wind intensity (V_w) is around 8 m/s < V_w < 11 m/s. The prevailing wind comes straight from the east with very little variations. Given that the wind is pretty strong in the region, it will be an important factor to take into account in the model and it could have a significant effect on local surface currents.

2.5.2 Wave Condition

Since waves generate surface turbulence and additional forces, the wave definition may govern the forces generating the surface current. Typical values for wave significant height, wave period and direction are needed to develop the wave simulation model. The wave condition will also affect the design of a rubble mound groyne because the wave's significant height dictates the minimum rock size that should be used (U.S. Army Corps of Engineering, 2008). The compiled data for the graphs in Figure 2.5 were made using the daily observations between December 2011 and March 2016:

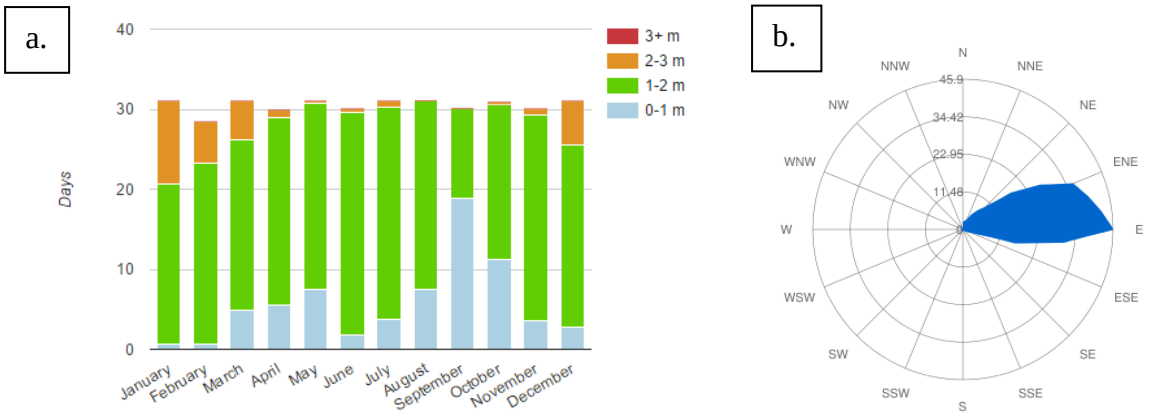

Figure 2.5: Wave Statistics at Friendship Bay (wisuki, 2016)

The wave condition shown in Figure 2.5 is for the swell approaching the bay, not the waves in the bay. Therefore, these wave conditions will be used as a boundary for the model. The typical significant wave height (H_s) throughout the year is between 1 m < H_s < 2 m, with very few days exceeding H_s = 2 m. As for the maximum wave significant height, Figure 2.5(a) indicates that no swell over H_s = 3 m was recorded in the past 4 years. To use a conservative approach, it could be assumed that the largest waves arriving in Jetty Bay are approximately H_s = 3 m. Figure 2.5(b) illustrates the wave direction in the past 4 years. The prevailing swell comes straight from the east. This can be considered as a typical condition for the wave model. The last characteristic needed for the model is the wave period (T). This period is typically forecasted to be between 7 < T < 9 seconds (wisuki, 2016).

2.5.3 Tide Condition

Assuming the tidal cycle is responsible for inducing different current patterns in the bay, (Figure 3.6) the influence of the former cannot be ignored in the model. To get an approximation of the tide at Jetty bay, the tide forecast for Friendship bay was used. To validate the source, it was compared to the predicted tide in the islands around it. (wisuki, 2016) (Meteo365, 2016) (NOAA, 2016). The comparison confirmed that the tidal cycle is 'mixed semidiurnal' with a maximum amplitude (A_t) of A_t = 0.7m. (NOAA, Ocean Service Education, 2008) Figure 2.6 illustrates the tide forecast for the period of June 1st to June 5th 2016:

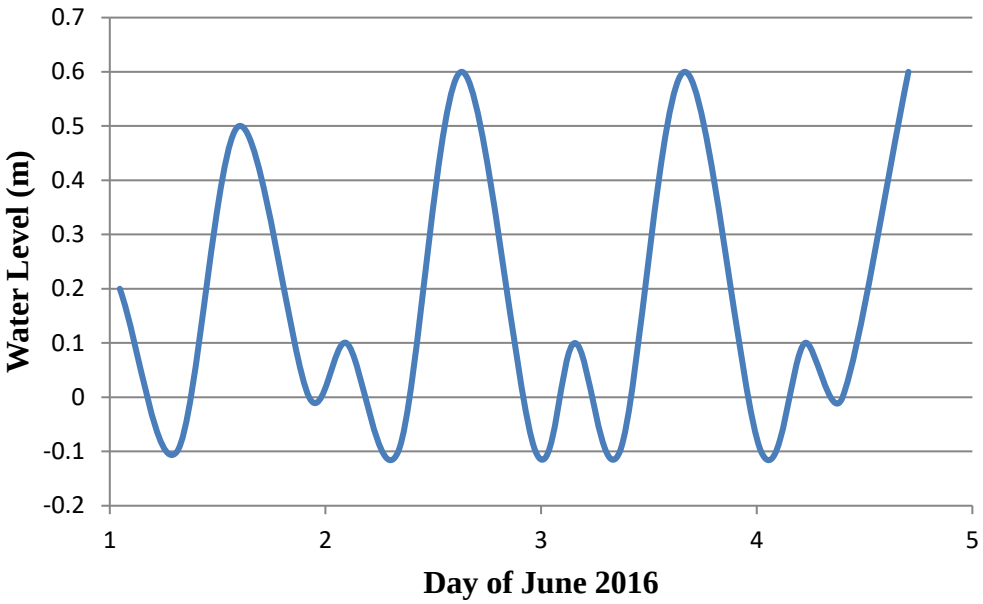

Figure 2.6: Sample of Friendship Bay Tide (wisuki, 2016)

2.6 Bathymetry

The bathymetry is crucial for the development of the computational grid. Only a very coarse bathymetric map was found on the Windows application Marine Navigation – Caribbean (see Figure 2.7). This resolution was found to be too coarse for the more refined portions of our model grid, such as the 'nearshore' sections. Therefore, additional field data needed to be collected in order to refine the grid in certain critical areas.

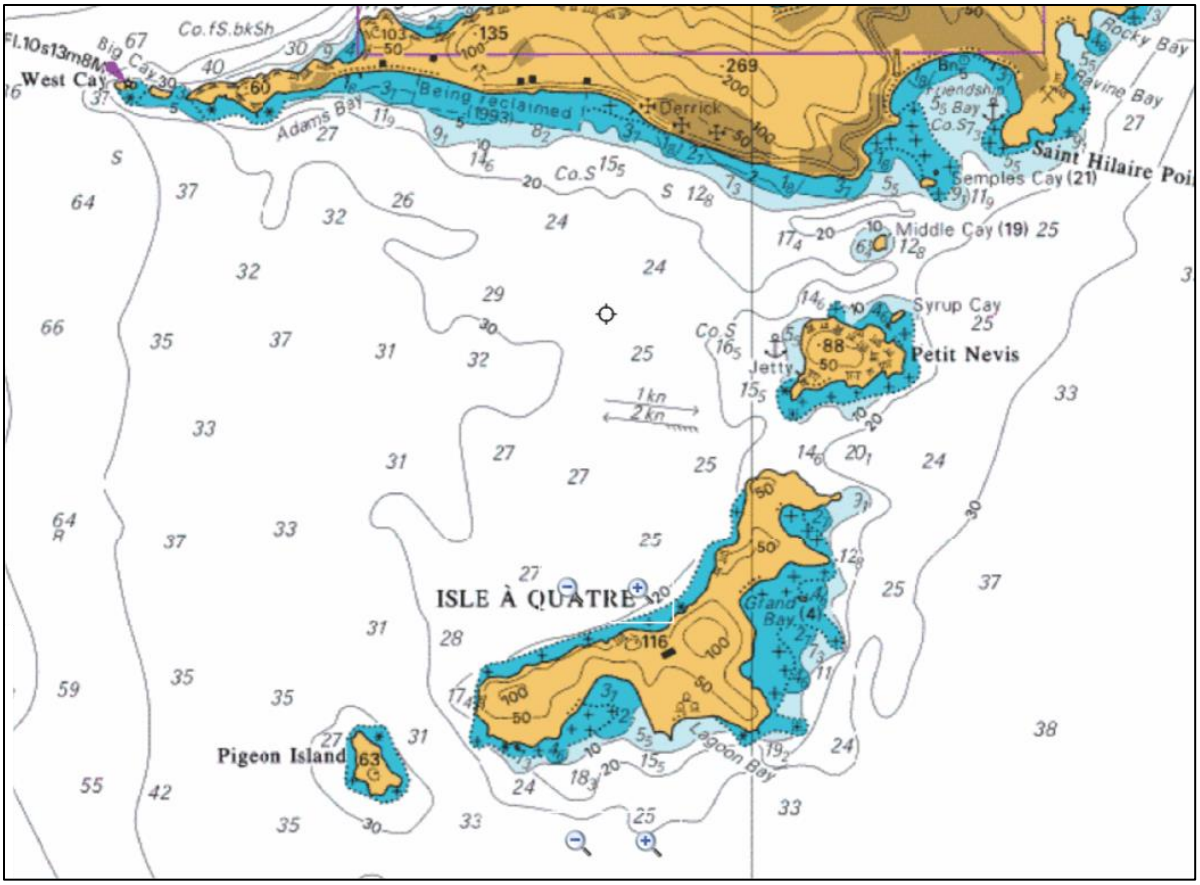

Figure 2.7: Navigation Map Bathymetry (Bist LLC, 2016)

A few different options were considered to increase the resolution of the bathymetric map. It was decided that using Acoustic Doppler Current Profiler (ADCP) would be the most appropriate tool for this work. The methodology used in the field measurements, as well as a description of the equipment used in the data acquisition, is provided in the section 3.2 Data Collection.

2.7 Discussion

Several conclusions and findings from the literature review proved useful in regards to guiding our study. It was found that:

- It is well within the capacity of Delft3D to simulate the coastal hydrodynamics of the Paget Farm area.
- A groyne structure can be represented in Delft3D-FLOW by using the function ‘dry points’ to stop the exchange of water across the groyne. It is important to also include ‘obstacles’ in Delft3D-WAVE to mimic the influence of the groyne on the wave action.

- Manning's coefficient for the sandy area of the bay can be calculated using Manning's formula. It provides an estimation of the coefficient based on the median grain size of the sand. For the bottom friction in a 'reef' area, the coefficient can be between $0.05 < n < 0.25$. A sand sample will then be necessary for the formulation of the bottom friction in shallow water and calibration for the area near-shore.
- Values of the JONSWAP coefficient, which depends on many factors, can vary from $0.019 m^2 s^{-3} < C_b < 0.067\ m^2 s^{-3}$. Values across this range will need to be tested in the formulation of the SWAN model.
- The 'sea conditions' information necessary to complete the model (wind, wave and tide) was found. Daily observations will be used for the calibration of the model. Sea condition statistics obtained for the past 5 years will be used to create scenarios that will test the groyne arrangements.
- A coarse bathymetric map of the region was obtained. While this map is adequate for completing the numerical model's grid in its "deep water" areas, it is not sufficiently fine to handle the "shallow water" areas of the coastal regions.

3 Field Campaigns

A total of two field campaigns were organized during this study (the schedule of the campaigns can be found in Appendix A). The goals of these two campaigns were to get a better understanding of the problem that the villagers are experiencing, get better knowledge of the area and collect the necessary data to build a numerical model. The subsections presented in this chapter are:

- Field investigations
- Data collection
- Soil Samples collection and analysis
- Meeting with local decision makers
- Presentation to the community

3.1 Field Investigations

3.1.1 Site description

A visit to the village and its surroundings was important to get a better understanding of the relevant problems and their underlying mechanisms. Observations were made on the following:

- Litter accumulations along the Paget Farm coastline (1),
- Litter accumulations in the Jeff Gregg inlet (2),
- Local tide-induced currents (3),
- Airport armoring (4).

The locations of the various observation sites are indicated by the above numbers in Figure 3.1: Field Investigation Location.

Figure 3.1: Field Investigation Location

3.1.2 Paget Farm Coastline Features

At present, the shoreline to the east of Paget Farm contains three groynes. One is the fishery factory groyne and the other two smaller ones are located west of the factory. These small groynes were installed by local fishermen and their purpose is to accumulate sand so that they can safely haul their boats.

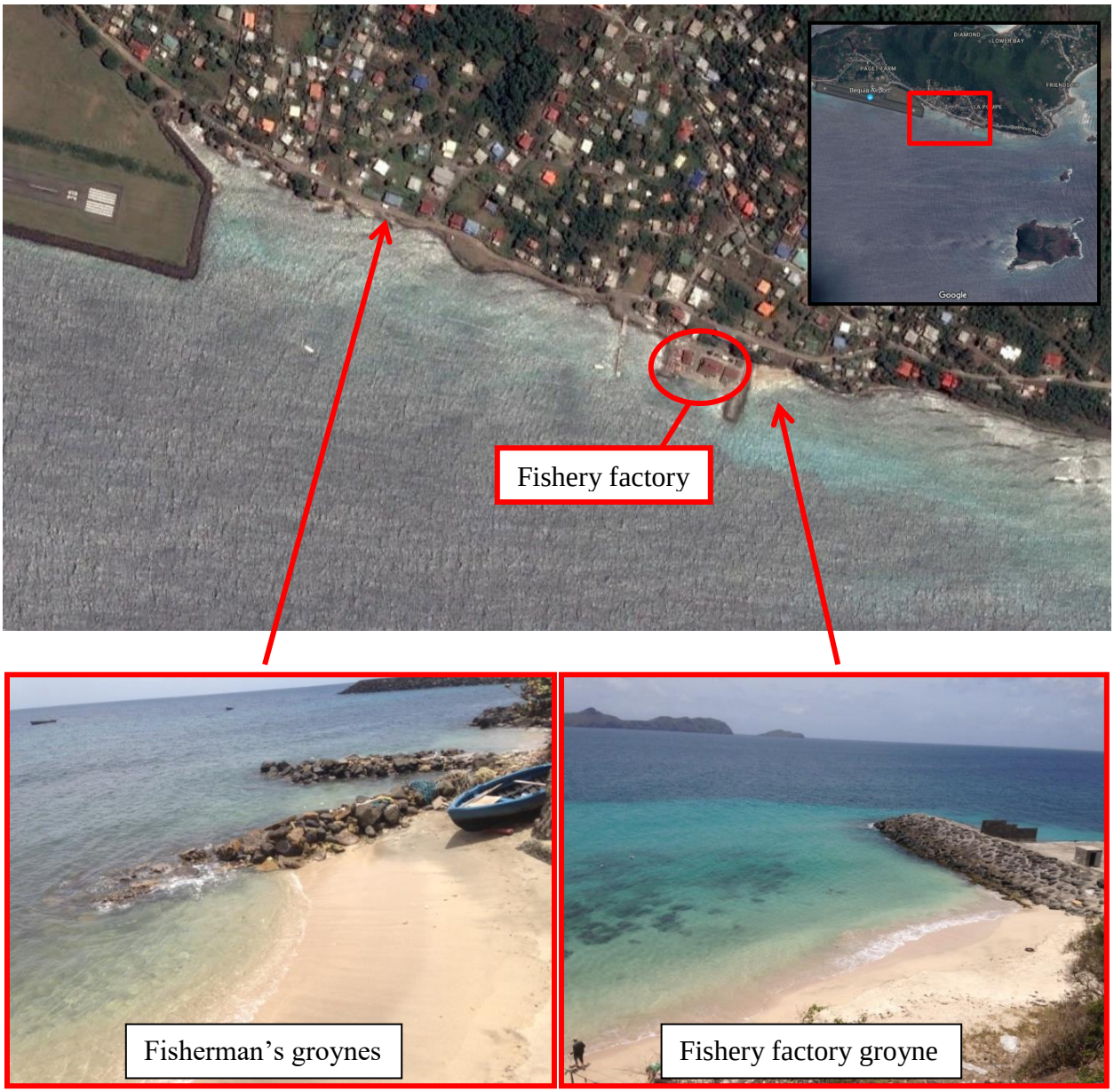

Figure 3.2: Sand Accumulation along the Coast

Sediment accumulation is notably higher on the windward side of those structures than elsewhere along the coast. This is a good indication that sediments are being transported along the shore and that they can be successfully trapped by the groynes. According to Belmar "the rate of sediment accumulation in the small groynes and in the inlet itself has increased since the start of the road enlargement program." The goal of this program is to protect Paget Farm's main road from erosion. This road protection program is enhanced by encouraging the villagers to dump soil, which comes from various construction activities in the village, at an erosion site along the coast. Since 2013, the road shoulder at that location was widened by 25m. This dumping of soil has imported sediments into the ocean. The small sediment particles, coming from the enlargement, are being washed out by waves and are being transported by the longshore current into the groynes and the inlet.

Figure 3.3: Most Suitable Starting Location for the Proposed Groyne

During the initial visit, a suitable location for the attachment of the proposed groyne was identified by the authors and Belmar. This area is the most suitable for such a construction because of the easy access to the ocean, there is plenty of free area along the shore and no demolition is required. This area is also very close to the access road that was built to move the rocks from the quarry to the airport, which is still in good condition. The area also features a small concrete ramp that would allow machinery to access the beach (Figure 3.3(b)). This ramp could also be used after the groyne's construction as an access ramp to the groyne and a location for a fish cleaning station.

When traveling along the shore road, a large amount of litter can be observed on both sides of the road, with higher concentrations in some locations. Figure 3.4 show samples of the types of littering that is present along the shore:


b
c
a
d
Google


a


b

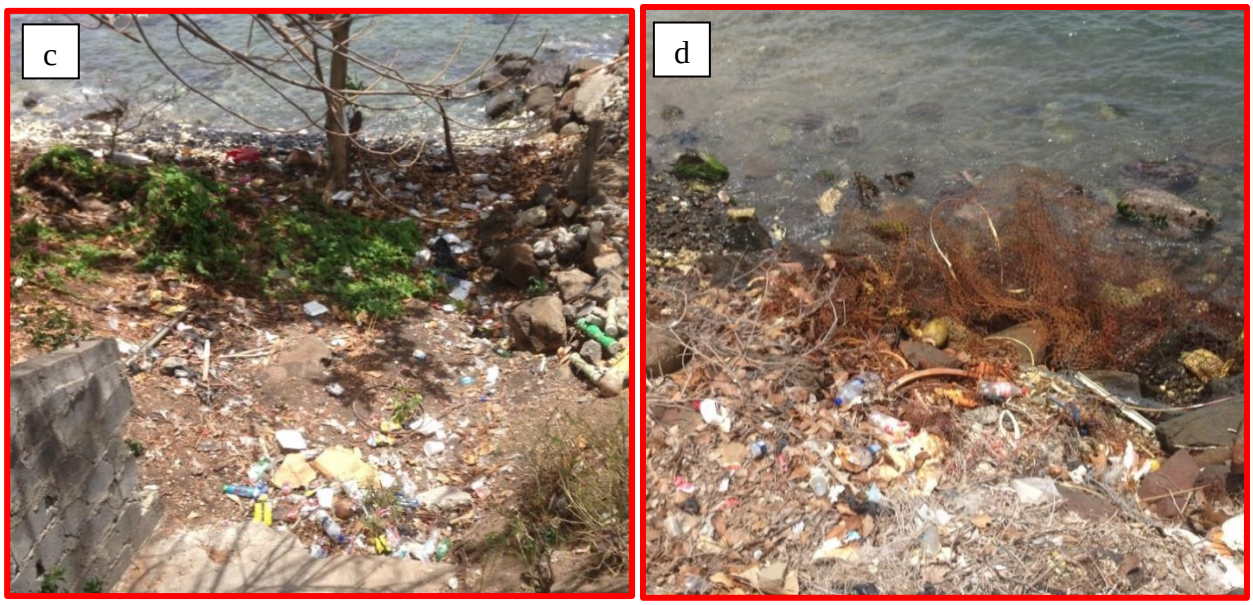

Figure 3.4: Litter along Paget Farm's Main Road

A close inspection of these litter deposits will confirm that, while some of it is ocean-borne debris, much of it can be attributed to 'garbage dumping' practices by the villagers themselves. For example, significant amounts of the litter are broken glass and various metal materials (Figure 3.4(c) and 3.4(d)). In Figure 3.4(a), a broken garbage container, full of garbage and left on the side of the road, is visible. Figure 3.4(b) illustrates debris that has accumulated in the drain on the land side of the road. Given that the ocean water level never reaches this height, the only possible source for this debris is from the land. This also indicates that some of the coastal litter is essentially garbage that was thrown into the drain.

It was also noted that the litter is not evenly spread along the shoreline. In fact, litter quantities are typically higher close to the convenience store, the ice cream shop and other busy establishments. So, there is a strong correlation between the amount of debris at a given location and human activities at these same locations. Clearly, the quantities and types of litter along the shore is largely reflected in the poor waste-disposal activities of some in the village community.

3.1.3 Jeff Gregg Inlet

The debris in the inlet is a mix of floating debris, non-floating debris and sargassum algae (see Figure 3.5(b)). According to the locals, the inlet was cleaned a week prior to when the picture of

Figure 3.5(b) was taken, therefore the picture doesn't represent the normal (high debris volume) situation of the inlet:

Figure 3.5: Litter Accumulation in the Inlet

In a more normal situation, the smell of the rotting sargassum can be unbearable and it spreads across the whole village. Moreover, while there is typically little or no accumulation of

sargassum along the coast, significant concentrations are frequently found in the inlet. These observations would suggest that local sea currents are largely responsible for collecting and directing this form of alga into the inlet. Also, this inlet is just 25m away from the only road that leads to the airport. So when tourists land, this is one of the first things they see and smell. When analysing the litter along the entire length of the inlet, it was observed that the non-floating debris were only at the end of the inlet, whereas the debris found between the rocks of the armoring were exclusively floating (mainly plastic water bottles) debris (Figure 3.5(a)). Given that the airport armoring areas are closed to the public, it can be assumed that the littering at these locations is exclusively deposited by sea action.

As this side of the island is exposed to the Atlantic Ocean and its currents, it would seem logical that floating debris from disparate ocean areas would be channeled and deposited by these currents. However, the brands of the water bottles found in the inlet and along Paget Farm's coast were found to be from the Saint-Vincent and the Grenadines region, only.

Belmar observed that "the 'brands' of bottle-type debris found along the coast, aside from the debris in the inlet, are almost exclusively European and African types". Our observations of the types of local debris, together with Belmar's shared anecdote on the source of same, would strongly support the premise that floating debris in the inlet are mainly supplied by Paget Farm residents.

3.1.4 Tide-induced Currents

A few investigative dives were undertaken along the coast to better understand the type of sea bottom in the area. Up to depths of ~5m, the sea bottom is a mix of coral reefs and sand patches. Beyond depths of 5m, the reef formations disappear and the ocean bottom is composed of fine sands. Also, it was observed that a strong current exists between the islands located east of the airport and that its direction changes with the reversal of the tide. At flood tide, the current moves in an east to west direction, while it moves from west to east at the ebb tide. Knowing that the current direction changes depending on the hour of the tide, the latter is most likely responsible for the driving forces creating this current phenomenon. (Bist LLC, 2016)

Figure 3.6: Tide-Induced Current Direction

3.1.5 Airport Armoring

In regards to the design of the proposed new groyne, an inspection of how the existing airport armoring has performed under severe wave attack would undoubtedly prove useful.

The nominal size (d_{50}) of the rocks that form the present armoring varies in the range: $0.5m \leq d_{50} \leq 2.0m$ (Figure 3.7(a)). During the dives, it was noted that there was a large amount of rocks found at the bottom of the ocean next to the eastern-facing side of the armoring (see Figure 3.7 (b)), while on the south-facing side, there was virtually no rock accumulation on the sea bed. This means that some of the armoring rocks were not heavy enough to resist the wave action and, as a result, were dislodged from their original location. Indeed, some minor damages were observed along most of the east-facing side of the armour berm while the south-facing side was almost intact. One factor that may have influenced this phenomenon is the ocean swell that approaches the airport area always coming from the east (see Figure 2.5), whereas the south side is less exposed to the waves, unless a storm creates waves that propagate north. Only dispersion of wave phenomena from the Isla a Quatre will end up affecting the south-facing side.

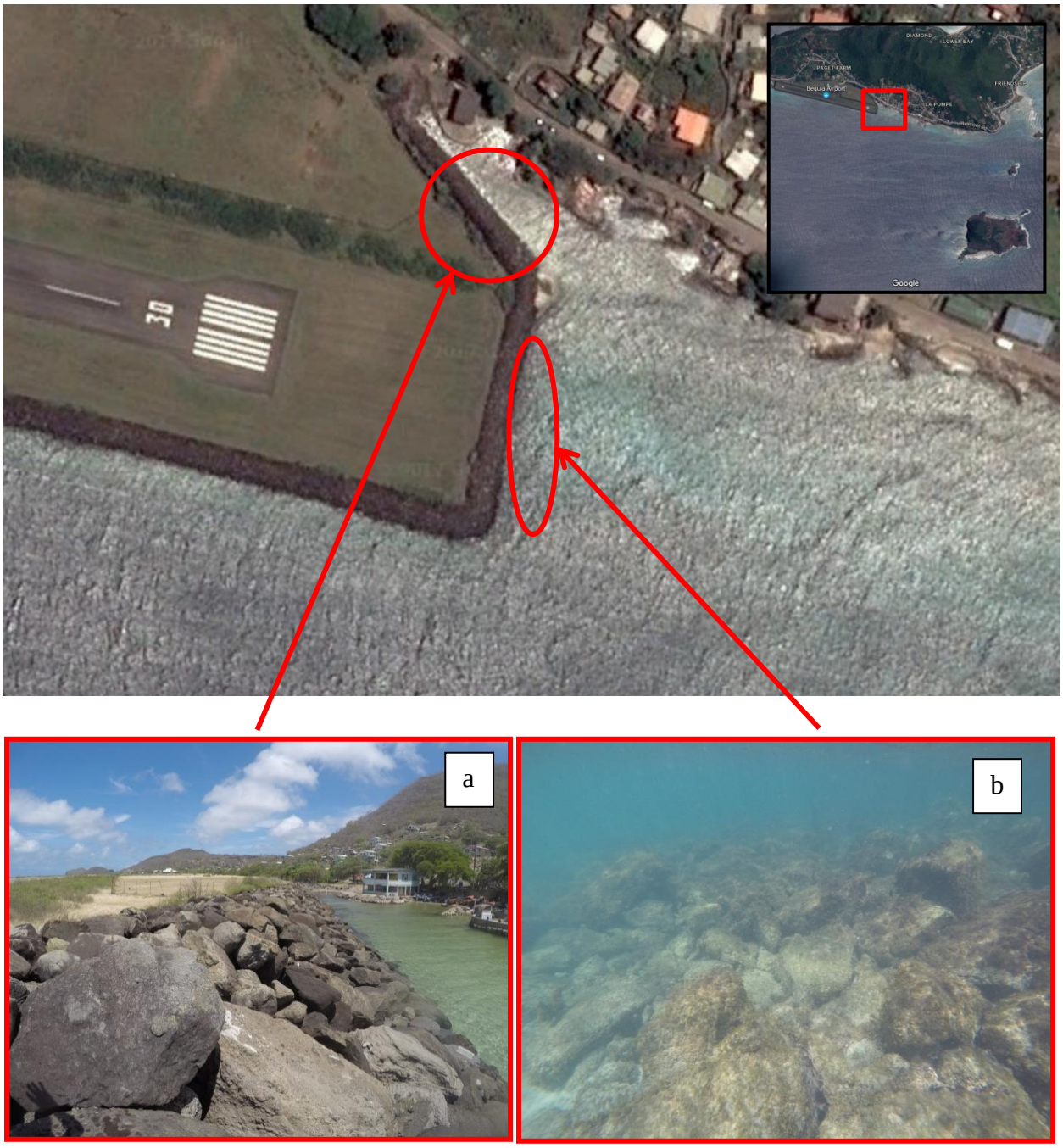

Figure 3.7: Airport's Rock Armoring

3.2 Data Collection

3.2.1 Equipment used for Hydrodynamic Survey; Acoustic Doppler Current Profiler

The missing data, needed for the development of the hydrodynamic model, are high-resolution depth mapping in critical areas, such as the coast and between the islands, and numerous Eulerian point velocities. The depth mapping, combined with the existing navigation map, will be used to construct the computational grid necessary for the numerical model. The Eulerian point velocities at critical locations will be used for the calibration of the model. The role of the collected data is fully explained in the section 4.4 Hydrodynamic Calibration and Validation. During the field campaign, an Acoustic Doppler Current Profiler (ADCP) was used to collect these necessary field measurements.

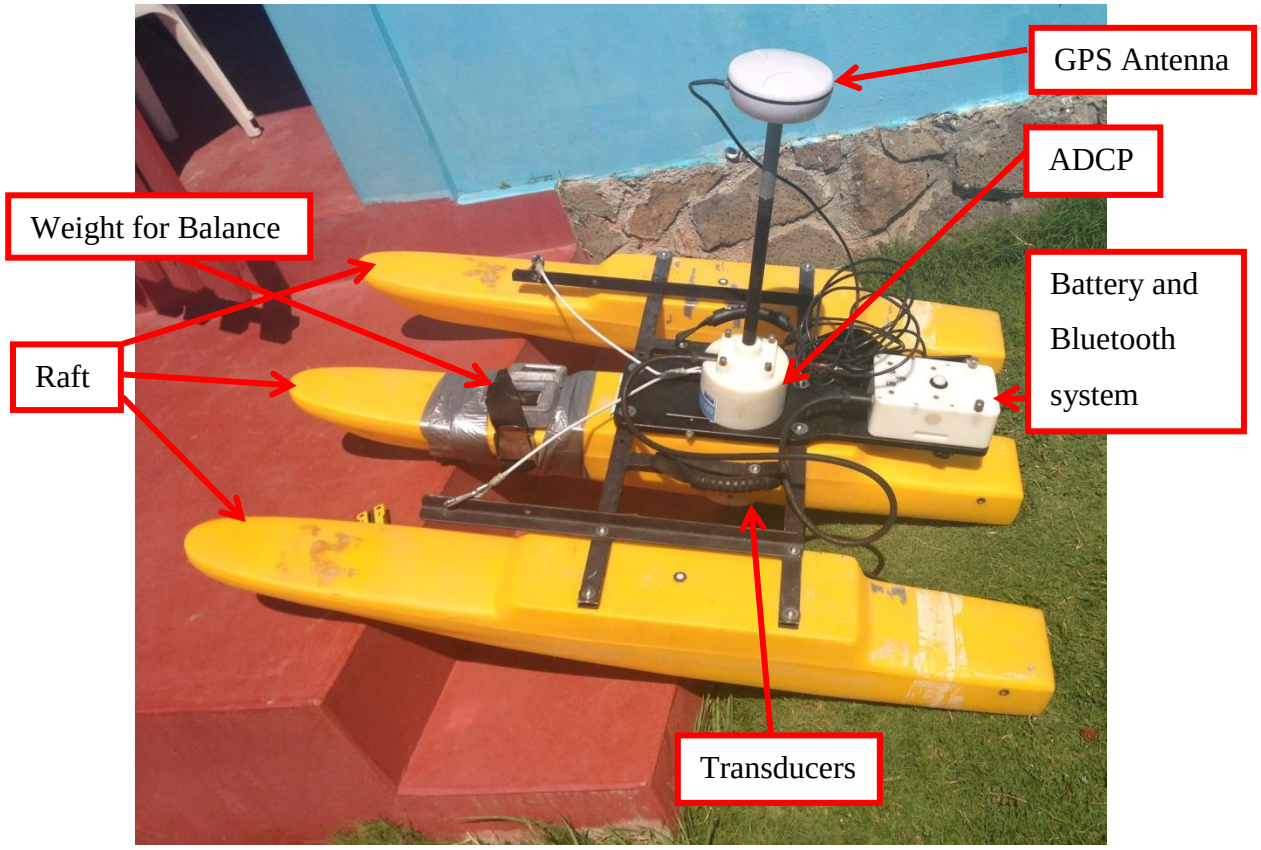

Figure 3.8: ADCP Components

The ADCP is a measuring device that uses acoustics to measure velocity throughout the water column. The velocity is measured using the transducers that compare the reflection of sound waves on small particles in the water column between two time steps. Given that the bottom will

reflect a very strong signal, the ADCP can also read the depth using the same transducers. An integrated GPS unit is used to obtain X and Y coordinates as well as correcting the depth with elevation variations caused by waves and changes of tide. This gives an absolute elevation of the bottom, not only relative depth. A differential resolution was achieved for the GPS, meaning that its absolute error was less than one meter. (SonTek, 2009) The monitoring and control of the ADCP was accomplished using Bluetooth technology, which allows the user to perform a remote control of the apparatus.

3.2.2 Bathymetry Survey

Continuous bathymetry measurements in the study area were obtained using the ADCP unit tethered to a boat, moving at around 2 m/s to 2.5 m/s. This speed was the highest that could be achieved while maintaining a high quality of depth reading. Over the course of the campaign, a total of 23400 usable x-y-z points were collected around the different areas where more resolution was needed (e.g. close to shore). The points were collected by travelling parallel to the shore and increasing the distance from the shore for each run and also including some diagonal transects to maximize the area covered by the survey. A greater amount of data points were collected close to the inlet to ensure that the model's representation of this critical area was accurate. Figure 3.9 shows the transects that were done in these exercises.

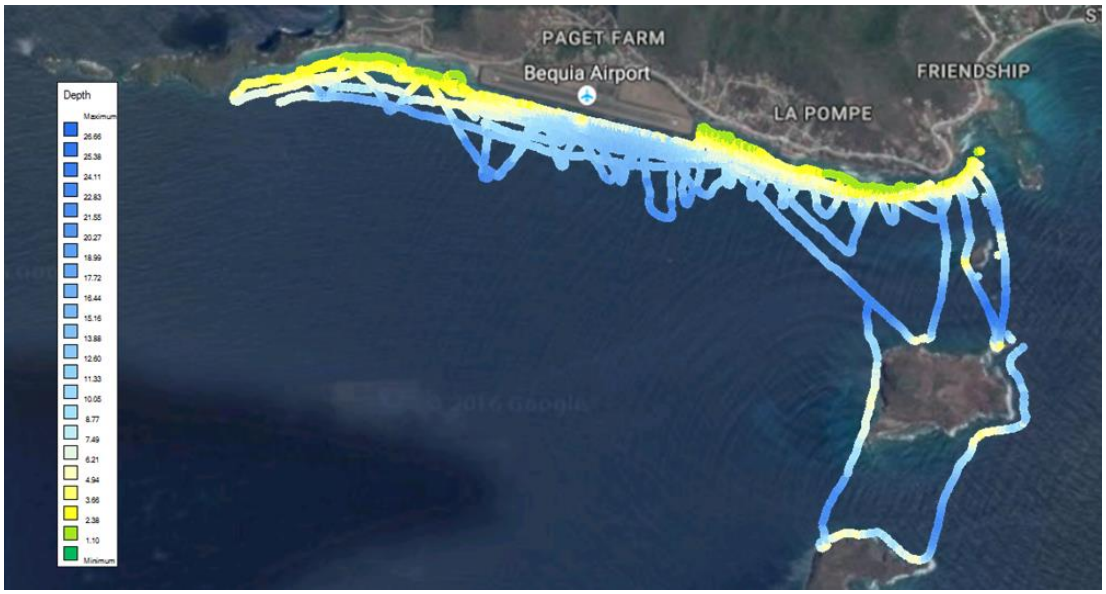

Figure 3.9: Map of the Transects

A good portion of the area close to shore was surveyed. The depths for the rest of the area covered by the computational grid will be calculated using a navigation map and by triangulation approximation using Delft3D.

3.2.3 Velocity Data Collection

Eulerian point velocities in the water column were also collected to assist in the calibration of the model. Using the ADCP, velocity can be measured using the transducers that compare the reflection of sound waves on small particles in the water column between two time steps. This provides point velocities through the entire water column. The boat was anchored at a particular location, which was then noted using GPS. GPS was also used to correct velocities by adjustments that reflected movements of the boat. In order to use these points in the calibration of the model, the velocities were averaged over time to account for fluctuations due to the waves and the movements of the boat. Since the software used (ADCP post-processing program) could not separate the velocity in the Z direction at any given time step, the velocity was also averaged over the whole water column. A total of 29 points were collected. Table 1 summarizes some of the points that were collected on August 29th 2016.

Time	Depth (m)	Velocity X (m/s)	Velocity Y (m/s)	Time of Measurement (s)	UTM(m)	UTM(m)
7:03:02	2.16	-0.055	-0.002	80	689243.04	1436328.50
7:05:11	2.66	-0.038	0.017	64	689238.87	1436322.48
7:10:53	2.08	-0.068	-0.036	77	689319.94	1436308.85
7:15:16	3.28	-0.118	-0.038	79	689397.92	1436262.99
7:19:13	3.29	-0.120	-0.034	74	689477.33	1436238.94
7:23:15	5.00	-0.170	-0.057	103	689485.18	1436189.92
7:27:31	5.67	-0.162	-0.059	85	689438.65	1436193.31
7:31:56	5.53	-0.144	-0.051	88	689351.88	1436223.49
7:35:46	5.70	-0.154	-0.038	75	689286.46	1436243.29
7:39:44	5.96	-0.127	0.004	83	689182.92	1436269.85

Table 3.1: Example of Point Velocities

Each point has a location defined in the UTM (Universal Transverse Mercator coordinate system) which helped trace back its exact position on the numerical model grid. The point

velocities were converted into X and Y components for an easier comparison with the Delft3D's default results format. (See Appendix B for the full post-processing method used)

The movements of floating debris just east of the inlet were observed during the velocity measurements. It was noted that the debris were moving approximatively parallel to the shore and were moving westward even when the current was moving eastward. This indicates that the tide-induced current is not the main driving factor of the surface current. Due to time constraints, the measurements were limited. If more time had been available, a tracking of floating debris, using GPS placed on floaters released at different times and sea conditions, could have extended the information available to validate the model. Also, a time series of the depth-averaged velocity over a full tide cycle at a location where the tide-induced current creates high velocities (such as between petit Nevis and Bequia in Figure 2.7) would have been preferable to create a better numerical estimation of the phenomenon.

3.3 Soil Samples Collection and Analysis

3.3.1 Sieve Analyses on Coastal Sediments

Local soil samples were analysed for the purpose of getting a better understanding of the material that form the sea floor in the area. The first type of analysis conducted is a grain size analysis on sand samples collected along the coastal water line (see Figure 3.10 for sample locations) where sediments were accumulating.

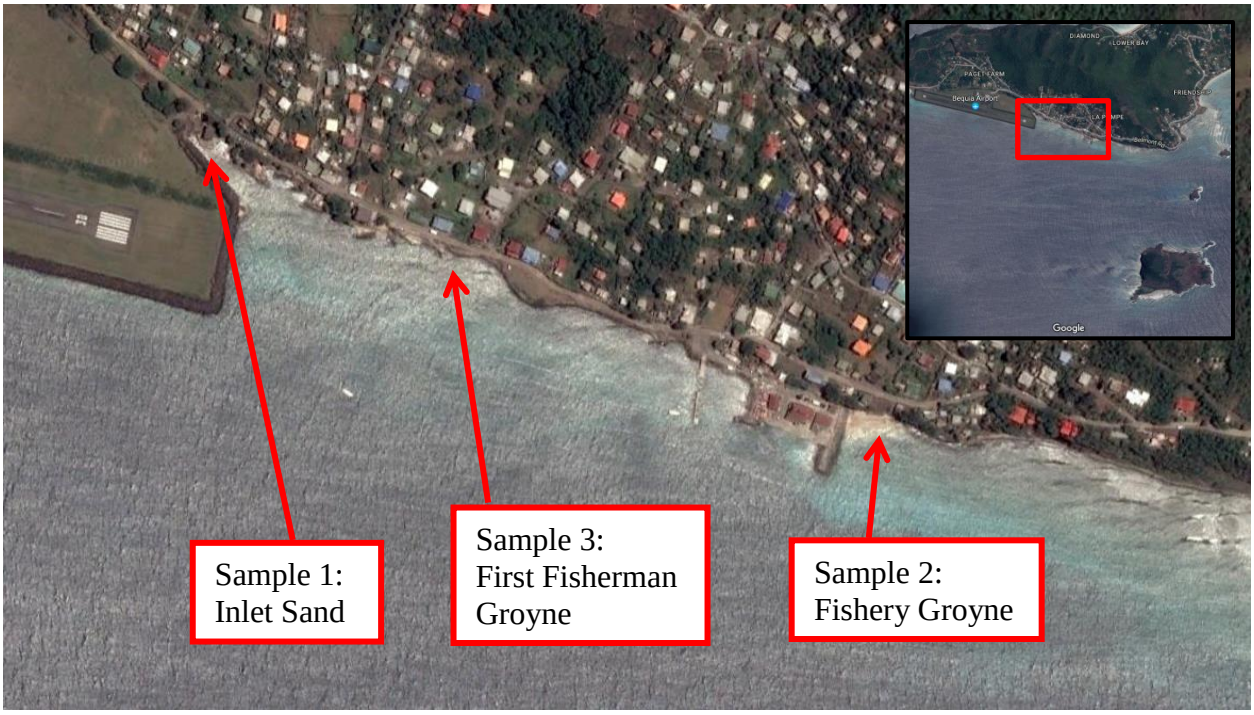

Figure 3.10: Sample location of the sieve analysis samples

The samples were tested according to the test method LS-602 recommended by the Ministry of Transport of Ontario (Ministry of Transport, 2006). The results of the sieve analysis done on the three samples are shown in Figure 3.11. (Individual graphs can be found in Appendix C)

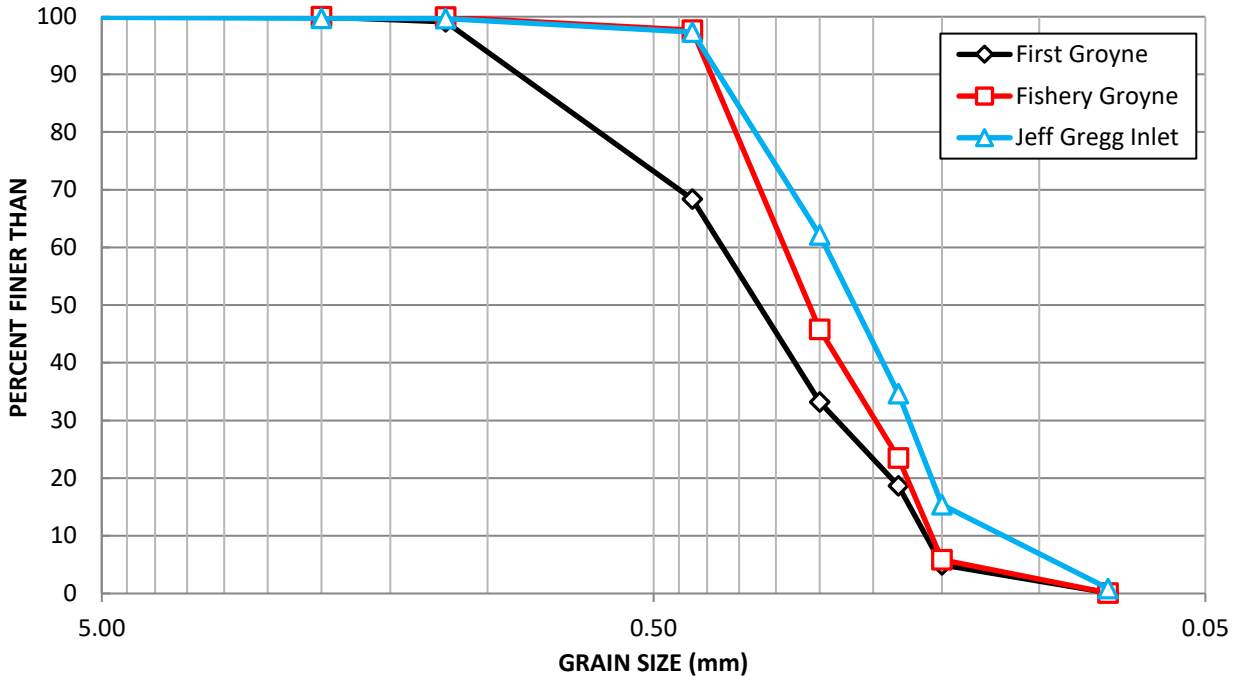

Figure 3.11: Sieve Analysis Summary

It can be concluded that all the samples consist of 'poorly distributed sand'. Table 3.2 is the summary of the passing soil at the different sieve:

		Fine Grain, Percent Finer (%)		
Sieve No.	**Sieve Size (mm)**	**First Groyne**	**Fishery Groyne**	**Jeff Gregg Inlet**
10	2	100.0	100.0	100.0
16	1.19	99.1	100.0	99.7
40	0.425	68.4	97.7	97.4
60	0.25	33.2	45.8	62.1
80	0.18	18.7	23.5	34.7
100	0.15	5.0	5.9	15.4
200	0.075	0.1	0.1	0.9

Table 3.2: Sieve Analysis Summary

There is a difference in the grain size distribution of the three samples. The results indicate that the first fisherman groyne has coarser sand. The sediments influx accumulating at that location comes from the road enlargement installed on the windward side of the groyne. The size of the sediments that come from the enlargement might be coarser than the natural sediment in the area. Also, the source is very close to the accumulation leaving no time to erode. This road

enlargement is described in the section 3.1.2 Paget Farm Coastline Features. Also, the inlet sample's grain size is the smallest. This can be explained by the fact that there is less wave action in the inlet which results in a beach with smaller grain size. (A. Heitor Reis, 2010)

3.3.2 Bulk Density Analysis on Quarry Rock

The second analysis executed is a density analysis on a rock sampled at the 'old quarry' (where the rocks used for the airport's armoring were quarried from). Given the quarry is very accessible and large size boulders are close to the surface, rocks could be easily quarried from that location and used for the rubble mound groyne. Also, the fact that the airport armoring has withstood for over 25 years proves that these rocks can resist the wave action of the area if the structure is properly designed. It also proves that this type of rock isn't affected by the chemical attack of salt water. Given that the design of a rubble mound structure is dependent on the rock's density (ρ), this analysis has to be done on the rock to ensure an appropriate design (U.S. Army Corps of Engineering, 2008).

The Canadian code that provides the recommendation for the coarse material density analysis is the CAN/CSA-A23.2-12A-14. However, this code is not providing a step by step technique to do the test. The method used for the experiment is the water displacement method. This method consists of using the principle of Archimedes to get an estimation of the bulk density of the rock. (Scogings, 2015) The rock is first weighted, then submerged and suspended in a water container. The difference of water weight, when adjusted according to the relevant density, is the bulk volume of the rock. The weight is divided by the bulk volume to get the bulk density of the rock. Table 3.3 summarizes the results from the experiment.

	Result
Weight of Rock (g) (1)	917.90
Weight of Displaced Water (g) (2)	312.08
Density of Water at 23C (g/cm³) (3)	0.9975
Density of Rock (g/cm³) (1)*(3)/(2)	2.934

Table 3.3: Results of the Bulk Density Experiment

The density of the rock is ρ = 2,934 kg/m³. This density is recommended to be used in the design of the proposed groyne.

3.4 Meeting with Local Decision Makers

A series of meetings were held with some of the local decision makers from Saint Vincent and the Grenadines. The first couple of meetings were with representatives of the different ministries involved in the various aspects of the project. The goal was to get their input and their approval on some of the activities required for the completion of the project, such as quarrying rocks and building on government land. Getting their approval will not only allow the proposed solution to be built when the plans are ready, it will also help with the granting of funds from the Caribbean Development Bank (CDB). The people present at these meetings were:

- Leah Belmar, Lucille Cozier, (Northern Grenadines Community Development Inc.)
- Herman Belmar (Directorate of Grenadines Affairs)
- Philippe April-LeQuere, Ioan Nistor PhD (University of Ottawa)
- Corliss Murray (Ministry of Lands & Surveys)
- Bentley Browne (Consultant CDB)
- Raymond Victory (Central Water & Sewerage Authority)
- Franklyn Haynes (Ministry of Transport & Works)
- Shelford Stowe (Physical Planning Unit)
- Houlda Peters (National Emergency Management Organization)
- Carlos Wilson (Public Health Department)

Meetings summary and outcome:

A consensus on a plan to address the problems of drainage, erosion and litter accumulation was reached by the end of the meeting. The proposed solution to fix the drainage problem is to build a long channel along the airport that would be deep enough to allow for the salt water to flow in. This channel will collect the water from the village drains. Therefore, the whole drainage system in the village will require recalibration and some new secondary drains require to be built to allow the water to drain in the main channel. The ministry of lands and surveys proposed to do the necessary surveys for the planning of the drains. A possible collaboration between the Physical Planning Unit and the Central Water & Sewerage Authority was mentioned to get additional funding for the construction of the new secondary drains and the recalibration of the existing drains.

The rubble mound groyne is the solution that was put forward to address the problems related to erosion and litter accumulation. The ministries' representatives approved the utilization of rocks and public lands for the project as long as the plans were sent and approved before the commencement of the construction.

The last meeting was with the Prime Minister of Saint Vincent and the Grenadines, Ralph Gonsalves. This meeting was considerably shorter than the others, given Mr. Gonsalves is a very busy man. After presenting the proposed solutions, Mr. Gonsalves confirmed his collaboration and suggested that NGCDI come up with a list of the approvals required. This list will be sent directly to the ministries and will be receive a higher priority than other projects.

3.5 Presentation to the Community

Given the project has a great community impact, their input is very important. Therefore, a presentation was organized by NGCDI to present to the population the proposed solutions to address the problems of erosion, litter accumulation and drainage. The attendees were welcomed to share their point of view and their perspective on the problems.

After a little presentation from the author (Philippe April LeQuéré), Herman Belmar and Bentley Browne on the physical side of the project, the attendees have indicated that they would welcome the proposed solutions. A concern was raised by the owner of a convenience store next to the inlet. She indicated that "a lot of people are throwing out their garbage along the coast and she saw the garbage moving into the inlet afterwards". This testimonial reinforces the hypothesis that most of the litter comes from the villagers littering habits.

3.6 Summary of the Field Campaigns

During the two field campaigns, important observations and data collection were achieved:

- Sand is accumulating along the shore, especially on the windward side of the existing groynes, (a)
- A large number of floating and non-floating debris was observed along the coast and in the inlet. It was concluded that most of the debris is coming from the villagers' bad habit of disposing their litter along the coast, (b)
- Only floating detritus were found stuck in the airport's armoring indicating that some of the debris is brought by the sea, (c)

- A tide-induced current was observed between the islands East of the airport, (d)
- The airport armoring was found to be in a very good condition indicating that a similar design can be used for the groyne,
- Local bathymetric data was successfully collected in areas where higher resolution is needed in the numerical model,
- Point velocities were collected along the shore to help with the calibration exercise of the model,
- A sieve analysis was done on three sand sample collected along the shore to help the formulation of the bottom friction in the area,
- A bulk density analysis was done on a rock sampled at the quarry where the airport armoring comes from. This result will help for the design of the rock size to be used in the groyne, The bulk density of the rock was found to be 2,934 kg/m^3,
- Meetings with the local decision makers, such as ministers and the Prime Minister, helped getting a consensus on which solution to implement and get a commitment for the approval of the project,
- A presentation with the local community has helped obtain the villager's feedback on the proposed solutions and to ensure they welcome the proposed groyne and new drainage system.

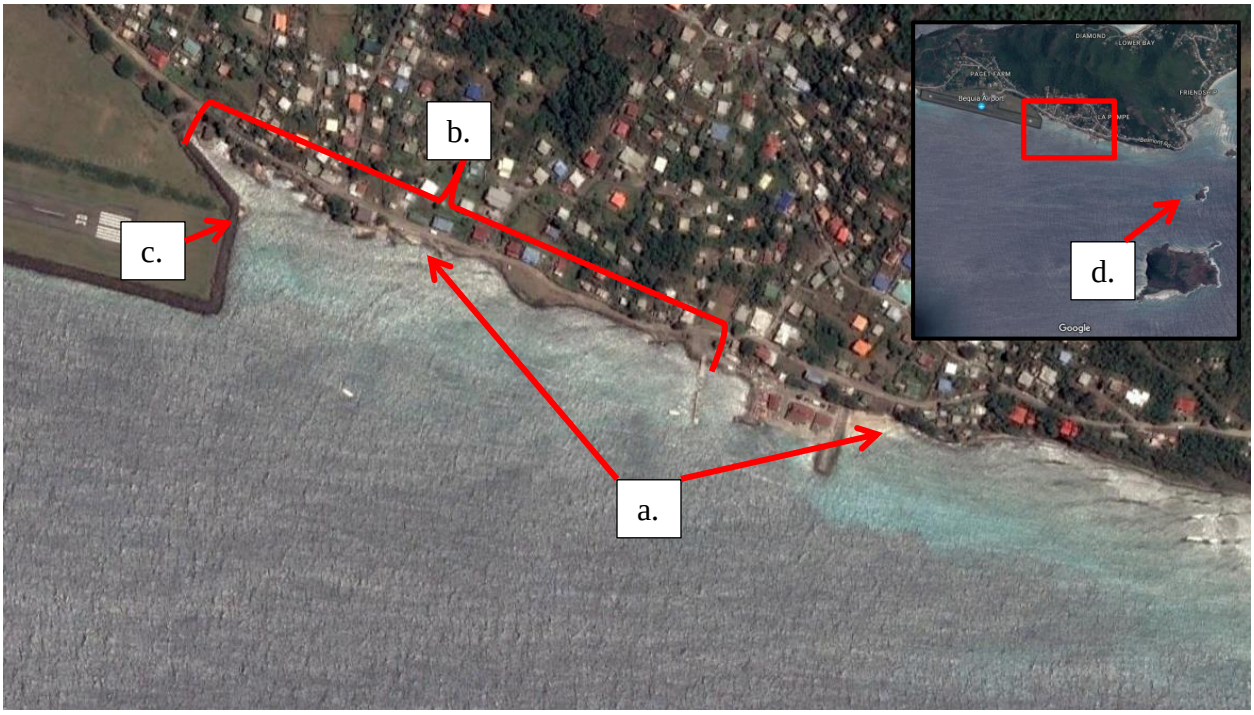

Figure 3.12: Field Investigation's Summary Map

4 Delft3D Model Development

As discussed in the 'Introduction' section, a new shore-line groyne structure is being proposed to, among other things, redirect floating debris in the Paget Farm coastal area away from the entrance to the Jeff Gregg inlet feature. Clearly, a better understanding of the complex coastal processes in the area, which largely govern the existing patterns of floating debris pathways, would assist in the design of the new groyne. To this end, a sophisticated computational model was developed to: (1) reproduce existing ocean current patterns and floating debris pathways in the region under different tidal and wind conditions, and (2) study the impacts of different arrangements of the proposed new groyne structure on the debris pathways.

The program chosen to construct the model is Delft3D by Deltares. This program is capable of generating hydrodynamic, morphologic and environmental simulations. The modules used for this study are FLOW and WAVE. FLOW simulates hydrodynamics while WAVE simulates the wave action based on the hydrodynamic results that FLOW calculates. After analysing some literature, it was confirmed that Delft3D-FLOW coupled with Delft3D-WAVE is an appropriate combination to simulate the hydrodynamics of a near-coast oceanic region (see section 2.2

Delft3D Numerical Modeling of Coastal Environment). The main equations and assumptions used to generate the model will be explained in this section, followed by an explanation of the model setup as well as the calibration procedure.

4.1 Theoretical Background of Delft3D Model

4.1.1 Model's Main Assumptions

In this section, Delft3D-FLOW's main assumptions are covered. The model simulates the hydrodynamics within a given grid by solving the 2D (depth-averaged) or 3D non-linear shallow water equations. These equations are an approximation derived from the Navier-Stokes equations for incompressible flow in shallow water. The following assumptions are some of the main ones used to approximate the Navier-Stokes equations (These are taken from the Delft3D-FLOW user manual. If more information is needed, the reader may refer to pages 187 to 189) (Deltares, Delft3D-FLOW, User Manual, 2011):

- Depth is assumed to be much smaller than the horizontal scale. Therefore, the vertical momentum equation is reduced to hydrostatic since the vertical accelerations are much smaller than the gravitational acceleration. (Shallow water assumption)
- In the Cartesian frame of reference, the earth curvature effect isn't considered. Therefore, the Coriolis parameter is constant throughout the domain.
- It is assumed that there is a slip boundary condition; a quadratic bottom stress formula is applied.
- The formulation of the increase of bed shear stress, when coupling wave and current forces, is generated from velocity approximated using a logarithmic distribution.
- The contribution of large eddies is simulated using the Eddy viscosity model. The k-ε model was used for the local turbulence. However, the parameters must be specified by the user in this particular model. For simplicity, the eddy viscosity approach, with the default parameters, is used in the model presented in this thesis.
- The production of turbulence is based on the vertical (the horizontal are ignored) gradients of horizontal flow in agreement with the aspect ratio for shallow water. If there is a case of a small scale flow, the horizontal gradients are included in the production term.

- The boundary conditions for the energy dissipation and turbulent kinetic energy at the bottom and free surface follow a logarithmic law of the wall.
- In the 'σ' coordinate system (used in the model), Delft3D solves the long wave equation. The model is not capable of resolving the scales of short waves, making the pressure hydrostatic. Consequently, the basic wave equations are averaged in analogy with turbulence introducing the radiation stresses term. Theses stresses are given by the wave forces provided by Delft3D-WAVE.
- The flux of particles through a closed wall and through the bed is equal to zero.
- The temperature and the density of the water are assumed to be uniform throughout the model.

The coordinate system used is the Cartesian system for the horizontal grid and 'σ' for the vertical grid. The Cartesian system is used to simplify the implementation of the tide asymmetry at the boundaries. The 'σ' co-ordinate system consists of a vertical grid with multiple 'σ' planes that aren't strictly horizontal (See Figure 4.1). The location of those planes is determined as a given percentage of the water depth. Consequently, these planes follow the topography and the surface of the water. This is different from a 'Z' grid system where each cell has a constant depth. The use of a 'σ-grid' allows a better resolution closer to the shore and the ability to get more resolution at the region of interest such as at the surface (example: for wind driven flows) or at the bottom (example: for sediment transport) while reducing the processing time because it is not necessary to add grid cells in deeper water.

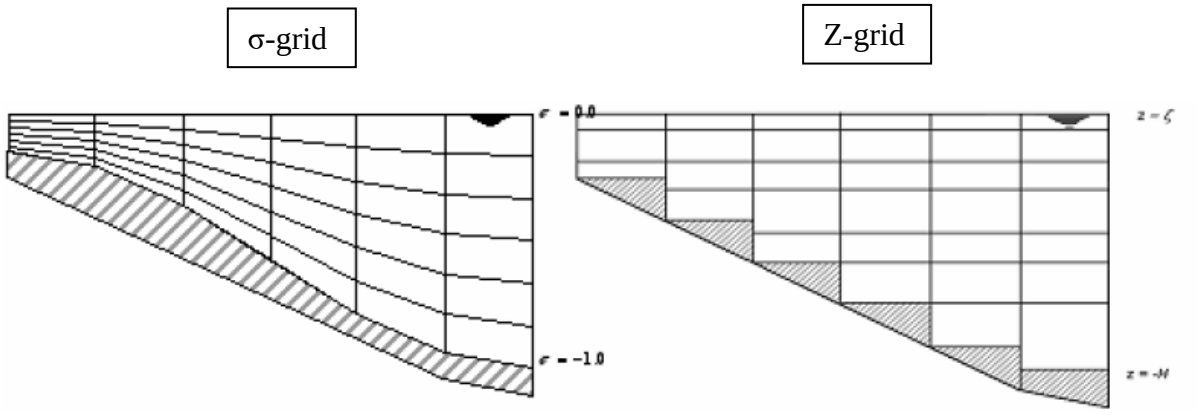

Figure 4.1: 'σ-grid' vs 'Z-grid' Comparison (Deltares, Delft3D-FLOW, User Manual, 2011)

$$\sigma = \frac{z - \zeta}{H} \qquad (2)$$

Where:

- z is the vertical coordinate,
- ζ is the free surface elevation above the zero plane (z=0), and
- H is the total water depth.

As described by equation (1), σ represents the ratio between the vertical co-ordinate (z) minus the free surface elevation above the reference plane (ζ) and the total depth at that location (H). Therefore, the bottom has σ = -1 and the surface of the water has σ = zero. The fact that the vertical grid split as a ratio of the total depth will provide a better resolution in shallower water than fixing the size of the grid in the vertical direction. Moreover, the 'σ-grid' was used instead of the 'Z-grid' because the coupling of the WAVE and FLOW modules in 3D can only be done if a 'σ-grid' is used.

4.1.2 Governing Equations

The following equations are the momentum equations solved in the two horizontal directions (2) and (3): (Deltares, Delft3D-FLOW, User Manual, 2011) (Elias, 1999)

$$\frac{\delta u}{\delta t}+\frac{u}{\sqrt{G_{xx}}}\frac{\delta u}{\delta x}+\frac{v}{\sqrt{G_{yy}}}\frac{\delta u}{\delta y}+\frac{w}{d+\zeta}\frac{\delta u}{\delta z}-\frac{v^2}{\sqrt{G_{xx}}\sqrt{G_{yy}}}\frac{\delta\sqrt{G_{yy}}}{\delta x}+\frac{uv}{\sqrt{G_{xx}}\sqrt{G_{yy}}}\frac{\delta\sqrt{G_{xx}}}{\delta y}-fv=$$

$$-\frac{1}{\rho_0\sqrt{G_{xx}}}P_x+F_x+\frac{1}{(d+\zeta)^2}\frac{\delta}{\delta z}\left(u_V\frac{\delta u}{\delta z}\right)+M_x \qquad (3)$$

Velocity Gradient; Advective Terms; Pressure Gradient; Bottom Roughness; External Forces (wind); Eddy Viscosity

$$\frac{\delta v}{\delta t}+\frac{u}{\sqrt{G_{xx}}}\frac{\delta u}{\delta x}+\frac{v}{\sqrt{G_{yy}}}\frac{\delta v}{\delta y}+\frac{w}{d+\zeta}\frac{\delta v}{\delta z}+\frac{uv}{\sqrt{G_{xx}}\sqrt{G_{yy}}}\frac{\delta\sqrt{G_{yy}}}{\delta x}-\frac{u^2}{\sqrt{G_{xx}}\sqrt{G_{yy}}}\frac{\delta\sqrt{G_{xx}}}{\delta y}-fu=$$

$$-\frac{1}{\rho_0\sqrt{G_{yy}}}P_y+F_y+\frac{1}{(d+\zeta)^2}\frac{\delta}{\delta z}\left(u_V\frac{\delta v}{\delta z}\right)+M_y \qquad (4)$$

Velocity Gradient; Advective Terms; Pressure Gradient; Bottom Roughness; External Forces (wind); Eddy Viscosity

Where:

- x, y and z are the three Cartesian coordinate directions,
- u, v and w are the velocities in the x, y and z directions respectively,
- G_{xx} and G_{yy} are the conversion terms between rectangular and curvilinear co-ordinates,
- d and ζ are the depth and the depth above datum respectively,
- fv and f_u terms are the Coriolis force,
- P_x and P_y are the pressure gradients created by the external forces such as wind and waves,
- F_x and F_y represents the unbalance of the Reynold's stresses in the horizontal directions,
- M_x and M_x terms represent the external source contributions or sinks of momentum, and
- u_V is the vertical eddy viscosity term.

All the density terms are neglected, except in the baroclinic pressure terms. The contributions of waves are added to the surface flow through the pressure terms and calculated using Delft3D-WAVE.

For the velocity in the z direction, the equation (4) summarizes the continuity equation that is solved:

$$\frac{\delta\zeta}{\delta t}+\frac{1}{\sqrt{G_{xx}}\sqrt{G_{yy}}}\frac{\delta\left[(d+\zeta)u\sqrt{G_{yy}}\right]}{\delta x}+\frac{1}{\sqrt{G_{xx}}\sqrt{G_{yy}}}\frac{\delta\left[(d+\zeta)v\sqrt{G_{xx}}\right]}{\delta y}+\frac{\delta w}{\delta z}=H\left(q_{in}-q_{out}\right) \quad (5)$$

Water Elevation Gradient | Pressure Gradients | Velocity Gradient | Local Sources and Sinks of Water

The terms are the same as the previous equation, only H , q_{in} and q_{out} are added. They represent the total water depth, the addition of water in l/s and the sink of water in l/s respectively. (Deltares, Delft3D-FLOW, User Manual, 2011) The acceleration in the vertical direction is neglected in the equation since the shallow water assumption was used by the program developers.

The FLOW module is capable of simulating flow induced by discharges from rain, tides and wind, but it cannot model wave contributions, an important factor in coastal areas. In fact, waves increase the turbulence due to wave breaking and white capping, and create a flux of mass that will affect the current profile, especially in the cross-shore direction. In the surf zone, the long shore current and rip currents generated by waves reshapes the current profile. This change of velocity in the water column changes the bed shear and stirs up the sediment. In Delft3D, the contribution of waves in the system is modeled using the WAVE module. Waves are simulated using the third generation wave model called SWAN (Simulating WAves Nearshore). This SWAN model uses the linear wave theory to derive its general equations. The linear wave theory is based on the assumption that the waves are very long, parallel and identical. The spectral action balance equation (5) describes the evolution of the wave spectrum: (Deltares, Delft3D-WAVE , 2011)

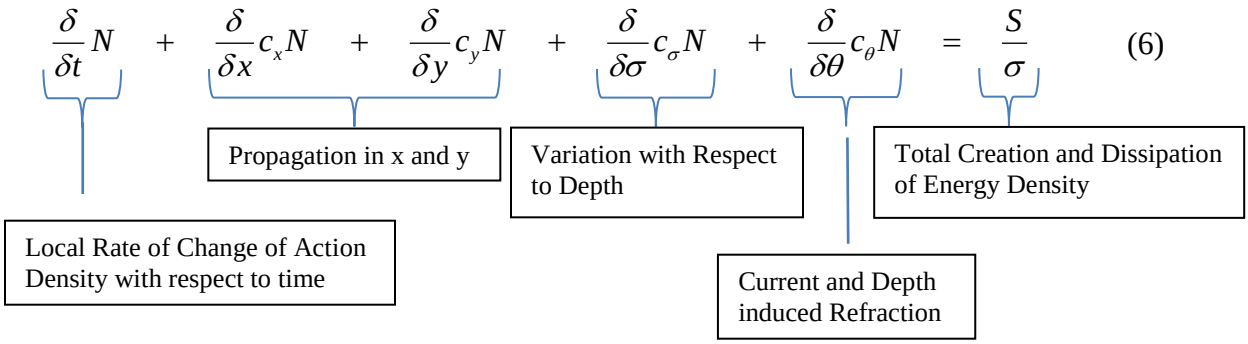

Where:

- σ represents the variation proportional to depth in the vertical direction,
- c_x, c_y, c_σ and c_θ are the celerity of the wave (wave speed),
- N is the action density, and
- S is the spectral action.

The equation models the increase or decrease of energy in the waves. Wind and non-linear wave-wave interaction increase the energy carried by the waves. Wave breaking, white capping, bottom friction and wave-wave interaction are factors that can decrease the wave's energy. Every source of creation and dissipation in the spectral action balance equation are described explicitly in the user manual. (Deltares, Delft3D-WAVE , 2011)

4.1.3 Coupling of FLOW Module and WAVE Module

The model was set up so that the FLOW module is coupled with the WAVE module. Figure 4.2 illustrates the interaction between FLOW and WAVE, and which inputs are used in the model:

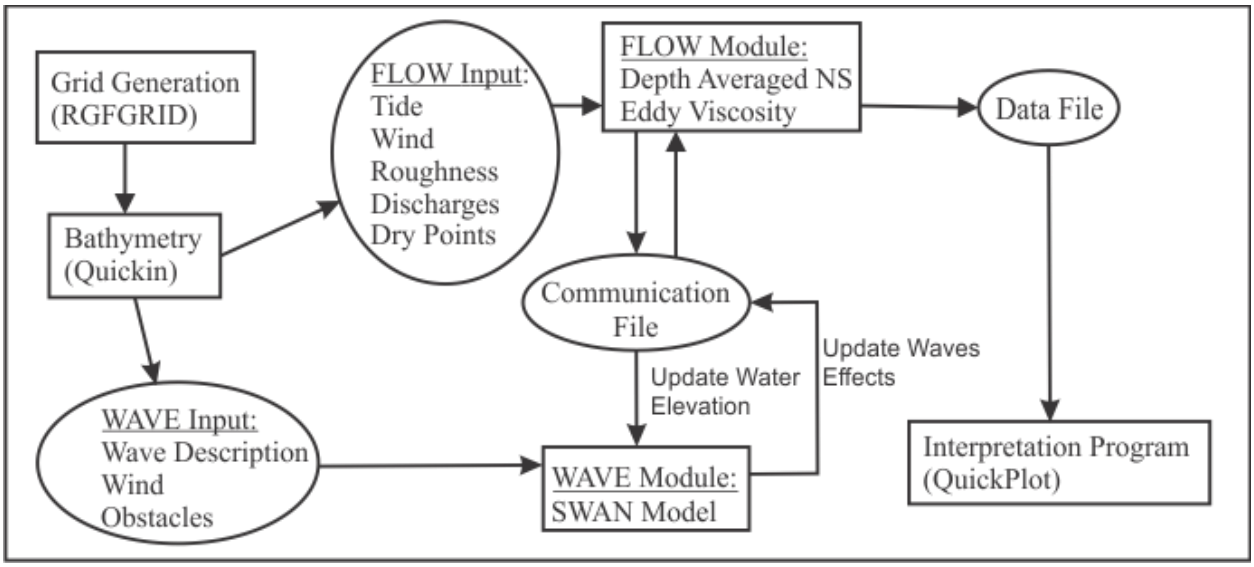

Figure 4.2: Flowchart of FLOW-WAVE coupling in Delft3D

Following Figure 4.2, the modules RGFGRID and Quickin are the tools that help create the grid and the bathymetry respectively. The grids and bathymetry, combined with inputs specific to each module, are used by WAVE and FLOW during their computation. FLOW simulates the hydraulic processes within the mesh using an approximation of the Navier-Stokes equations and writes the results in a 'Data file'. At a given time step, the hydraulic properties within the grid, such as the water level, updated bathymetry, current velocities, etc., are written in a 'Communication file'. The information that is written in that file is interpreted by WAVE to solve the SWAN model. Then, WAVE writes the wave action in the 'communication file' so that FLOW gets the wave forces input used in the momentum equations. At the end of the simulation, the 'Data file' can be interpreted by using the post-process module QuickPlot which uses a Matlab code to generate graphs.

4.2 Computational Grids

4.2.1 The FLOW Grid

To set up a model in Delft3D, the first two steps are to construct a grid for FLOW and associate a bathymetry to that grid. Some groynes were defined along the coast, using the function 'dry points' in Delft3D, at the same location that the existing groynes that were noted in the field campaign (see Appendix D for the full list of 'dry points' location). The water level and the discharge at the boundaries were defined as sinusoidal functions to mimic the changes due to the

tide. A total of 14 Eulerian points, called ‘observations points’, were defined at the approximate locations where the point velocity measurements were taken in the field (see section 3.2.3 Velocity Data Collection). The depth- averaged velocity at those points was used for the calibration exercise: points 1 to 10 for the bottom roughness calibration, and points 11 and 12 for the tide-induced current calibration.

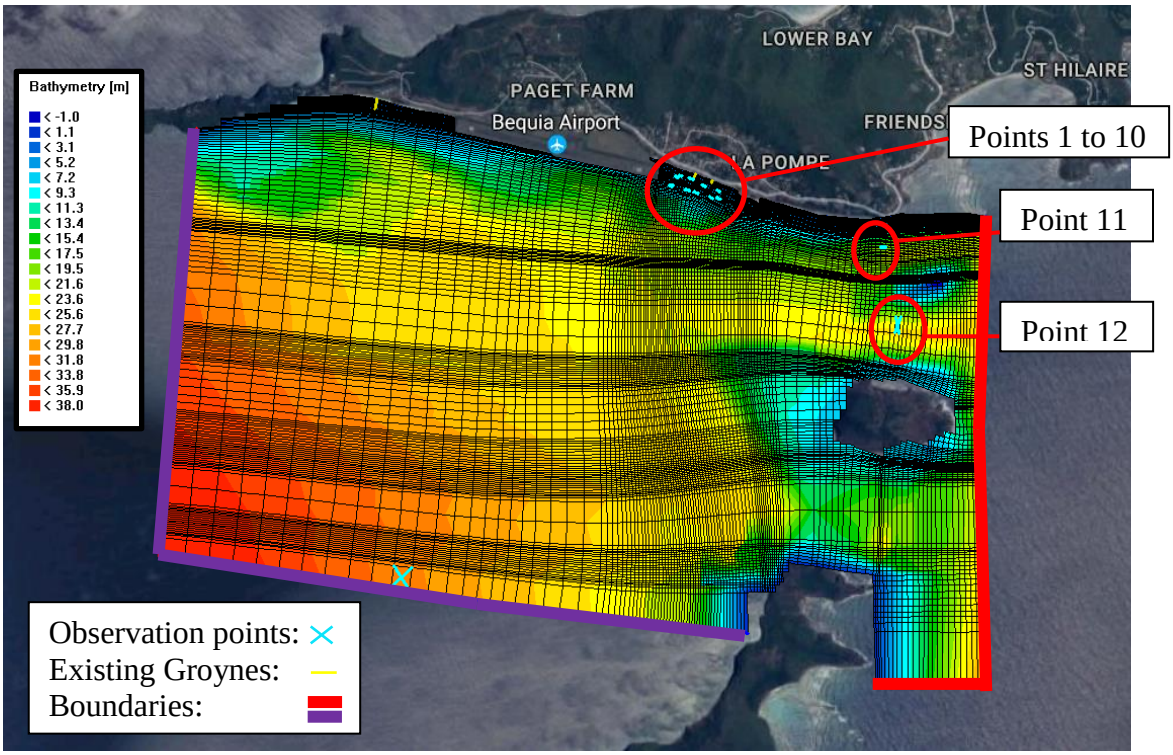

Figure 4.3: FLOW Module’s Grid

In Figure 4.3, the bathymetry is represented using a rainbow gradation following the legend labelled on the left of the graph. The grid was made such that the cell size is smaller both in X and Y directions in the area closer to the inlet. The grid was also refined around the islands East of the inlet. The effect of the refinement of the grid surrounding the islands was tested and has greatly improved the quality of the calibration. The total number of cells is 121 in the X direction and 153 in the Y direction. For the vertical direction, a σ-grid was set up. The grid in the vertical direction is divided into 6 cells each having a specific depth percentage: 2%, 15%, 20%, 40%, 15%, 8%. The σ-grid was refined closer to the surface to isolate the surface current from the depth-averaged current. This surface refinement has greatly improved the simulation of the

movement of floating debris in the model and has allowed to better reflect their movement as observed in the field. In total, the FLOW grid consists of 111,078 cells.

4.2.2 The WAVE Grid

A different grid was defined for the WAVE module. The grid used in FLOW could have been used alone, but WAVE's grid was built bigger to include wave diffraction from Isla a Quatre (see Appendix E). WAVE module was set up such that the wave condition is defined at the eastern boundary in the WAVE grid. The wave condition was only defined at the eastern boundary because the waves almost exclusively come from the East and are only coming from that direction in the modeled scenarios. The wave forces are then transferred to the FLOW grid at its boundaries.

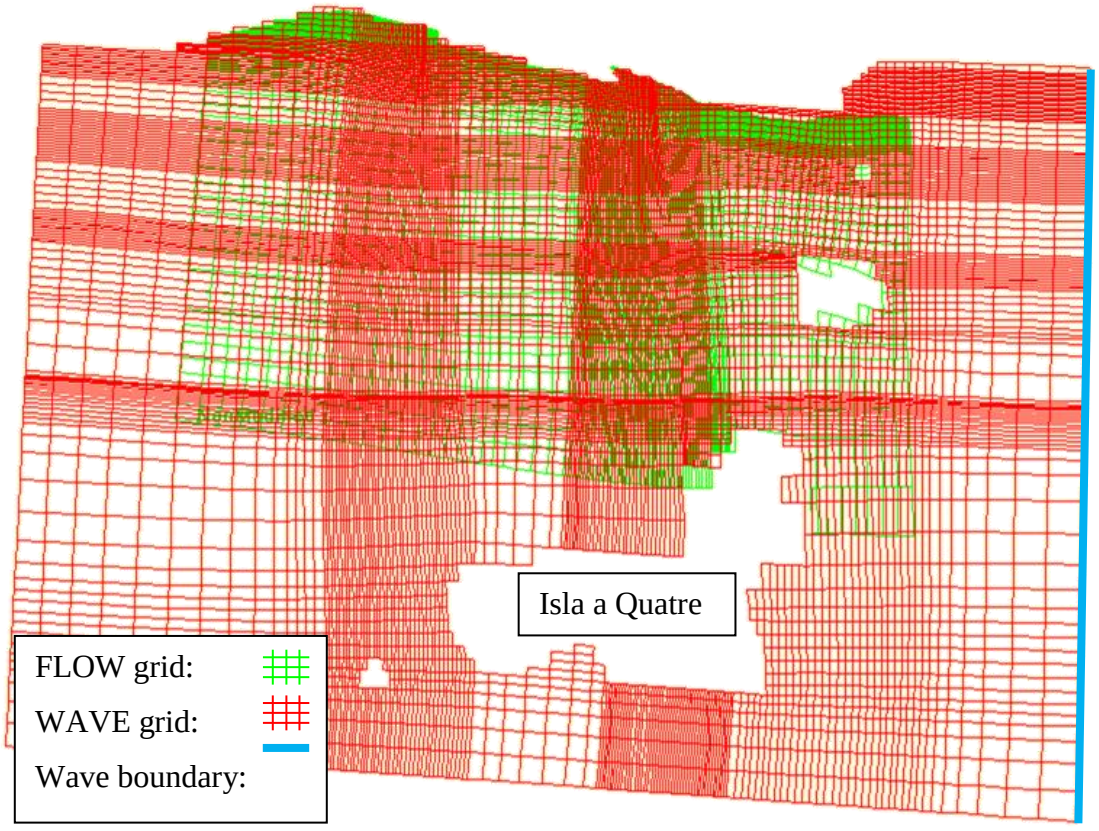

Figure 4.4: WAVE Module's Grid

The grid was refined around the islands and close to shore to provide a more detailed representation of the shallow water impact on the waves. Cells were defined as 'obstacles' at the location where groynes are defined as 'dry points' in the FLOW grid. The amount of cells is 141

in the X direction and 116 in the Y direction for a total of 16,356 cells. Unlike the FLOW grid, the WAVE module doesn't have a vertical grid. Now that the model setup is defined, additional data is required in order to complete the model.

4.2.3 Bottom Roughness

The bottom roughness in the model was defined using Manning's coefficient. The bottom roughness was divided into two areas: (i) a section near the Bequia shore, and (ii) the ocean section (the rest of the grid). Given that it was observed during the dives that the bottom near shore is different from the rest of the area, the roughness there is defined with a different value than the rest of the grid. The roughness in that area was assumed to be higher than the rest of the grid as the sea bed consists of reef outcroppings, a bottom that provides more resistance than sand. The sea bed in the ocean section consists of sand. This sand's grain size distribution was assumed to be the average of the grain size distribution from the local sand samples tested. Except for the grain size found in the laboratory, no information on the bottom roughness was found. Therefore, a calibration is needed in order to establish an appropriate bottom roughness value.

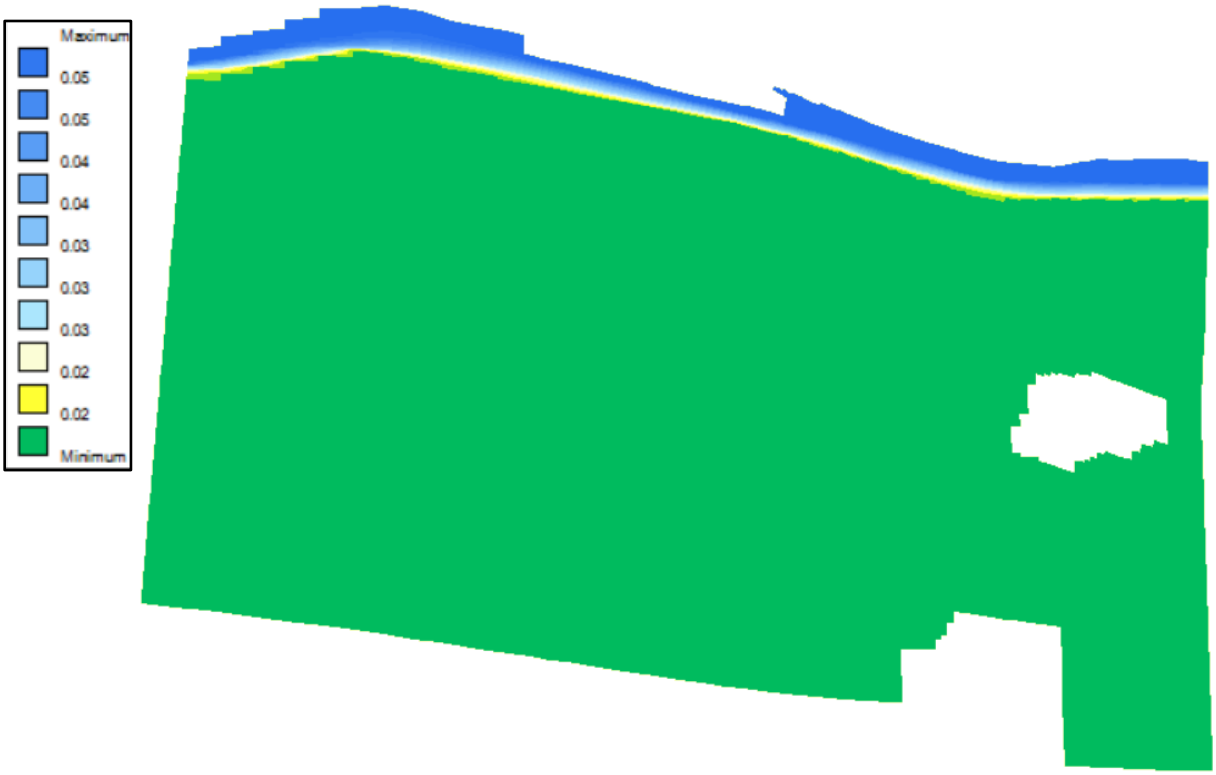

Figure 4.5: Manning's Roughness Grid

The grid shown in Figure 4.5 is the calibrated Manning's coefficient that varies through the grid. The roughness was found to be indeed higher along the shore.

4.2.4 Wind

The wind direction and intensity in the model was assumed to be constant throughout the whole simulation. In the computation, the wind forces were applied to the whole surface layer of the FLOW grid. The wind is also used in the WAVE simulation for induced white capping and wave generation found in a SWAN model. At the onset, it was planned to use the daily weather observation from the web site: 'wisuki.com' to perform the calibration, which indicated that the wind was always blowing from the east (90 degree from north). However, during the field campaign, it was observed that the airport windsock was pointing in the direction of the landing strip, at the nautical direction of 120 degree north. This could be attributed to the possible impact of the island's mountain on the wind direction. Therefore, the wind in the model was adjusted to reflect the observed phenomenon.

4.3 Boundary Conditions

4.3.1 Wave

The wave generating boundary in the model was defined at the East boundary WAVE's grid (blue line in Figure 4.4). The waves were modeled as being uniform throughout the whole boundary following the longwave assumption in SWAN. The waves were also assumed to have a constant significant height, direction and period throughout the simulation. The daily wave observations from wisuki.com were used in the model calibration to accurately represent the condition of that particular day.

4.3.2 Tide

The tide in the model was simulated by imposing its conditions at the three boundaries open to the ocean in the FLOW grid (red and purple lines in Figure 4.3). The tide condition was modeled using the harmonic function in Delft3D. This function makes the defined parameter vary following a sinusoidal function which represents a semidiurnal tide. This is not representing exactly the local condition since the local tide is a mix semidiurnal (Figure 2.6). The reason for the simplification is that velocities produced by the tide water level alone were too low and discharge (later added in the model) cannot be defined following the same pattern as a mix semidiurnal tide. However, the tide amplitude and rate of variation of water level during the time of the measurement were used for the calibration. Therefore, the calibration and results shouldn't be affected by this simplification. Two ways of defining the boundaries were attempted to simulate the tide and generate a tide-induce current: defining the east and west boundaries as two water levels and defining the west boundary as a total discharge and the east boundary as a water level.

First, by making a lag between the two sinusoidal functions that defines the water level at the two boundaries, the two water level model generates a tide-induced current, similar to the one observed during the field campaign. This lag creates a difference in water level between the two boundaries forcing the water to travel from the boundary with the higher level toward the other boundary. Since a sinusoidal function is used, the water level difference varies with the tide and changes the direction of the tide-induced current at the tide shift. No information is available on that lag. A calibration using the point velocities measured was done. However, this model was discarded as instabilities were experienced during longer simulations. This is possibly due to the

fact that imposing two water levels tends to create water accumulation and it is very sensitive to the orthogonality of the boundary.

Second, the discharge and water level model was implemented to solve the problems experienced when using the precedent model. The east boundary was defined as a water level that varies following a sinusoidal function, (Red lines in Figure 4.3). This boundary was chosen since it is the same side as Friendship bay, where the tide forecast used is made. The west boundary was defined as a total discharge. The discharge at the boundary is constant for every unit area and varies following a sinusoidal function that has the same rate of change as the water level at the east boundary. The amplitude of the total discharge was defined as a factor of the tide amplitude so that they vary proportionally. The new model has performed better than the previous model and has proven to be more stable. This is explained in more details in the section 4.4 Hydrodynamic Calibration and Validation.

4.4 Hydrodynamic Calibration and Validation

Because data on the bottom roughness and the tide-induced currents were missing, the model needed to be calibrated. It was decided to separate the calibration by adjusting two model parameters: the tide-induced current and the bottom roughness.

4.4.1 Calibration of the Tide-Induced Current

The tide-induced current was modeled by defining the east boundary as a harmonic water level and the west boundary as a harmonic total discharge. The east boundary was modeled following the tide's amplitude and speed (degree/h) at the moment that the point velocities were measured (see Table 4.1). The west boundary had three components that needed to be controlled: the total discharge for the west boundary and that for the south boundary and the lag between the East boundary, and the West and South boundaries harmonic cycles. The total discharge was defined by the authors as a factor of the tide amplitude, so that it varies proportionally when the tide amplitude is changed.

As the calibration process, by adjusting the bottom roughness, is intrinsically related to the calibration of the tide-induced current and vice versa, a value for the bottom roughness has to be assumed to first obtain a preliminary value for the boundaries' parameters. For simplicity, the bottom roughness value for the calibration of the tide-induced current was assumed to be the

same in the whole region. From scuba dives performed by the authors in the area, it was observed that, except near the shore, the ocean bottom in the area is covered mostly by sand. Samples of the sand were collected and analysed. The resulting grain-size distribution curves provided representative D_{50}–values for the three samples collected. The Manning's roughness value for the ocean bed was then calculated to be n = 0.018, using the equation (6): (California Departement of Water Resources. 1970)

$$n \approx 0.039 * D_{50}^{\frac{1}{6}} \qquad (7)$$

The required data on wave conditions, tide amplitude and wind conditions were obtained on the web site www.wisuki.com, where daily information on the local weather is continuously updated. As point velocities were recorded over two different days, under different weather conditions, two calculations were required. The following table summarizes the tide, wave and wind conditions for those two days:

	Date:	**August 21st**	**August 22nd**
Wave condition	Significant height (m)	0.8	0.8
	Direction (d)	90	120
	Period (s)	8	8
Wind Condition	Speed (m/s)	5	5
	Direction (d)	120	120
Tide condition	Time/Water Level	2:30 +0m	3:07 +0m
		8:38 +0.4m	9:24 +0.4m
		15:16 +0.1m	16:30 +0m
		20:23 +0.3m	21:27 +0.3m
Tide boundary definition	Tide amplitude (m)	0.3	0.4
	Tide speed (deg/s)	27.7	25.5

Table 4.1: Information required for the model's Tide Lag Calibration (wisuki. 2016)

The tide-induced current was calibrated using the velocity measured on those two days at approximatively the same location, which is between Bequia and Middle Cay and between

Middle Cay and Petit Nevis (Points 11 and 12 in Figure 4.3). Figure 4.6 summarizes the results of the calibration:

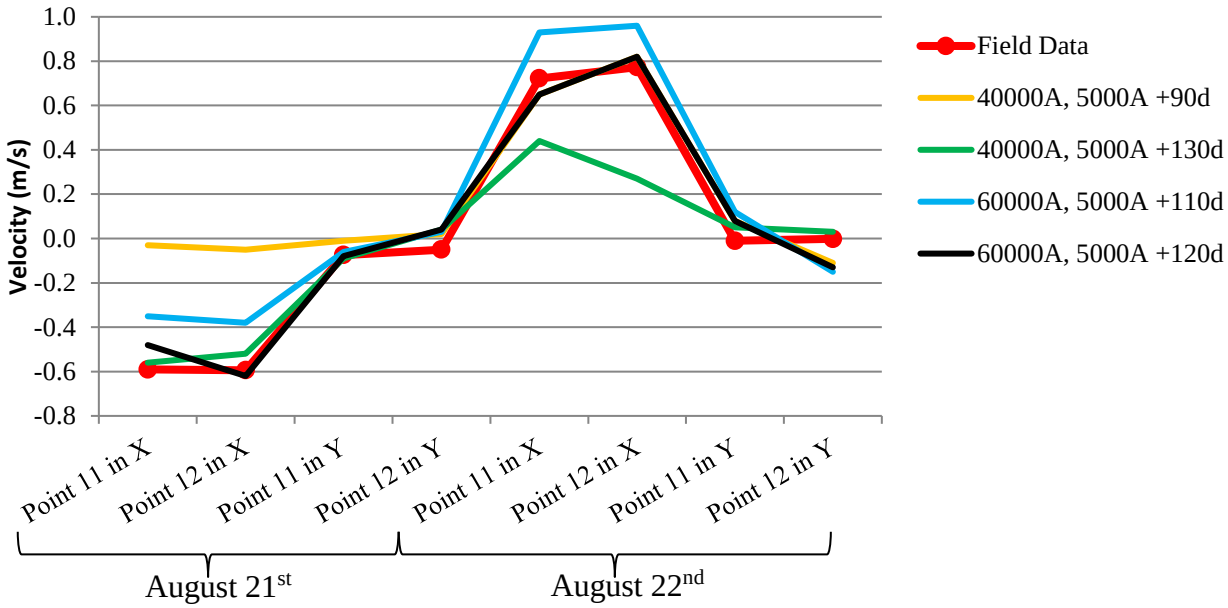

Figure 4.6: Tide-Induced Current Calibration Results

After analysing the data, it was observed that a total discharge for the West and South boundaries, of 60000 times the tide amplitude and 5000 times the tide amplitude respectively, represents most accurately the tide-induced current. A lag between the definitions of the two boundaries of 120 degrees was also found to be more appropriate. A root mean square error of 0.083 m/s was calculated. The main source of that error stems from the fact that the measured velocities at points 11 and 12 under the two conditions are similar and almost identical when considering velocities in the Y-direction. In the numerical model, point 11 exhibits lower velocities in the X-direction while the velocities in the Y-direction indicating that the currents are not parallel. This can probably be attributed to the uniform conditions for the eastern boundary. Full calibration results can be found in a table format in Appendix F.

4.4.2 Calibration of the Bottom Roughness

As soon as the tide lag was correctly reproduced, the second element used in the calibration is the bottom roughness. When diving in the area for visual confirmation of the nature of the bottom terrain, it was observed that the bottom near the coast (within 100m of the shore)

consisted of small reefs and sand patches. This fact was also observed via satellite imagery. As there is no precise information on a Manning's roughness for that type of bottom, the bottom roughness adopted for this region will have to rely on a calibration process. As a reference, Manning's roughness was estimated to be between $0.05 < n < 0.22$ for some reef systems in earlier similar-type studies (Prager, 1991) (Cialone & McKee Smith, 2007). For the rest of the grid, the roughness was assumed to be constant with a Manning's $n = 0.018$, a value that was used to verify tide-induced current calibration. At a specific distance, the bottom roughness was assumed uniform with a Manning's $n = 0.018$ and the roughness was then increased close to shore as needed. As all the measurements used for this calibration were taken on the same day, only one sea condition was used in the model. Table 4.3 summarizes the wave, tide and wind information inputted into the model:

	Date:	**August 29th**
Wave condition	Significant wave height (m)	1.2
	Direction (d)	90
	Wave period (s)	7
Wind condition	Speed (m/s)	7
	Direction (d)	120
Tide condition	Time/Water level	3:14 +0.2m
		8:23 0m
		15:03 0.5m
		23:03 0m
Tide boundary definition	Tide amplitude (m)	0.2
	Tide speed (deg/s)	36

Table 4.2: Model Information for Roughness Calibration (wisuki. 2016)

As the data was collected between 7:00AM and 7:40AM on August 29th 2016, only the ebb tide between 3:14AM and 8:23AM will be simulated. The points used for the calibration are shown in Figure 4.3 and marked from 1 to 10. All these points are very close to the location of the intended groyne. Figure 4.7 summarizes the results of the calibration for bottom roughness:

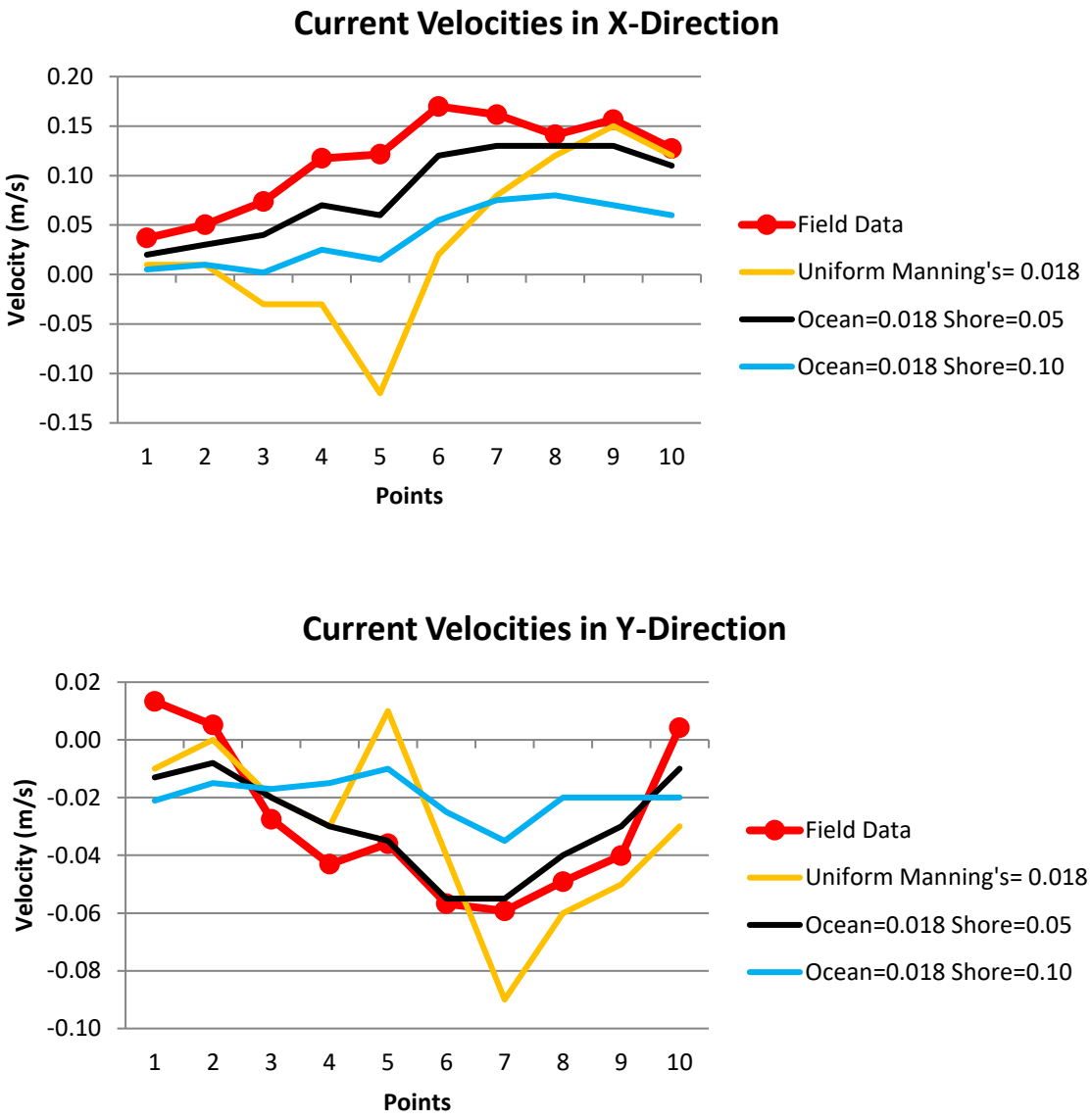

Figure 4.7: Bottom Roughness Calibration

After analysing the data, it was observed that when the bottom roughness for the first 100m of shore is increased to a Manning's coefficient of n = 0.05, while keeping the rest of the grid at n = 0.018, the model was most accurately representing the field measurements. The calculated root mean square error is 0.0264 m/s. This difference is acceptable since it is within the mean averaging error of 0.048 m/s for the data set. Also, the model is representing correctly the trend of the measured velocities. This gives a good indication that it will accurately model the movement of the floating debris. Knowing that the shore is composed of a mix of small reefs and sand, it is in line with previous studies that have also found that a reef bottom will have a higher

roughness. (Cialone et al. 2007) Previous authors have also suggested similar Manning's coefficient for reefs systems in shallow water. (Prager, 1991) (J.H. Rosman, 2011) Full calibration results can be found in a table format in Appendix F.

4.4.3 Floating Debris Pathways Validation

Validation of the model was done by tracking the movement of floating debris and testing if the surface current along the shore will push the debris toward the inlet. This is done by releasing floating buoys, defined as 'drogues' by Delft3D. It was observed that using the default value of JONSWAP's bottom friction in Delft3D (C_b = 0.067 m^2s^{-3}), the debris are moving offshore perpendicularly to the shore. This observation is contrary to what was observed during the field campaigns. So, different values of JONSWAP were tried and it seems that a lower value is more appropriate for this situation of 'shallow water with reefs' bottom. This confirms the newest findings that the assumed value of JONSWAP for wind driven waves is too high. (Cialone & McKee Smith, 2007) (Vledder, 2010). Figure 4.8 illustrates the movement of floating debris released at 3 locations every hour during a full tide cycle.

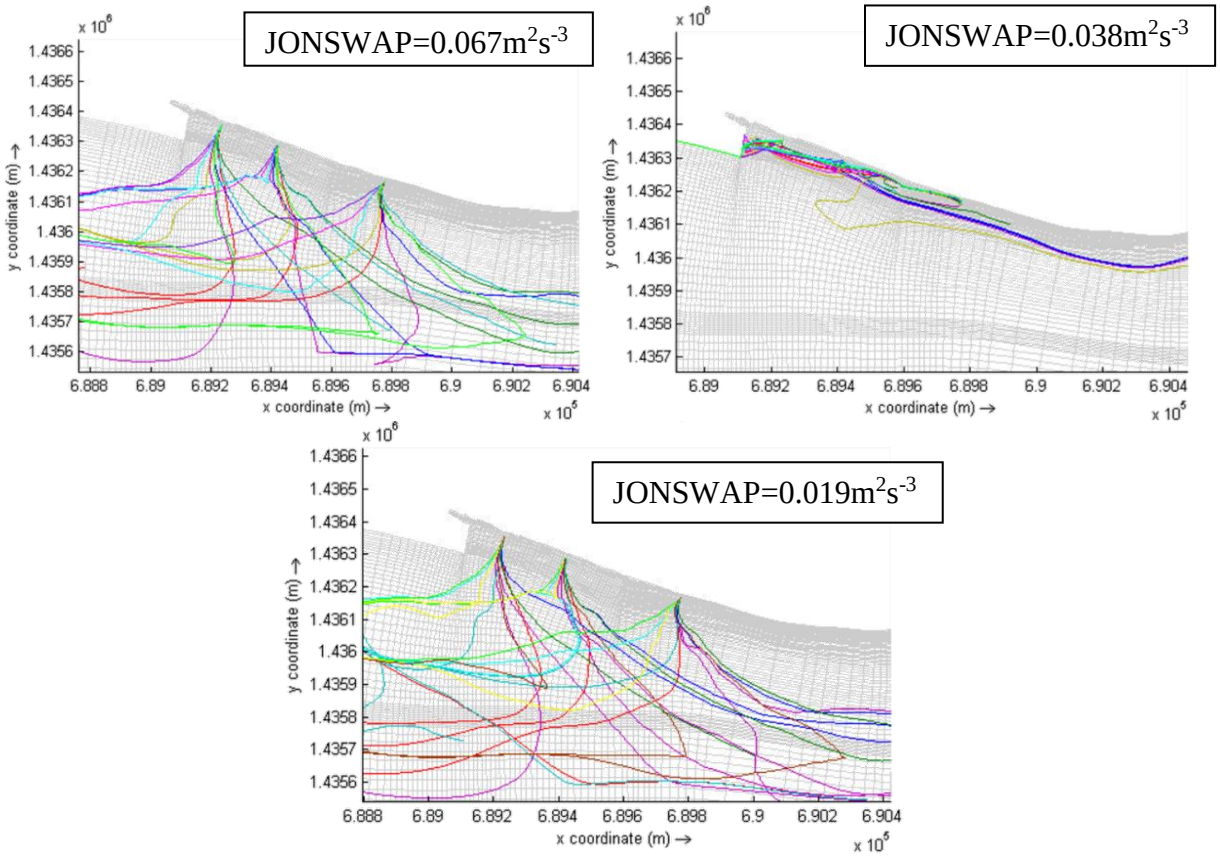

Figure 4.8: Floating Debris Patterns with Different JONSWAP

The value for Caribbean sand type bottom proposed by the SWAN team (C_b = 0.019 m^2s^{-3}) gave similar results as the wind driven wave value (C_b = 0.067 m^2s^{-3}), (The SWAN team, 2017). A JONSWAP parameter of C_b = 0.038 m^2s^{-3} will be used as it was proposed as a more appropriate value for this situation and represented better the observed floating debris pathways, (Vledder, 2010). However, the value of JONSWAP can't be adjusted further since no actual floating debris tracks were measured in the field. The change of JONSWAP has had little effect on the depth-averaged velocity calibration and the values presented for the calibration are for the reduced JONSWAP parameter.

5 Modeling of Existing Condition

Three different "sea" scenarios were investigated in order to study the possible pathways of floating debris in the vicinity of the proposed groyne:

1. Typical condition
2. High wave, high wind
3. Low wave, regular wind

These conditions were used to simulate the existing condition and then investigate the impact of the different groyne configurations on the debris pathway. The assumption is that these first conditions will help eliminate some groyne configurations on the basis of insufficient performance.

5.1 Modeled Conditions

The conditions that were chosen to test the groyne configurations were influenced by the conditions on August 29th 2016, the day that the point velocities used in the bottom calibration were collected.

		Typical	High Wind, High Wave	Low Wave, Regular Wind
Wave condition	Significant wave height (m)	1.2	2	0.5
	Direction (deg)	90	90	90
	Wave period (s)	7	7	7
Wind Condition	Speed (m/s)	7	11	7
	Direction (deg)	120	120	120
Tide condition	Amplitude (m)	0.4	0.4	0.4
	Speed (deg/h)	36	36	36
	West boundary total discharge (m^3/s)	24000	24000	24000
	South boundary total discharge (m^3/s)	2000	2000	2000

Table 5.1: Sea Conditions used for the Existing Condition and Groyne Configurations tests

In all of the scenarios, the tide amplitude at the East boundary and the total discharge at the West and South boundaries were doubled to match the average tide amplitude (wisuki, Statistics, Friendship Bay, 2017) Wisuki. The tide speed was kept the same. The specific changes done on each scenario are the following:

- In the 'Typical' scenario, the wind and wave conditions were kept the same as the weather observations from August 29th 2016.
- In the 'High Wind, High Wave' scenario, the wind speed and wave significant height were increased in order to mimic a 'windy' day. The wave height and wind speed are not exceeding the typical values for the area.
- In the 'Low Wave, Regular Wind' scenario, the wind speed is kept the same but the wave's significant height is reduced. Comparing the 'Typical' scenario to this one will help identify the effect of waves on debris accumulations.

All the simulations were done over a period of 56 hours and finished at the end of the flood tide. The first 22 hours of simulation were used to stabilize the model. During the following 9 hours, numerous floating trackers were released. In the remaining 25 hours, the movements of the trackers were monitored.

In the model, a function in Delft3D called ‘drogues’ was used to study the floating debris movements. These drogues are floating trackers released at the surface and they follow the velocity calculated in the surface cells. Their starting positions were chosen to be along the shore since the field campaigns had revealed that it is very likely that most of the debris were the result of community littering (see section 3.1 Field Investigations).

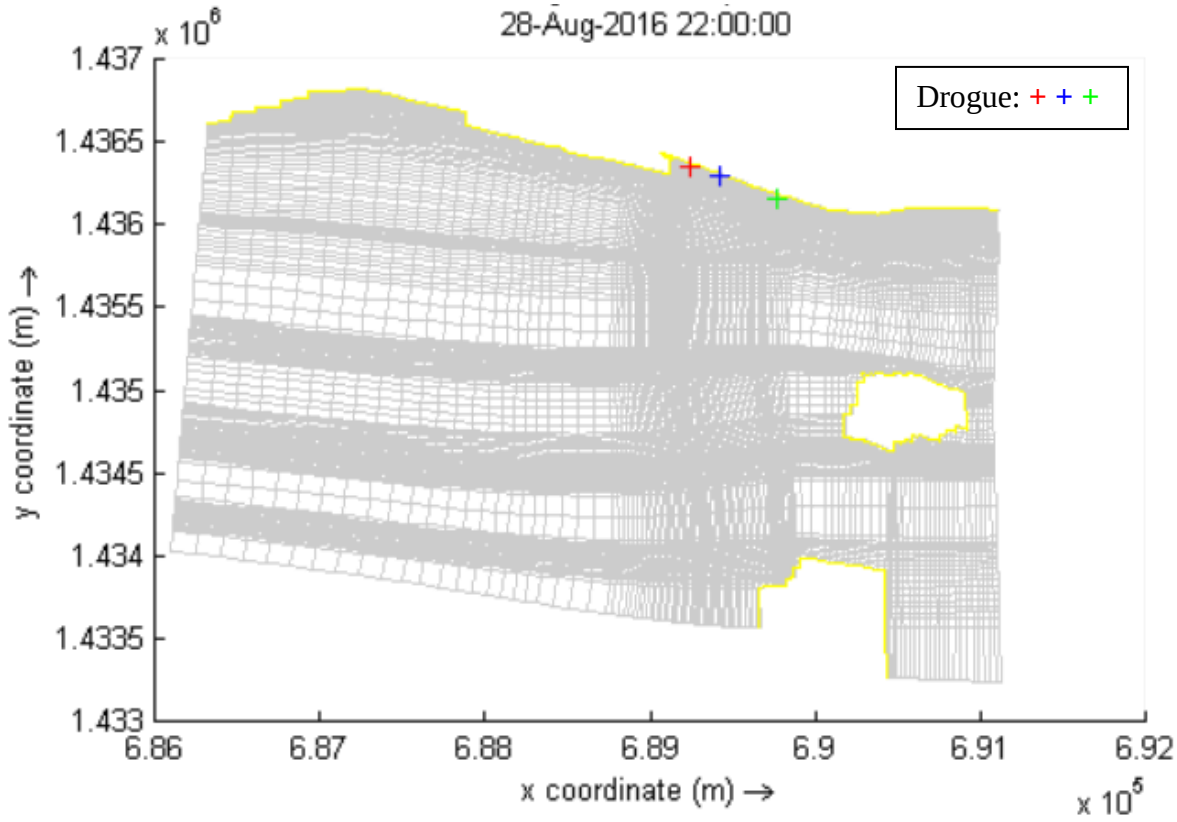

Figure 5.1: Starting Position of the Drogues

Three starting locations were defined where drogues were initially released (represented by a cross in Figure 5.1) during a full tide cycle, between the 22nd and 31st hour of simulation for a total of 30 drogues. Their position was registered at every time step (0.004 seconds). The red and blue crosses were located on the leeward and windward sides of the starting position of the proposed groyne, respectively and the green cross was located on the windward side of the fishery groyne. These locations were chosen because they were identified as areas where the litter accumulation was observed on the shore.

5.2 Existing Condition of Floating Debris Accumulation

The existing condition, without the proposed groyne, was first modeled using the same drogue set up used for testing the different groyne configurations' performance. The results from this simulation provided a 'benchmark' that helped in judging the influence of the proposed groyne. Also, an additional simulation was set up without the WAVE module to verify the influence of waves on the litter accumulation phenomenon. These particular simulations were done under the conditions of the 'typical' scenario and the scenario was run for 36 hours, only.

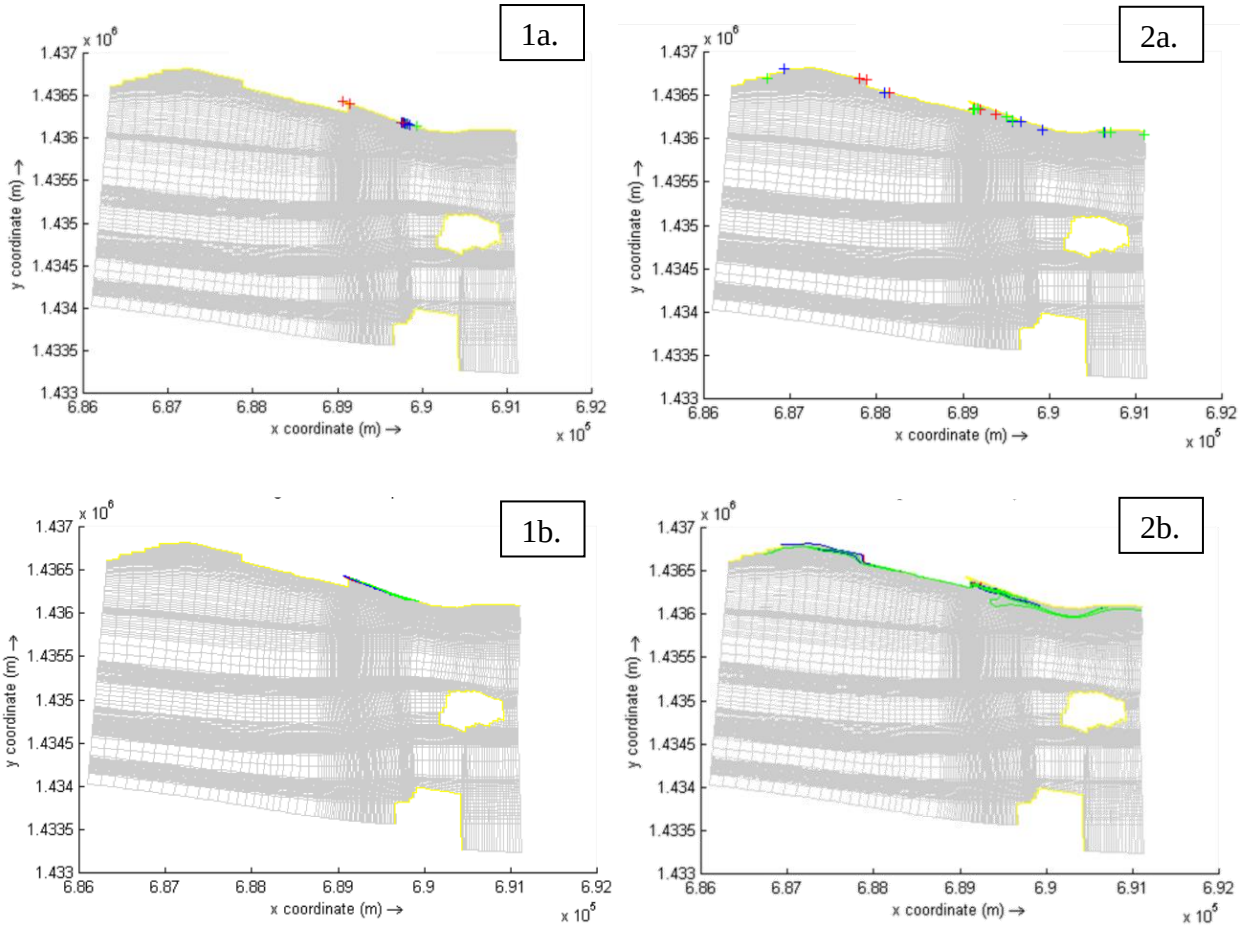

No Waves: 15 inlet, 15 shore

Waves: 12 inlet, 18 shore

Figure 5.2: Drogues Final Position (a) and Drogues Track (b) in Existing Condition Simulation; With Waves (1) vs Without Waves (2)

The drogues in the simulation with waves present are much more scattered than in the simulation without waves. In the simulation without waves, 15 drogues ended up far down the inlet. The drogues that did not end up in the inlet finished their course next to the fishery groyne. Some

drogues released during the ebb tide (when the depth-averaged velocity was in the West to East direction) were still accumulating in the inlet. This was in agreement with an observation made during the field campaign. In the simulation with waves present, no drogues entered the inlet. Twelve drogues were found at the mouth of the inlet and the rest were found scattered along the shore. In the 'no waves' simulation, the drogue pathways indicated that the drogues went toward the shore and stayed along the water edge during the whole simulation (Figure 5.2 (1b) and (2b)). When waves were added, the drogues stayed fairly distant from shoreline. Clearly, the waves were creating a "disturbed" water body next to the shore, thereby causing floating debris to be pushed away from the shoreline and thus preventing debris accumulation in the inlet. Therefore, according to the model, the wind is the driving force that generates the debris accumulation.

5.3 Benchmark Results for Existing Conditions

The same method was used to count the amount of debris accumulating in the three scenarios without the groyne being present. The number of drogues that accumulated in the inlet were adopted as a benchmark in assessing the performance of the different groyne configurations.

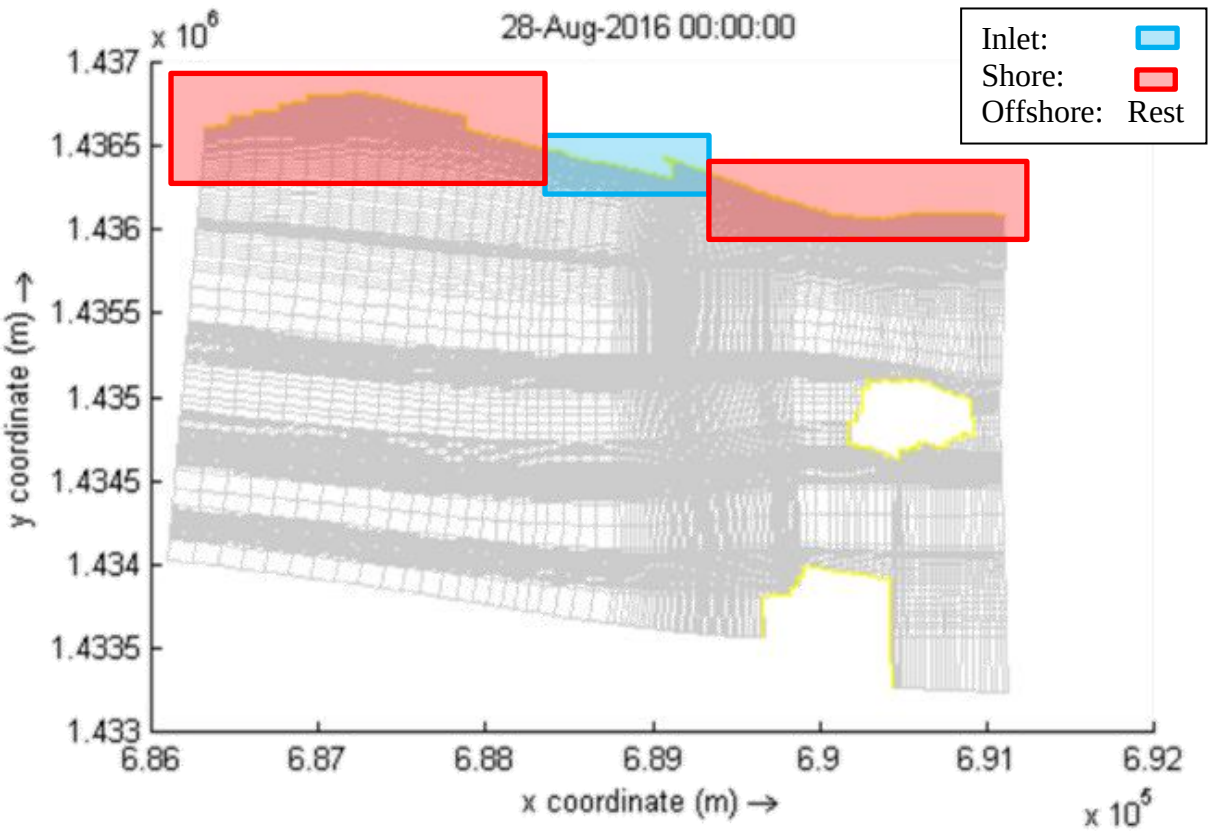

Figure 5.3: Benchmark Areas: Inlet, Coastline and Offshore

The grid was split into three different areas in order to describe the drogues' final positions: Inlet, Shore, Offshore (as shown in Figure 5.3). These three areas were designed to test the ability to prevent litter accumulation in the inlet of the proposed groyne configurations. The area of the 'inlet' was extended past the physical inlet to account for the fact that the drogues weren't accumulating at the end of the inlet (see Figure 5.2 (2a)). The 'inlet' area is defined from the location of the start of the groyne to the middle of the airport landing strip. The drogues' final position in the three scenarios is compiled in Figures 5.4 to 5.6 and in Table 5.2.

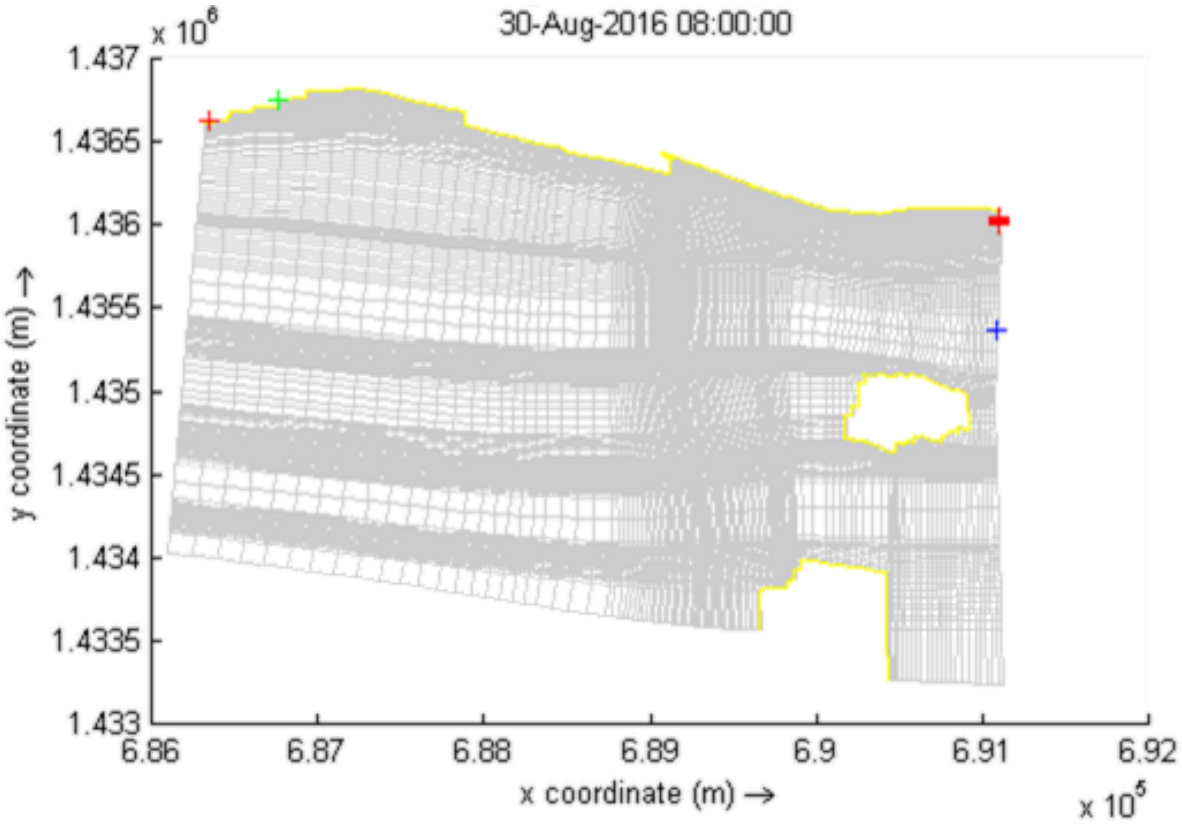

Figure 5.4: Drogues' Final Location Benchmark in Typical Condition

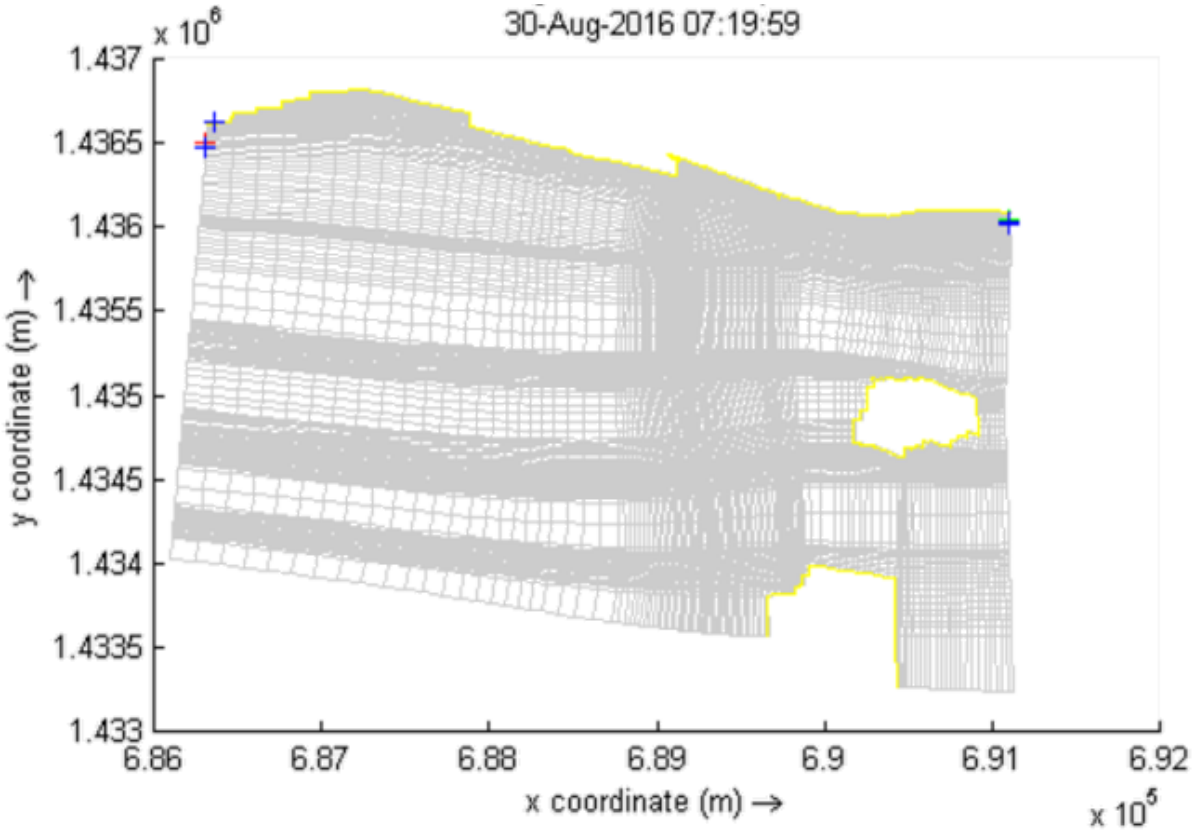

Figure 5.5: Drogues' Final Location Benchmark in High Wave, High Wind Condition

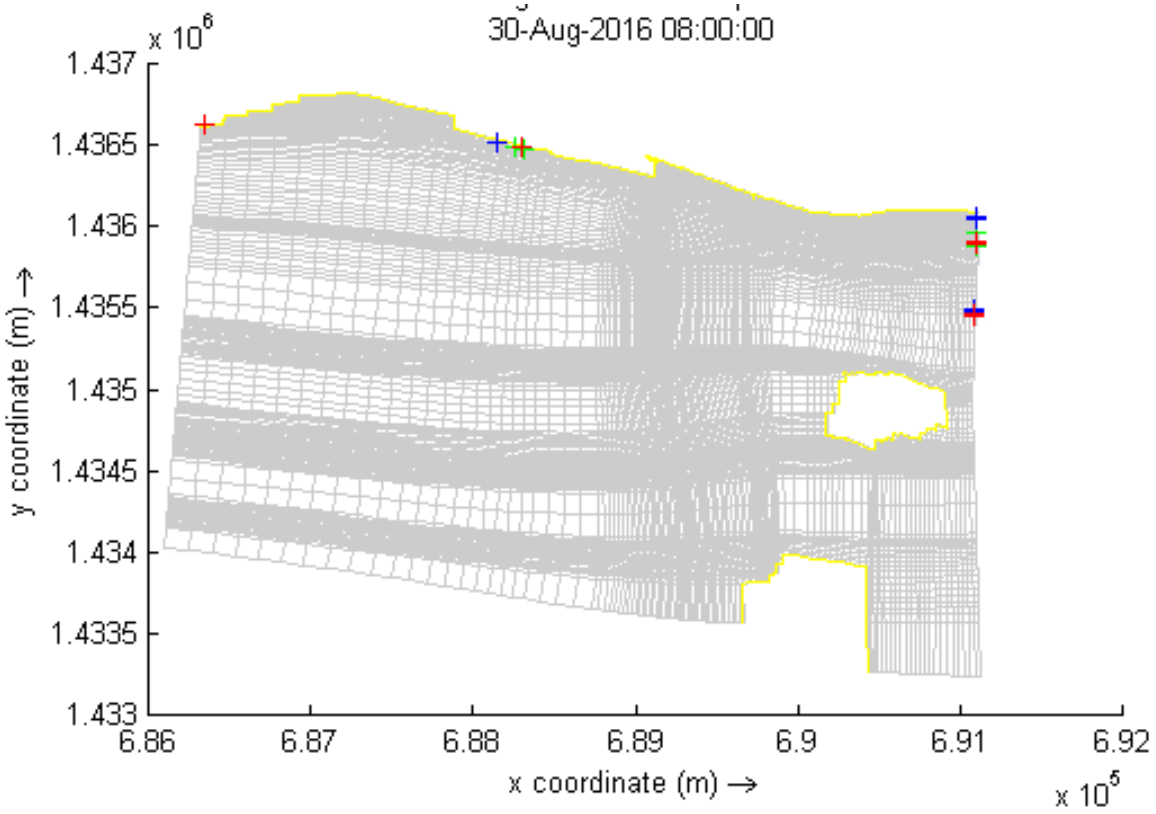

Figure 5.6: Drogues' Final Location Benchmark in Low Wave, Regular Wind Condition

Conditions	Drogues final position	Red	Blue	Green	Total
Typical	Inlet	0	0	0	**0**
	Shore	10	9	10	29
	Offshore	0	1	0	1
High Wind, High Wave	Inlet	0	0	0	**0**
	Shore	10	10	10	30
	Offshore	0	0	0	0
Low Wave, Regular Wind	Inlet	3	2	5	**10**
	Shore	5	5	5	15
	Offshore	2	3	0	5

Table 5.2: Drogues' Final Location Benchmarks Summary

In the 'typical condition' and 'high wave, high wind' scenarios no drogues accumulated in the 'inlet' area meaning that, under those conditions, debris accumulation does not occur. So, any debris accumulation in the inlet during the testing of the groynes indicates that the groyne enhances the accumulation of debris. In the 'low wave, regular wind' scenario, debris accumulation was observed in the 'inlet' area. A total of 10 drogues from the three starting

locations accumulated on the side of the airport. The debris accumulation patterns do not exactly recreate the conditions observed in the field, which is that litter from the nearshore area is accumulating in the inlet. However, it was closer represented at lower wave intensity. This fact confirms that the waves are preventing the debris from accumulating in the inlet.

It is also observed that the lesser the wave energy, the more debris leave the shore area. In the 'high wave, high wind' scenario, no drogues were found offshore. In the 'typical condition' scenario, one drogue left the shore area. In the 'low wave, regular wind', 5 drogues were found in the 'offshore' area. This may be caused by the fact that the tide-induced current would take more importance in the surface currents. The waves' intensity was reduced from a scenario to the other and the tide's properties were kept the same. Therefore, the tide became a bigger factor in the 'low wave, regular wind' scenario. Also, during the ebb tide, the tide-induced current is going toward the East while the wind and waves are going westward. This means that it is the only force input that is pushing the drogues toward the west.

6 Proposed Groyne Configurations

The proposed solution to reduce the litter accumulation is to build a rubble mound groyne in front of the inlet to redirect the floating debris away from it. In an attempt to optimise the groyne arrangement, six different potential configurations of the structure were tested in the modeling exercises. These included: two different angle settings, between the groyne and the shoreline (one was perpendicular to the shoreline and one was set at 50 degrees to the latter and angled towards the inlet), and three different groyne lengths ('long', 'medium' and 'short') for each 'angle' arrangement tested.

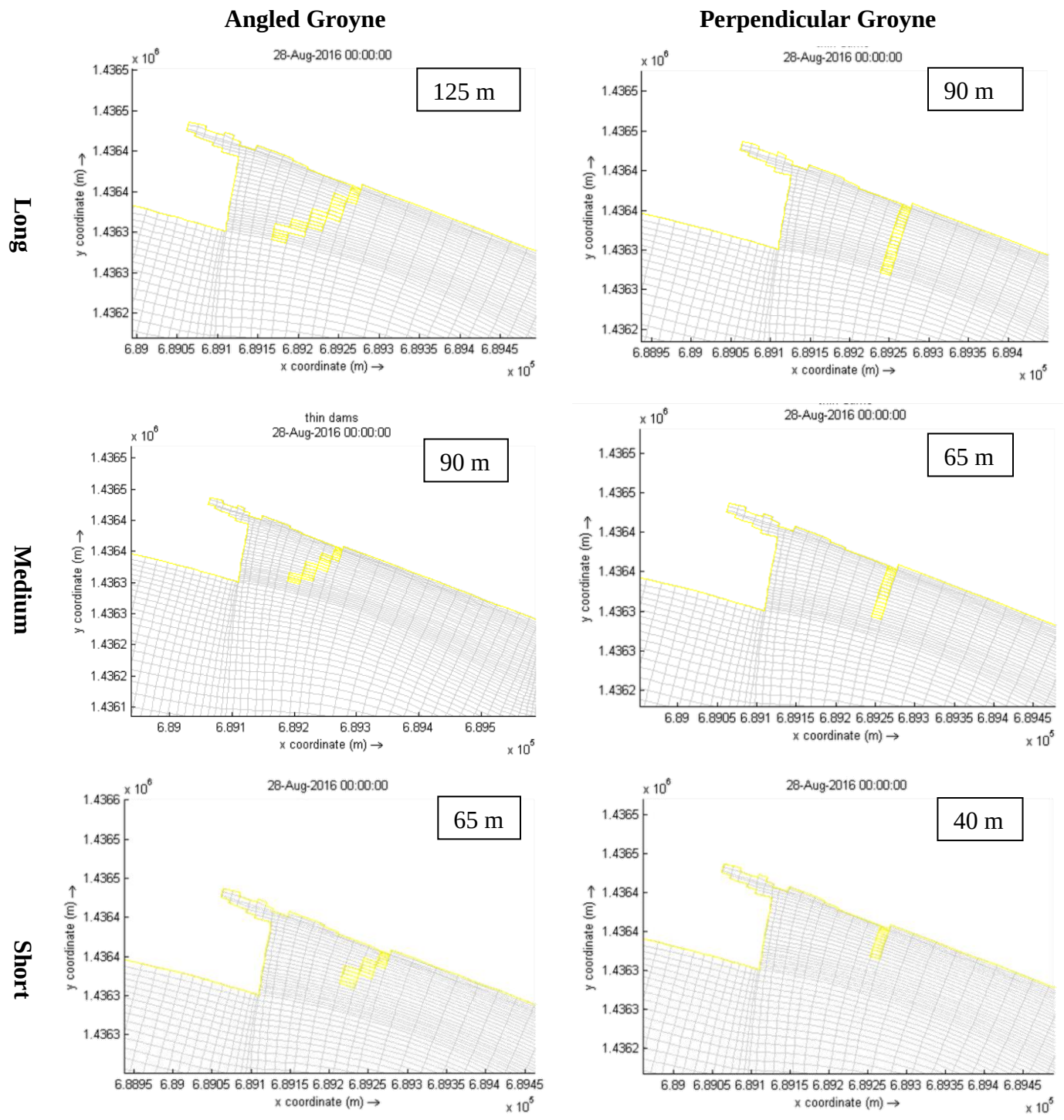

Figure 6.1: Tested Groyne Configurations, including Overall Length

The groyne lengths were selected, such that the distance between the tip of the structure and the coastline was the same for every pair of ('long', 'medium' and 'short') groynes tested, see Figure 6.1. The location of the groyne, relative to the inlet entrance, was the same for all of the testing

scenarios, as this particular site was virtually the only one where the construction of such a structure could be achieved (see section 3.1.2 Paget Farm Coastline Features).

As was discussed in the ‘literature review’ chapter, in the Delft3D model the grid cells occupied by the groynes are defined as ‘dry points’ in FLOW and ‘obstacles’ in WAVES. The cells occupied by the groynes are catalogued in Appendix D.

7 Results for the Groynes Configurations

Six different groyne configurations were tested in order to optimize the ability of the groyne to mitigate debris accumulation. Three different scenarios were employed to verify the performance of the configurations under different conditions: (i) typical condition, (ii) high wind, high wave, (iii) low wave, regular wind. A total of 30 drogues were released in the same tide cycle and their movements were tracked for 25 hours. Their final position was recorded and used as a point of comparison to recommend a final design. Figures 7.1 to 7.18 are showing the results from the different groyne configurations under the different scenarios and Table 7.1 summarizes all the results.

7.1 Results for Short Perpendicular Groyne

The first configuration modeled was a 40m long groyne perpendicular to shore. Figure 7.1 illustrates the position of the drogues at the end of the simulation under the 'typical condition' scenario.

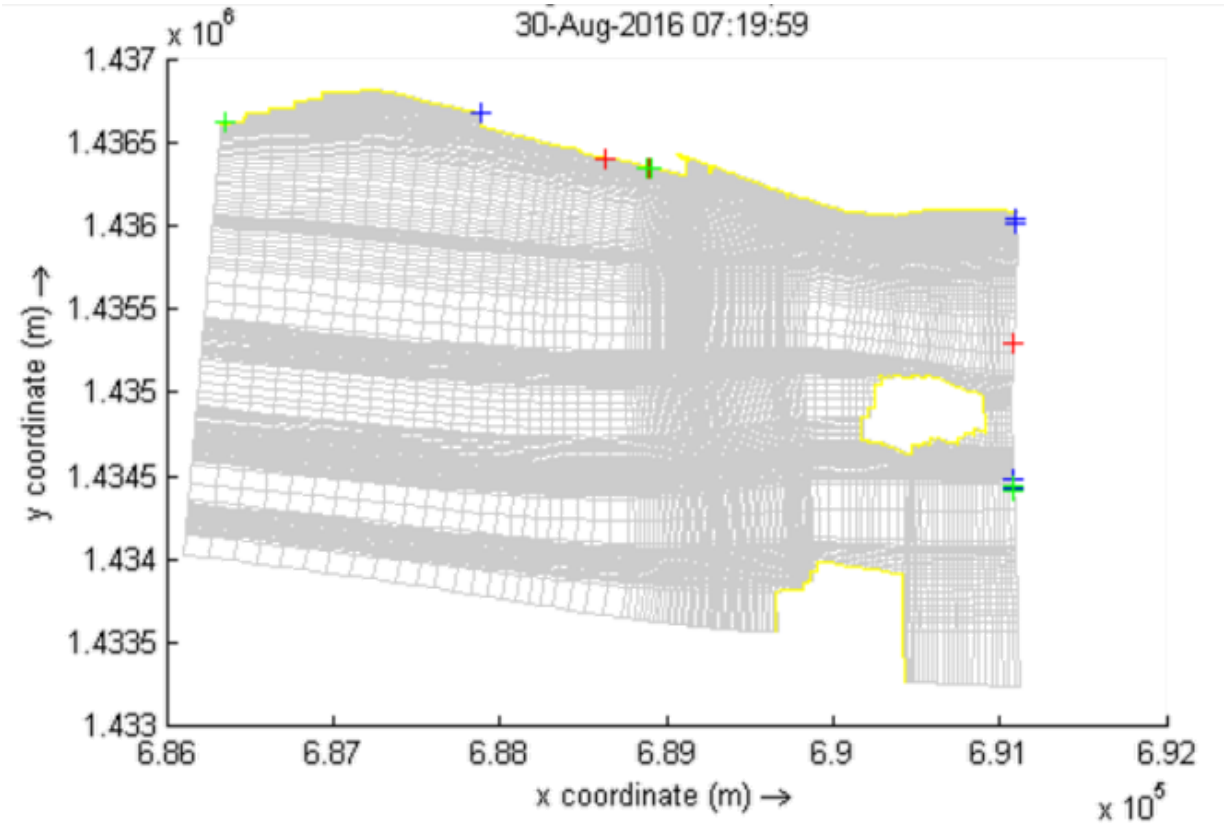

Figure 7.1: Drogues' Final Location for Short Perpendicular Groyne in Typical Condition Scenario

In this scenario, a total of 6 drogues finished their course in the area defined as ‘inlet’. It was also noted that 5 drogues were found to go offshore and 19 along the shore.

The same groyne configuration was then simulated under the ‘high wind, high wave’ scenario. The results are found in Figure 7.2.

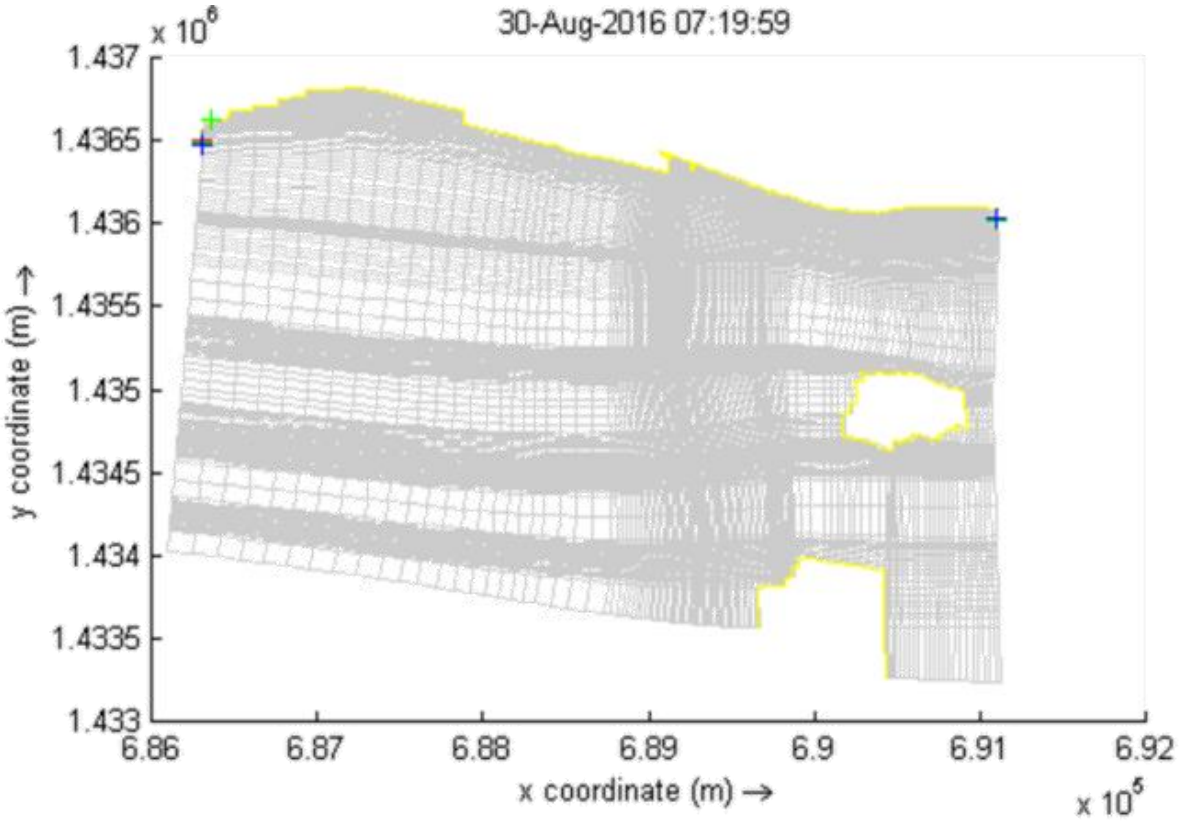

Figure 7.2: Drogues' Final Location for Short Perpendicular Groyne in High Wind, High Wave Scenario

In this simulation, the groyne has prevented any drogues from staying in the inlet area. This means that the groyne is not disturbing the existing condition's mechanism that prevented the drogues from collecting in the inlet. This may mean that the groyne may not be able to protect the boats in the area from incoming wave, a secondary objective that was defined.

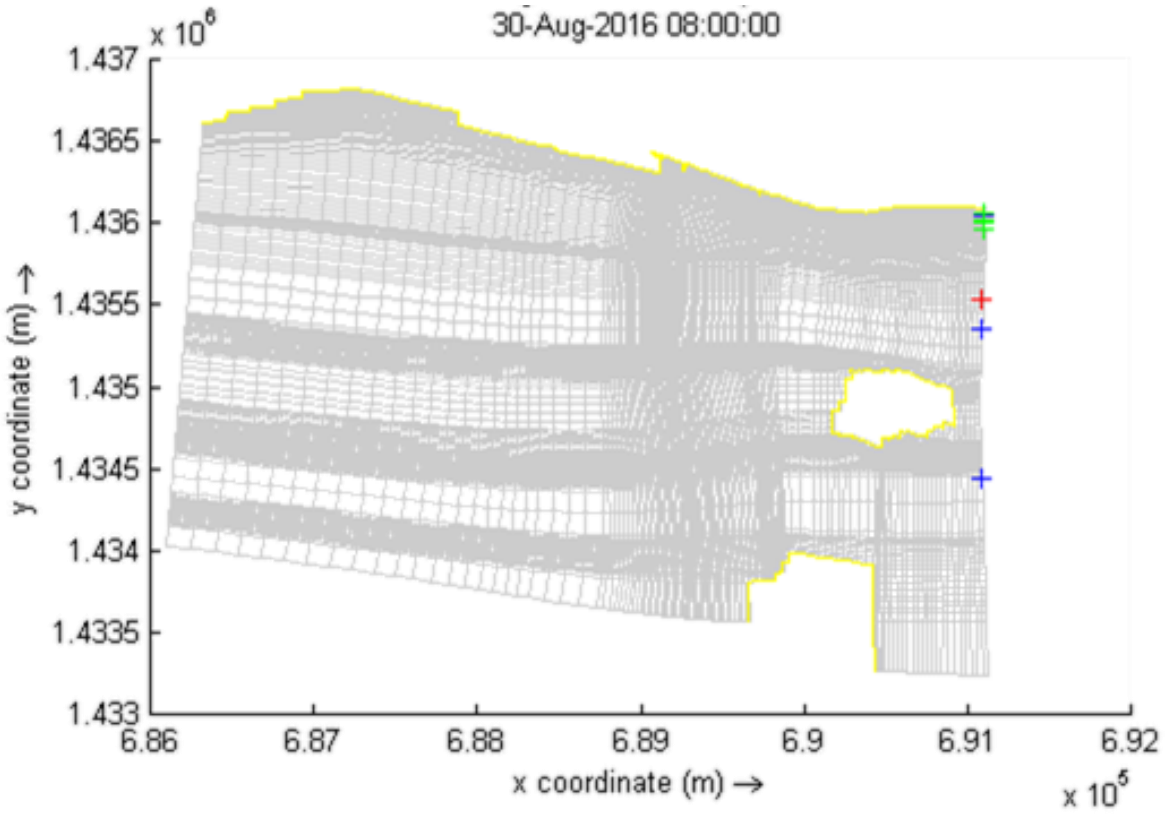

Figure 7.3: Drogues' Final Location for Short Perpendicular Groyne in Low Wave, Regular Wind Scenario

For the third scenario, the groyne has prevented any accumulation in the 'inlet' area (Figure 7.3). Three drogues were found in the offshore area and 27 in the shore area.

Overall, this groyne configuration has limited the accumulation of drogues to a total of 6 when adding the three scenarios. Also, eight drogues left the shore area reducing the amount of possible litter along the shore.

7.2 Results for Medium Perpendicular Groyne

The second configuration that was modeled is the 65m long perpendicular groyne. The first scenario that was tested is the 'typical condition' scenario. Figure 7.4 illustrates the end position of the drogues' track.

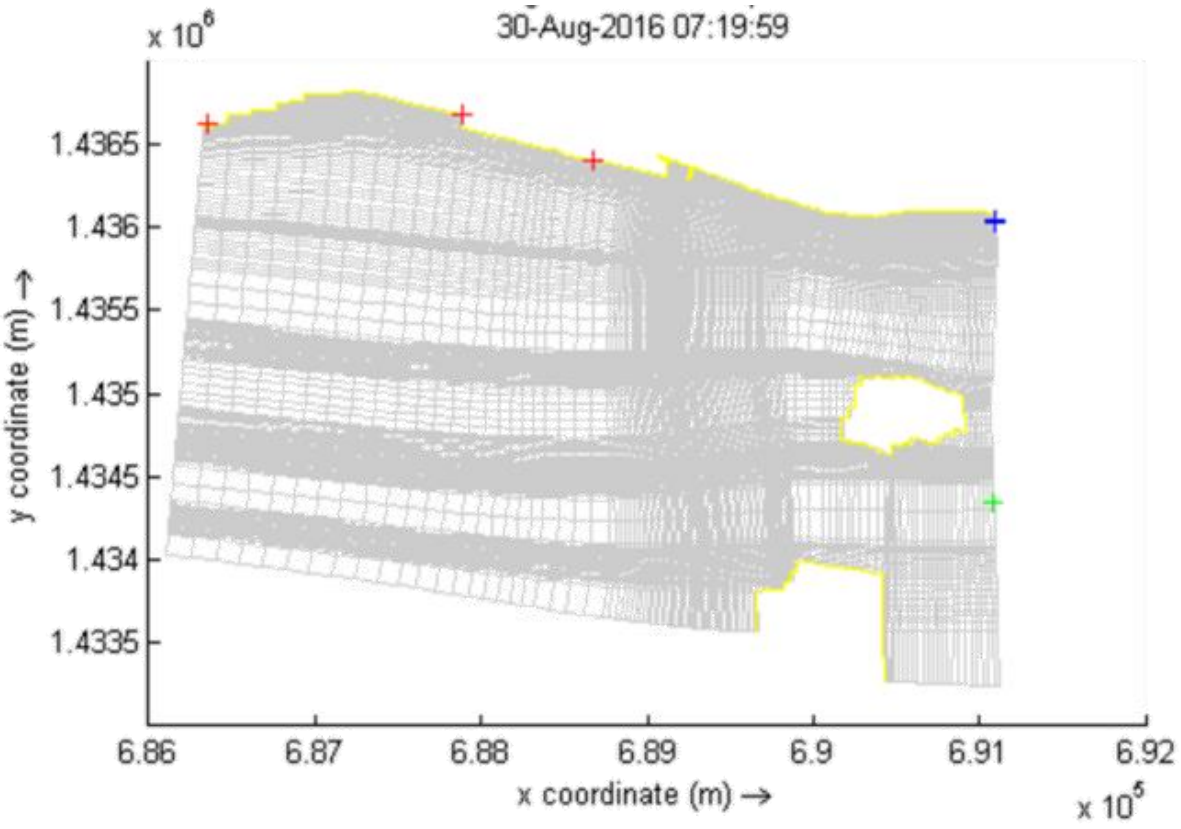

Figure 7.4: Drogues' Final Location for Medium Perpendicular Groyne in Typical Condition Scenario

A total of 13 drogues ended up in the ‘inlet’ area. They were found to be all stacked at the same location, around the middle of the airport. Also, only one drogue has left offshore and the other 16 were found along the shore.

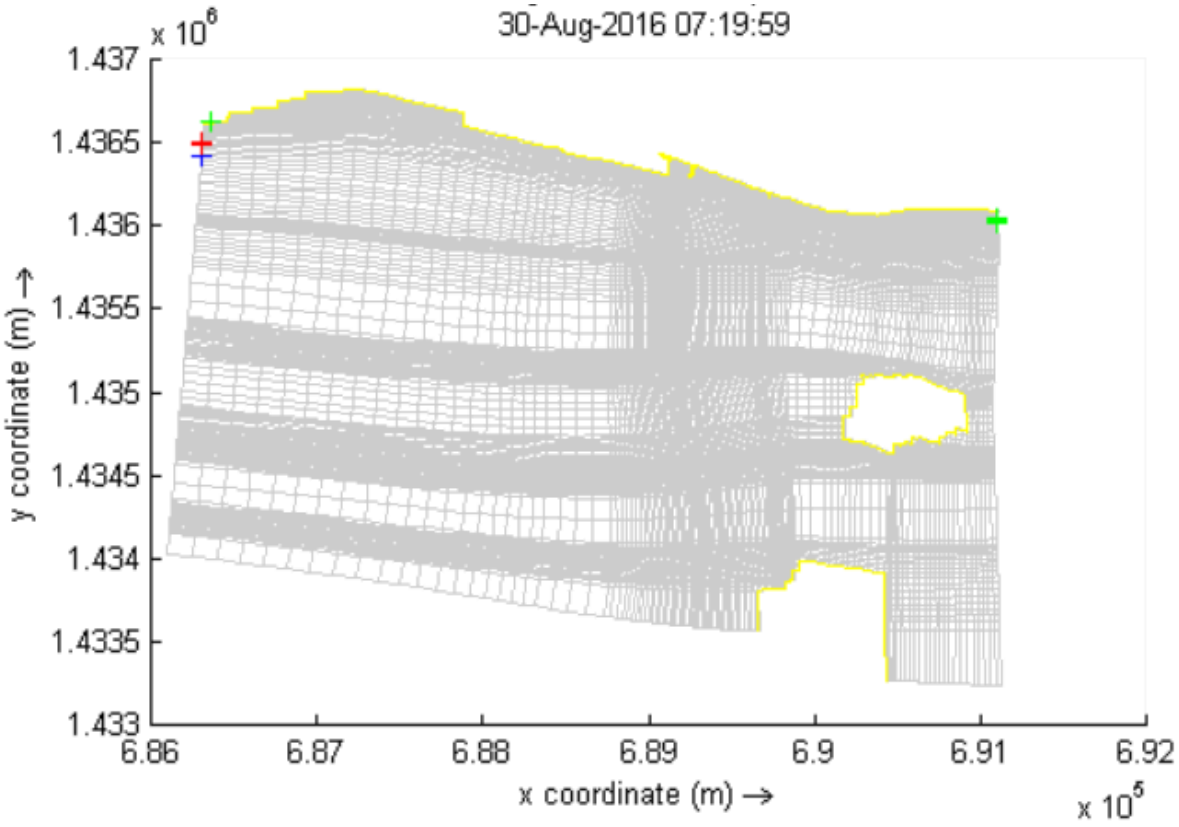

Figure 7.5: Drogues' Final Location for Medium Perpendicular Groyne in High Wind, High Wave Scenario

Shown in figure 7.5 is the final position of the drogues in the 'high wind, high wave' scenario. Just like the existing conditions, no drogues accumulated in the inlet and all were found elsewhere along the shore. Therefore, the groyne might prevent the debris from entering the inlet or is not big enough of a barrier to disturb the water movement in the existing condition that was preventing the accumulation of debris in the existing condition.

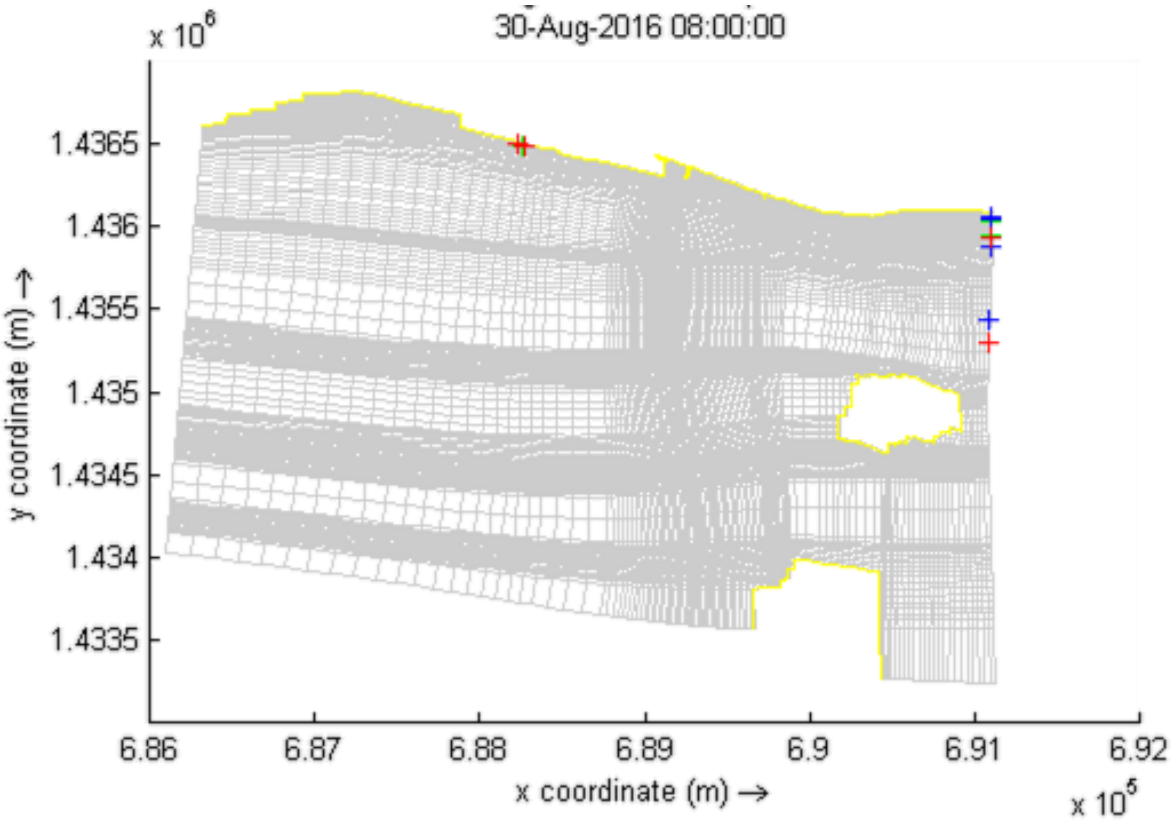

Figure 7.6: Drogues' Final Location for Medium Perpendicular Groyne in Low Wave, Regular Wind Scenario

Shown in Figure 7.6, is the performance of the medium perpendicular groyne under the 'low wave, regular wind' scenario. A large amount of drogues were found along the airport. These drogues were included in the 'inlet' area. 15 drogues were found at that location originating from the three starting locations. Four drogues were found in the 'offshore' area.

This groyne had a great negative effect on the debris accumulation. A total of 28 drogues were found in the 'inlet' area and 5 off shore. Also, the drogues that accumulated in the inlet were coming from the three starting locations. Therefore, it is not simply caused by a lack of circulation on the leeward side of the groyne that would prevent drogues from leaving the area behind the groyne. The groyne is not able to prevent debris from the coast to accumulate in the 'inlet' area.

7.3 Results for Long Perpendicular Groyne

The next configuration that was modeled is the 90m perpendicular groyne. Figure 7.7 shows the final location of the drogues in the 'typical condition' scenario.

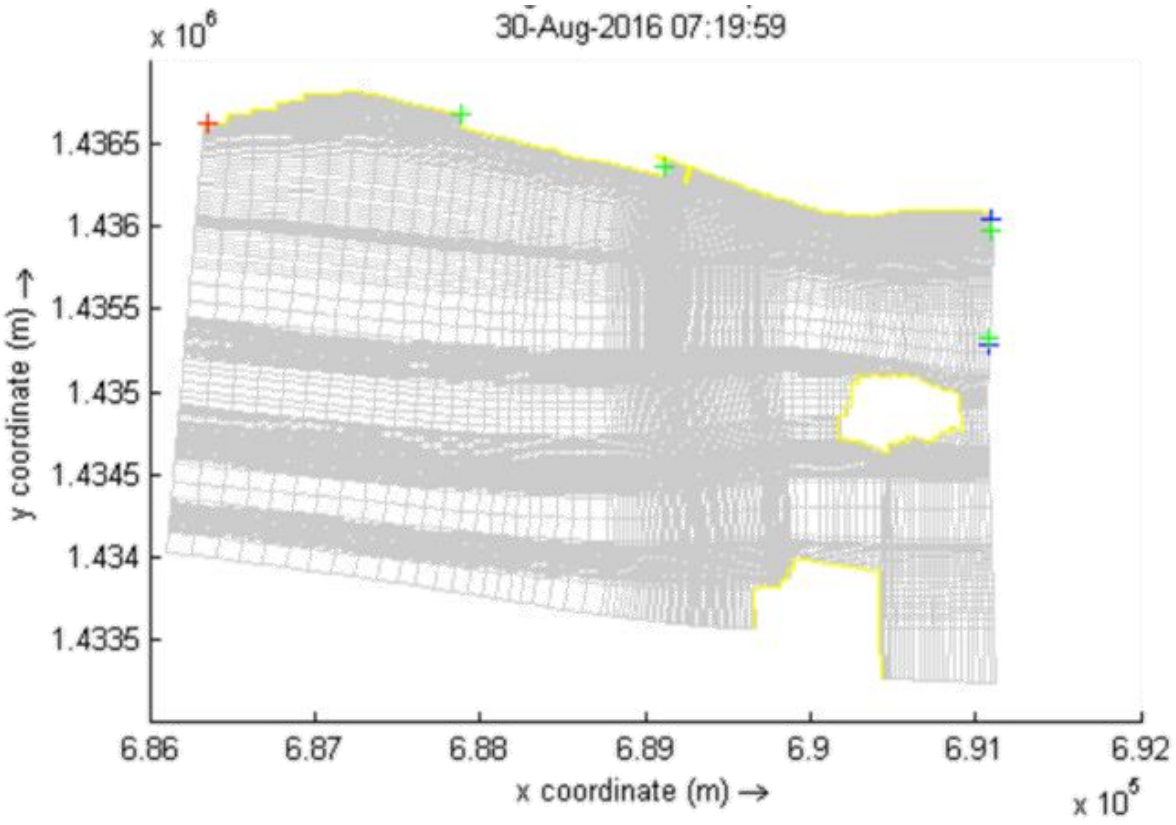

Figure 7.7: Drogues' Final Location for Long Perpendicular Groyne in Typical Condition Scenario

In this simulation, 7 drogues were found in the approximate same location in the inlet, 21 along the coast and 2 offshore. It was noted that 6 of the 7 drogues that were found in the inlet had a starting location outside of the inlet. Therefore, they were entrained behind the groyne and all got stuck at the same location.

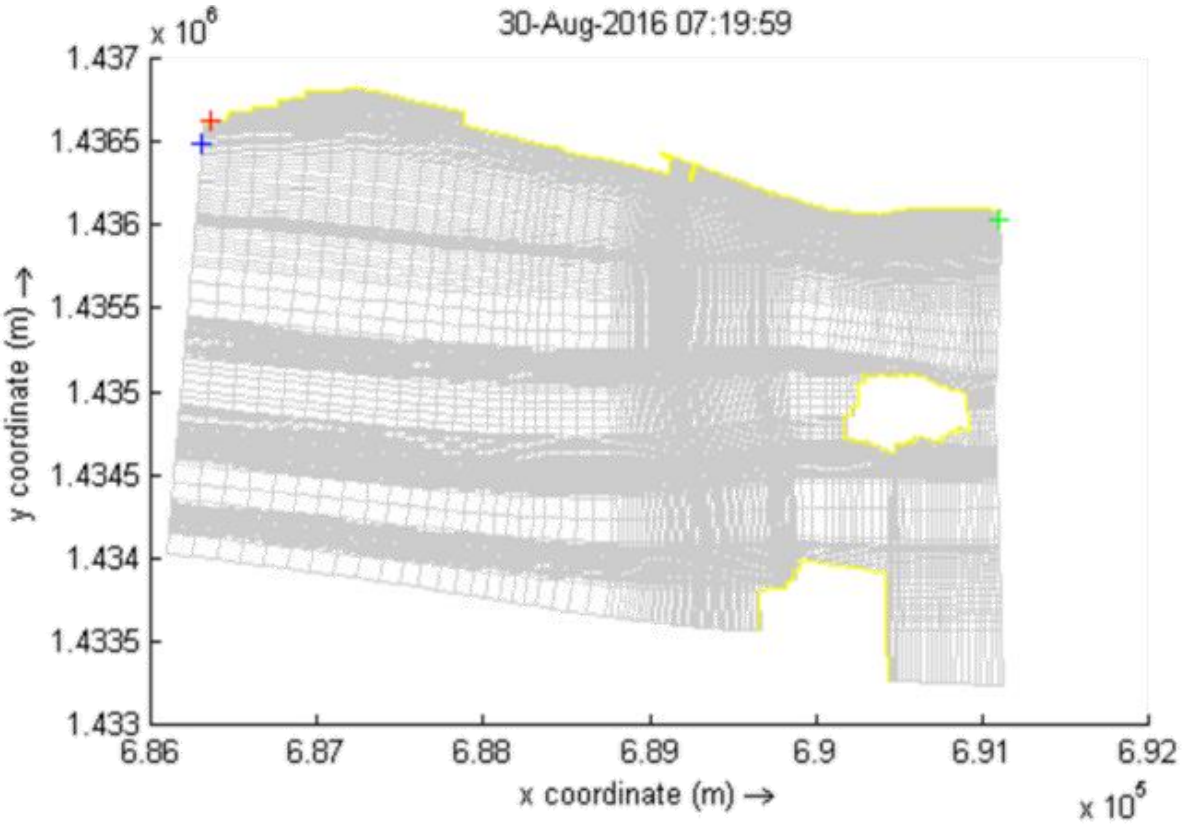

Figure 7.8: Drogues' Final Location for Long Perpendicular Groyne in High Wind, High Wave Scenario

Shown in figure 7.8 is the results from the 'high wind, high wave' scenario. Once again, no accumulation was generated in this scenario. Like the other perpendicular groynes, the existing condition of non-accumulation was not changed by the addition of the groyne.

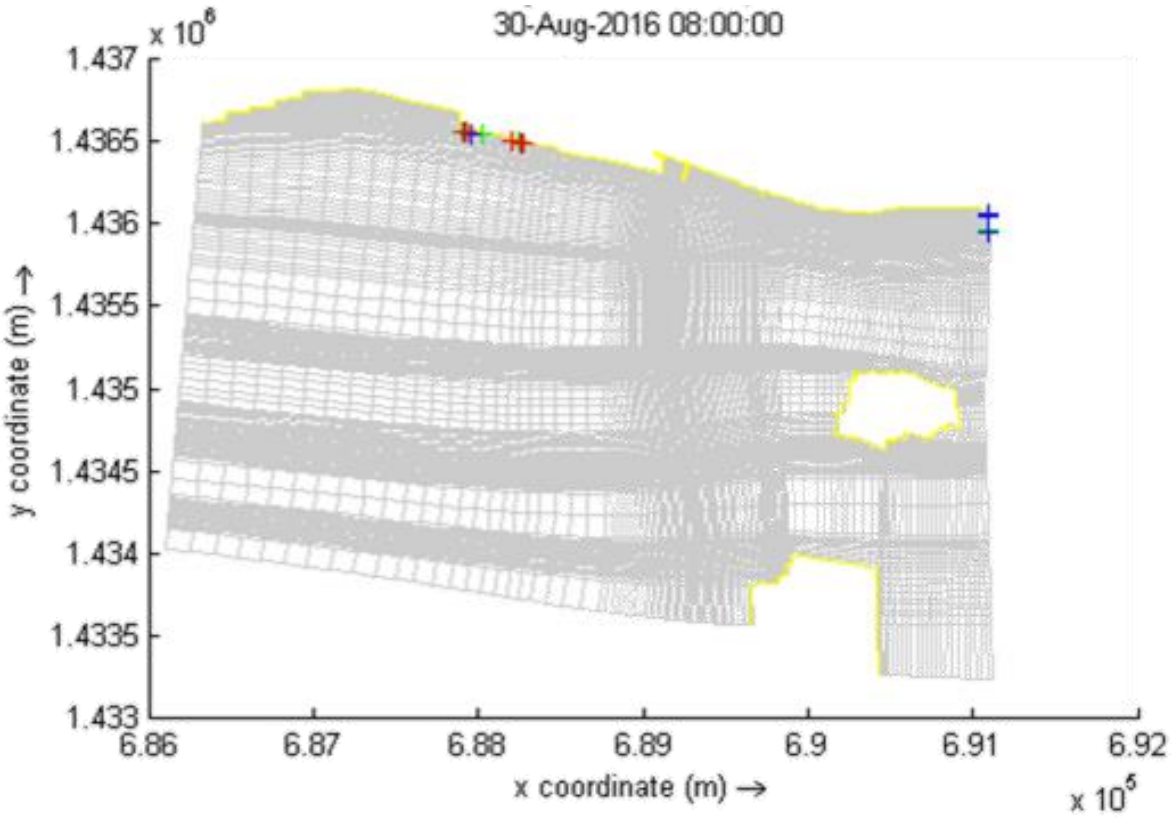

Figure 7.9: Drogues' Final Location for Long Perpendicular Groyne in Low Wave, Regular Wind Scenario

Figure 7.9 shows the final location of the drogues at the end of the 'low wave, regular wind' scenario. 8 drogues were found in the 'inlet' area. 10 more drogues were found just west of the 'inlet' area, but were not included. No drogues were found in the 'offshore' area.

7.4 Results for Short Angled Groyne

The next set of results presented is for the 65m angled groyne. Figure 7.10 shows the final position of the drogues at the end of the simulation.

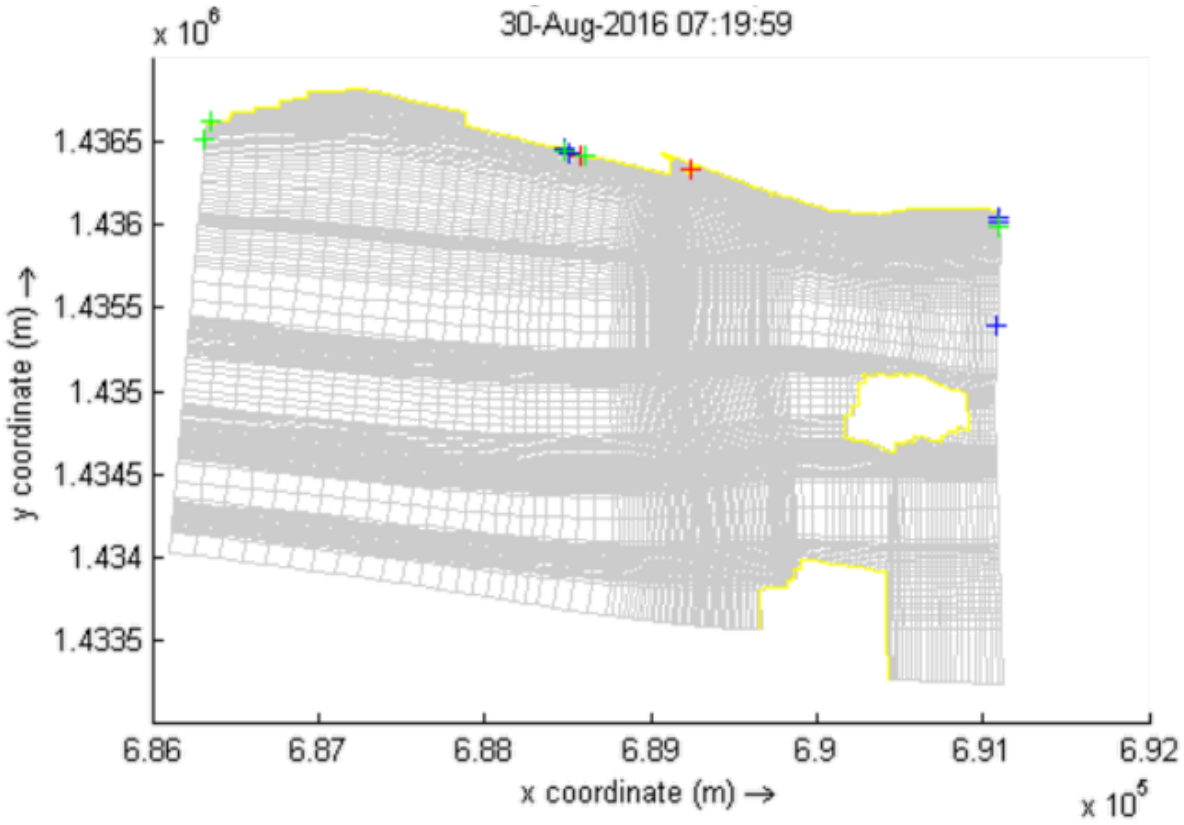

Figure 7.10:Drogues' Final Location for Short Angled Groyne in Typical Condition Scenario

In this scenario, 9 drogues were found in the 'inlet' area, one offshore and 20 along the shore. The drogues were found at the same gathering point observed in previous scenarios. Also, two red drogues were stuck on the leeward side of the groyne. The drogues were found at the corner of a grid cell. It is possible that the fact that the groyne is simulated in blocks, not as a smooth straight line, has created an area where the drogues get caught during the simulation. This can create an overestimation of the number of drogues that are accumulating in the inlet area. This point will be considered when comparing the different configurations.

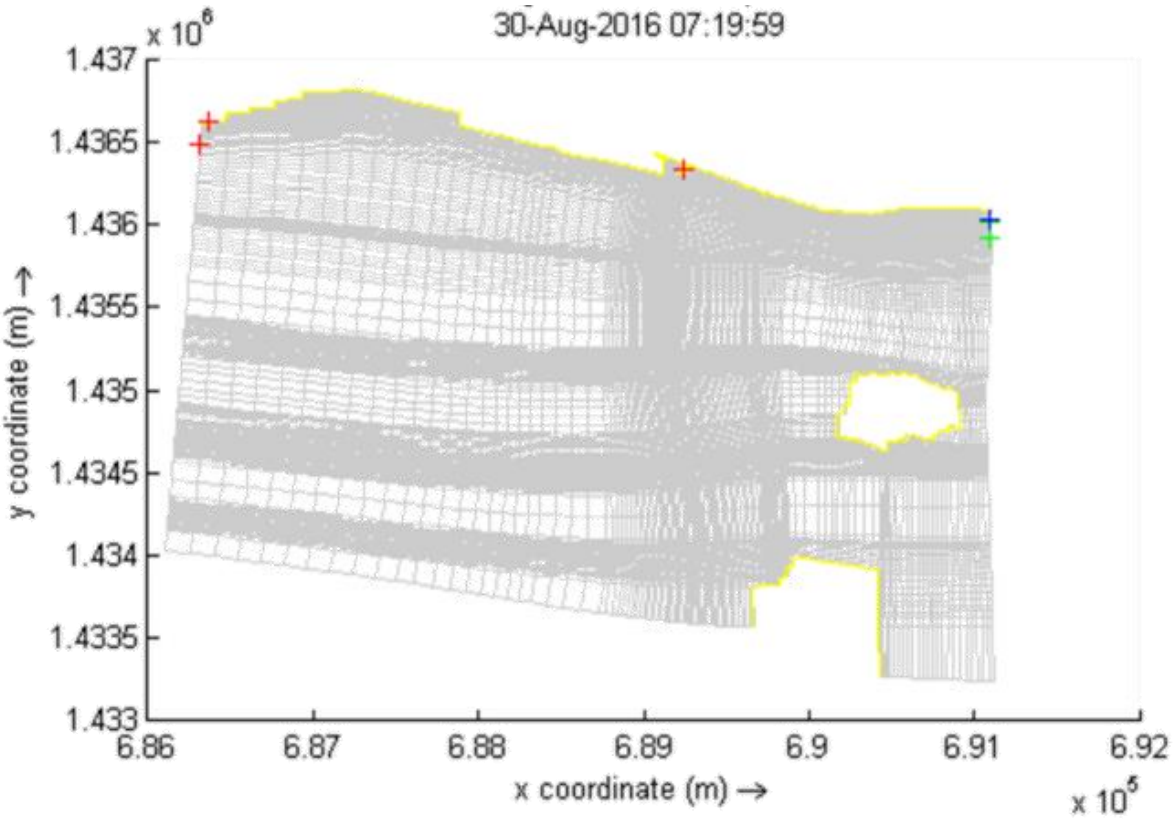

Figure 7.11: Drogues' Final Location for Short Angled Groyne in High Wind, High Wave Scenario

Figure 7.11 shows the results from the 'high wind, high wave' scenario. Three drogues were found in the 'inlet' area. This means that the addition of the groyne has generated some debris accumulation. However, these drogues all collected at the location described earlier. So, there might be a problem with the smoothness of the groyne. Not having a groyne shaped in steps would have let the drogues glide along the structure. Therefore, no accumulation would have occurred on the leeward side of the groyne.

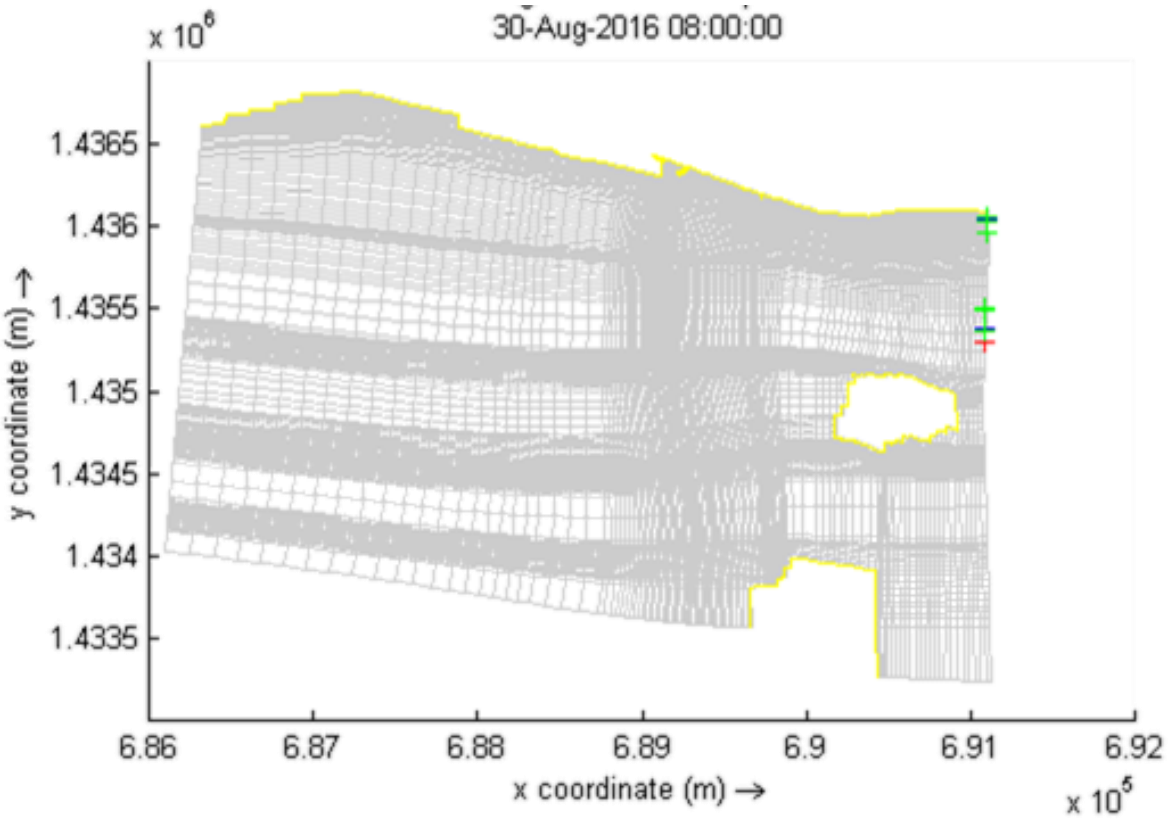

Figure 7.12: Drogues' Final Location for Short Angled Groyne in Low Wave, Regular Wind Scenario

In the ‘low wave, regular wind’ scenario (Figure 7.11), the groyne has prevented any drogues from accumulating in the inlet. Also, 10 drogues finished their course in the ‘offshore’ area.

In total, 12 drogues accumulated in the ‘inlet’ area. During the analysis of the results, it was noted that this number might be overestimating the debris accumulation because of the way the groyne was modeled. Further investigation into this issue is presented in the Discussion section.

7.5 Results for Medium Angled Groyne

The next set of results presented is for the 90m angled groyne. Figure 7.13 shows the final position of the drogues at the end of the simulation.

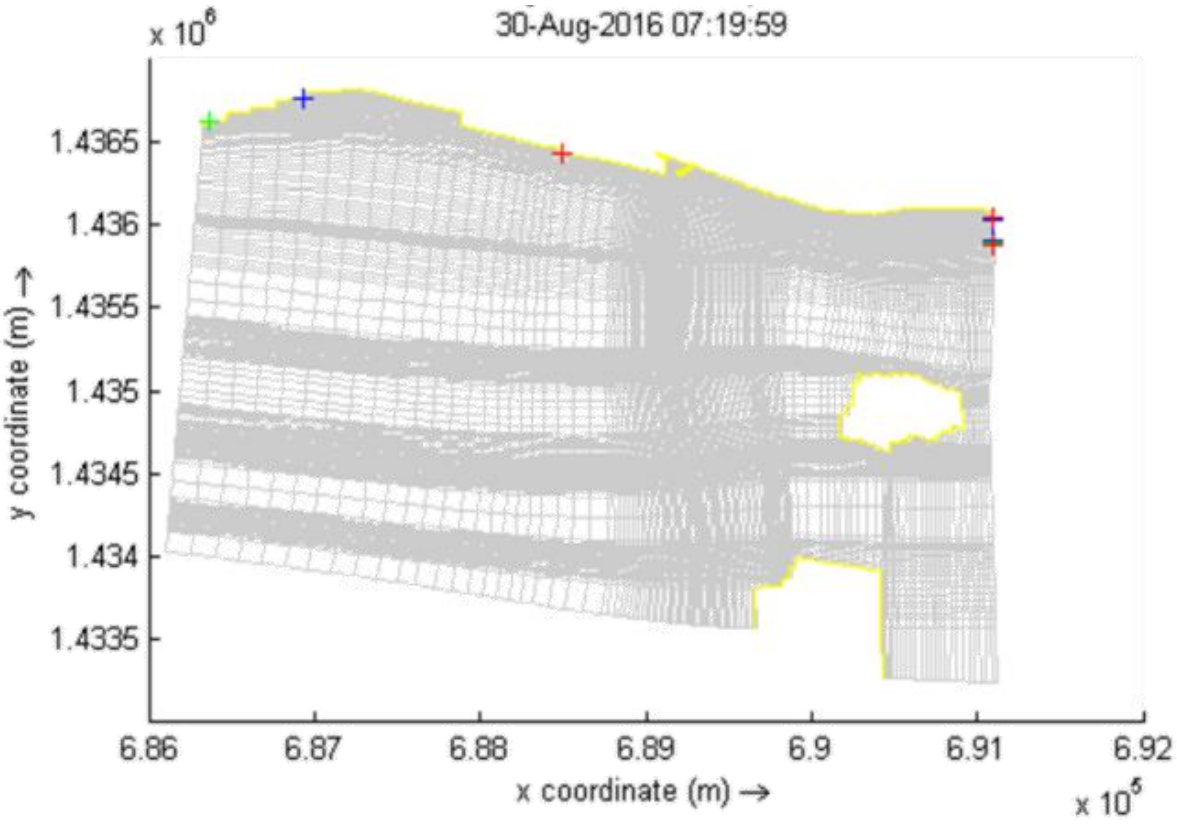

Figure 7.13: Drogues' Final Location for Medium Angled Groyne in Typical Condition Scenario

In this simulation, four drogues were found in the middle of the airport, in the 'inlet' area, and the rest along the shore (Figure 7.13). No drogues were found behind the groyne. Therefore, the drogues did not get stuck on the groyne, like observed in the short angled groyne configuration.

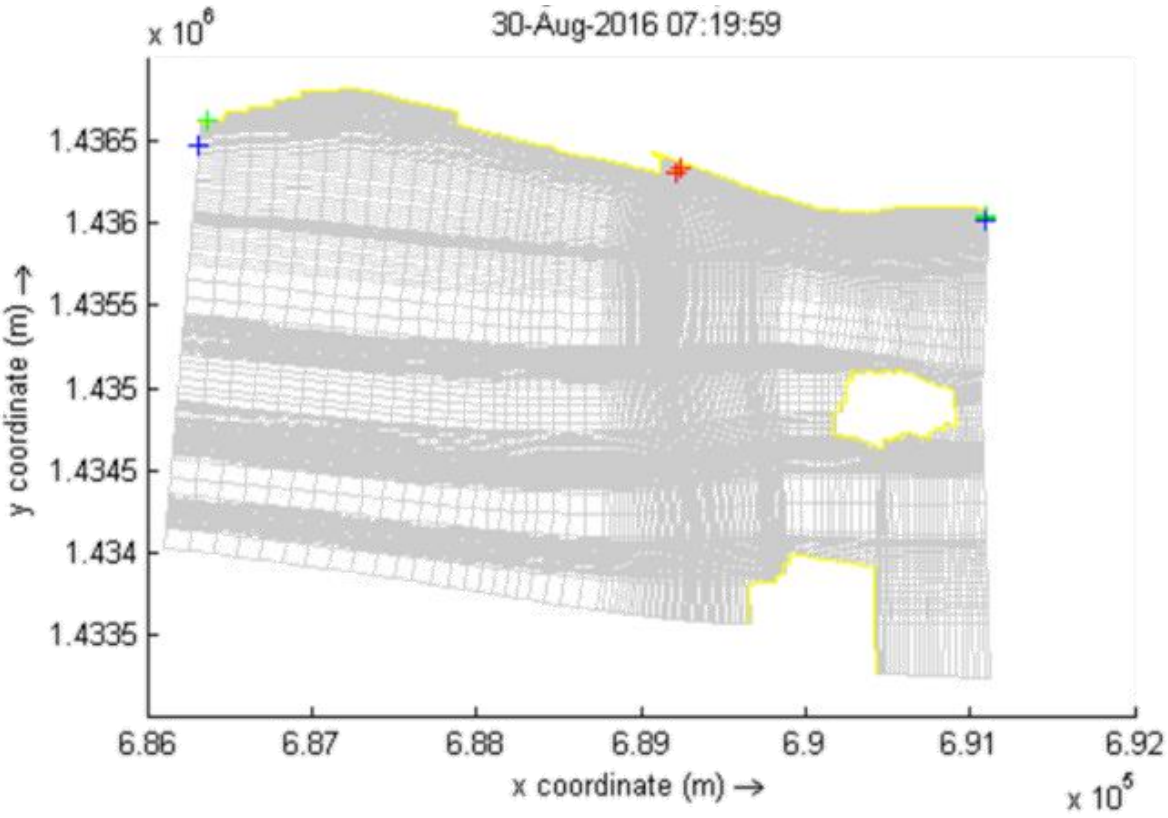

Figure 7.14: Drogues' Final Location for Medium Angled Groyne in High Wind, High Wave Scenario

In figure 7.14 is the results from the 'high wind, high wave' scenario. Four drogues were found behind the groyne in the corner of the cells. A typical pattern of groyne accumulation observed in the other angled groyne simulations. The rest of the drogues were along the shore.

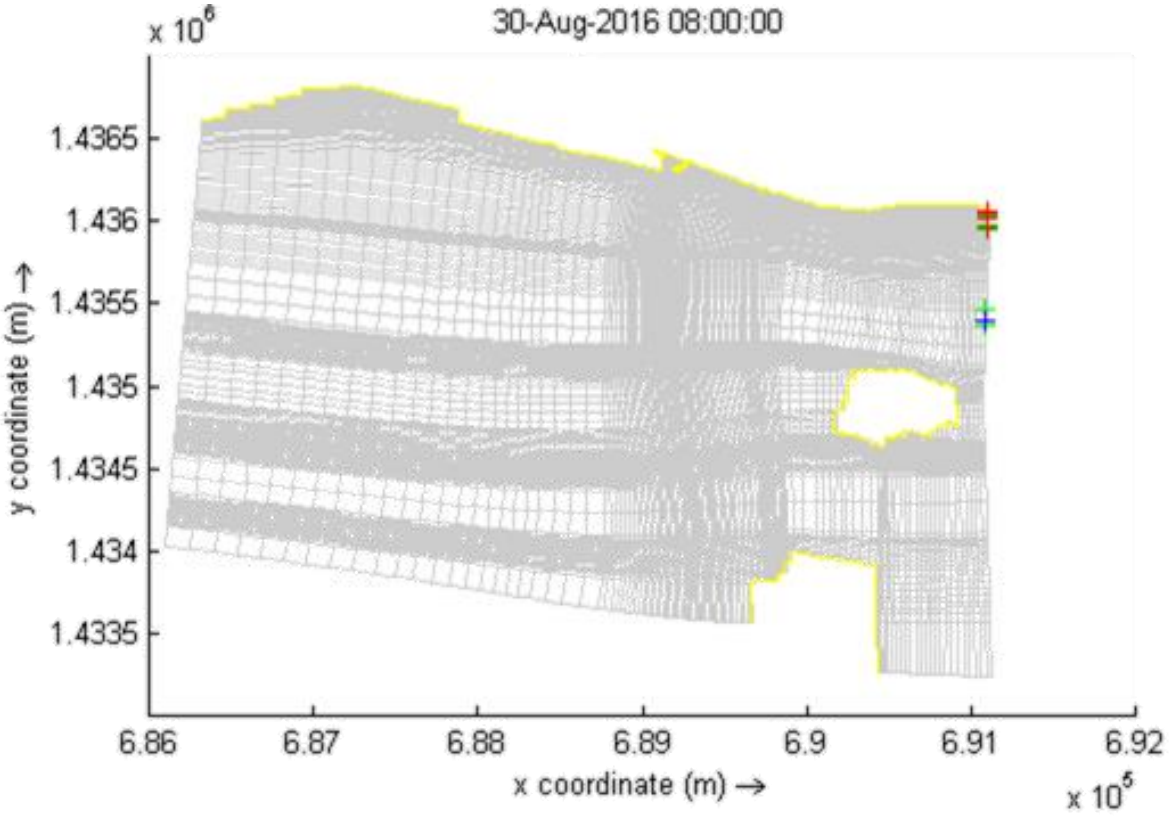

Figure 7.15: Drogues' Final Location for Medium Angled Groyne in Low Wave, Regular Wind Scenario

Shown in Figure 7.15 is the performance of the medium angled groyne under the 'low wave, regular wind' scenario. The groyne has prevented any drogues from accumulating in the inlet area. In addition to that, three drogues were found in the 'offshore' section and the other 27 in the 'shore' section.

Overall, 7 drogues were found in the 'inlet' area. Three of those drogues were stuck in the groyne, which might have happened because of the way the groyne was modeled. Also, 7 drogues moved away from the 'shore' area.

7.6 Results for Long Angled Groyne

The last configuration simulated is a 125m angled groyne. Figure 7.16 shows the final position of the drogues at the end of the simulation.

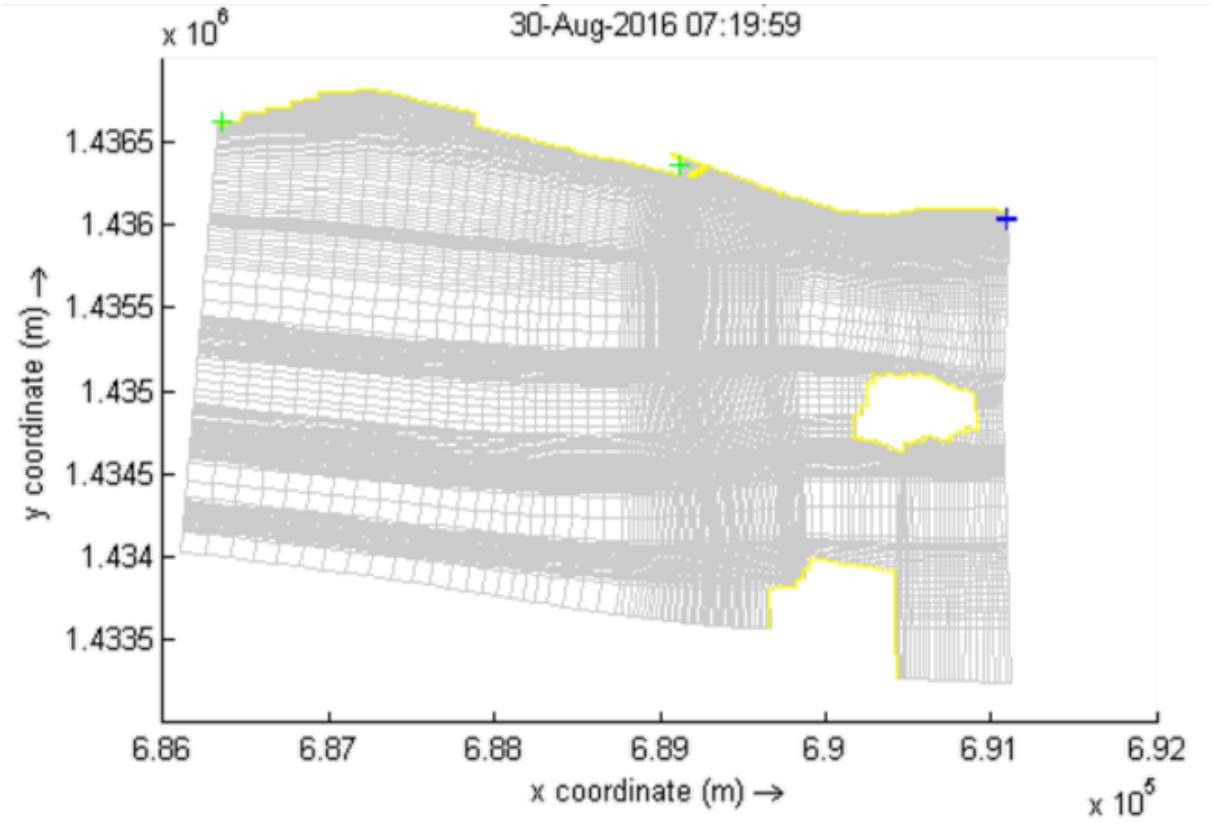

Figure 7.16: Drogues' Final Location for Long Angled Groyne in Typical Condition Scenario

In the simulation, 10 drogues were found at the exact same location behind the groyne, in the airport's armoring. This might be a sign that the groyne is too long for water to move in the inlet area and flush out the debris. The rest of the drogues finished in the 'shore' area.

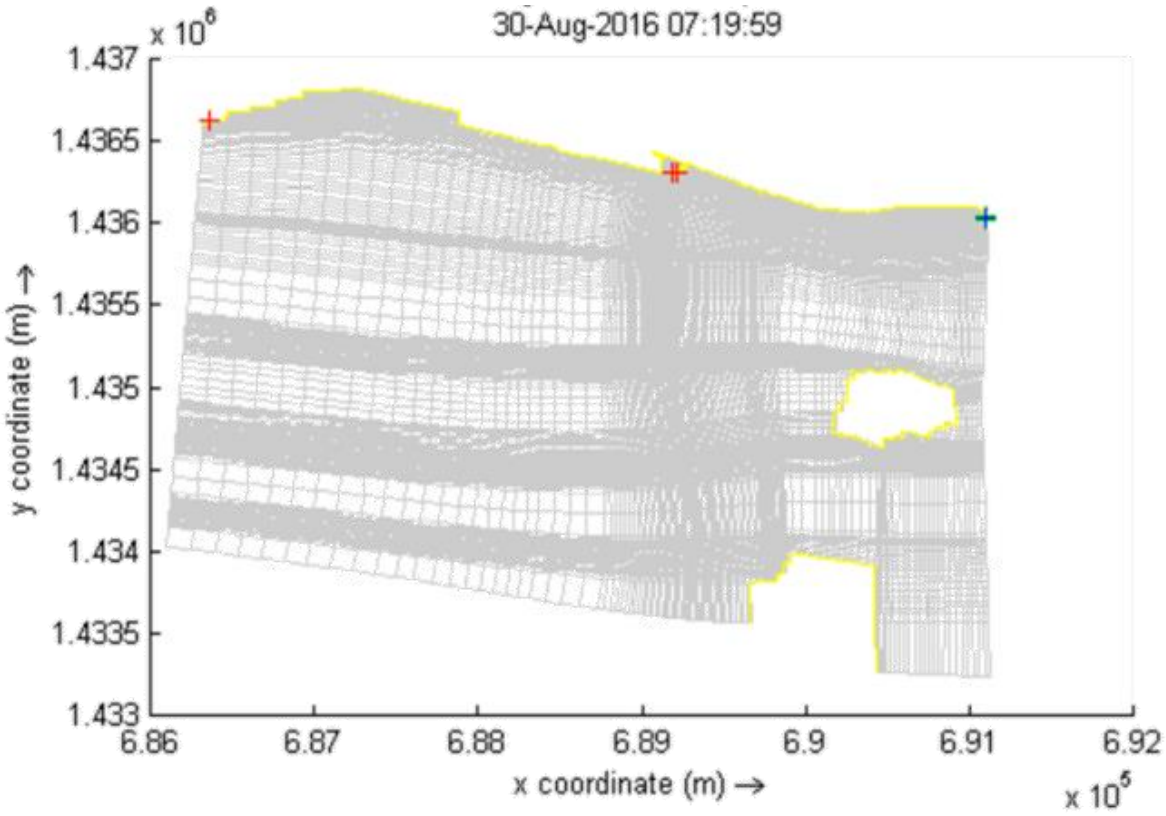

Figure 7.17: Drogues' Final Location for Long Angled Groyne in High Wind, High Wave Scenario

Figure 7.17 shows the results for the 'high wind, high wave' scenario. Three red drogues were found on the leeward side of the groyne in the corner of some grid cells. This may be caused by the way the groyne is simulated or the lack of circulation behind the groyne. Since the drogues had a starting positon behind the groyne, the groyne still has the capacity of preventing debris from the coast to enter the inlet area.

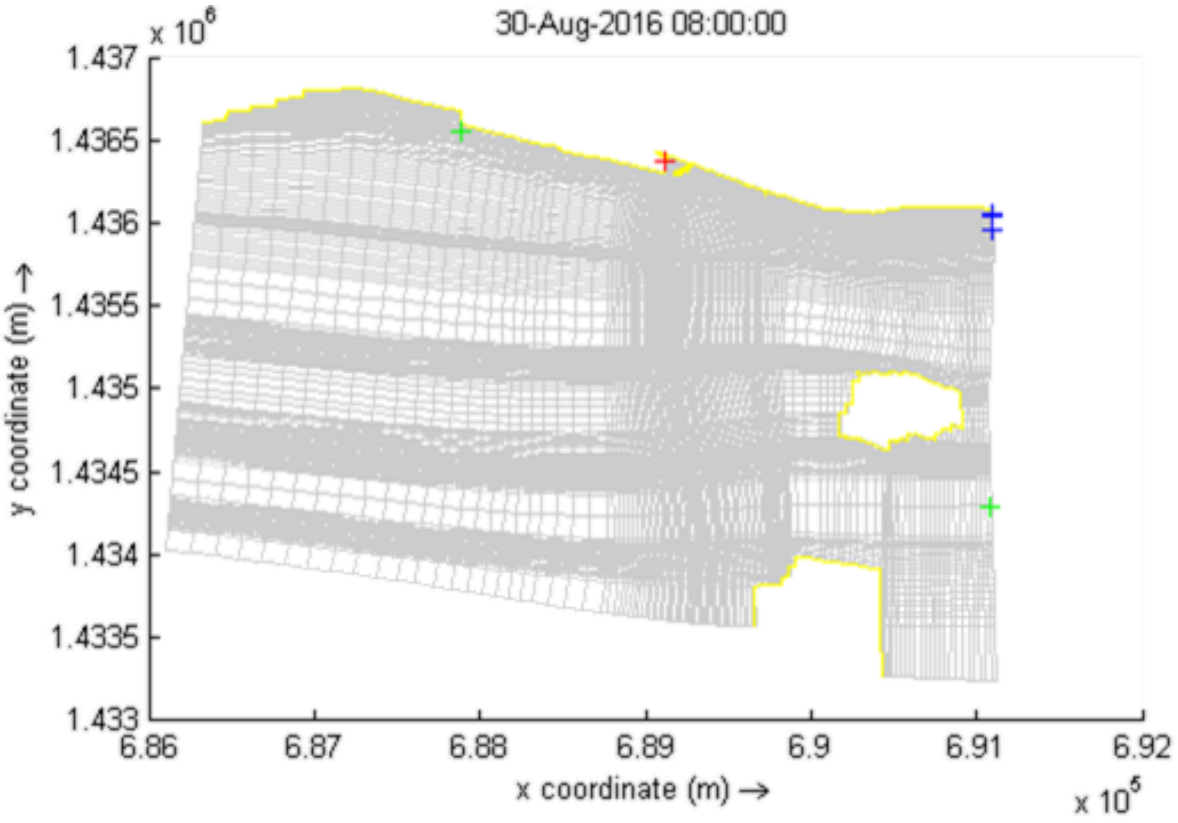

Figure 7.18: Drogues' Final Location for Long Angled Groyne in Low Wave, Regular Wind Scenario

Shown in Figure 7.18 is the performance of the long angled groyne under the 'low wave, regular wind' scenario. Six drogues finished their course behind the inlet, one offshore and 23 in the 'shore' area.

In total, 19 drogues accumulated behind the groyne. Three of those drogues got stuck in the groyne possibly due to the way the groyne was modeled. The rest of the drogues came from every location, proving that the groyne may not be able to prevent the drogues from going behind the groyne. This may be caused by a current entraining the drogues on the leeward side of the groyne. The study of the velocity field behind the groyne is necessary to understand the source of the accumulation.

7.7 Drogue Test Summary

Now that each groyne configurations were tested under the three different scenarios, a comparison between their performances was done. Table 7.1 summarises the test results. The

number in parentheses are the number of drogues that got stuck in the groyne cells. The reader can also refer itself to Appendix G for the detailed test result tables.

		Perpendicular Groynes			Angled Groynes		
Scenario	Location	Long	Medium	Short	Long	Medium	Short
Typical Condition	Inlet	7	13	6	10	3	9 (-2)
	Shore	21	16	19	20	23	20
	Offshore	2	1	5	0	4	1
High Wind, High Wave	Inlet	0	0	0	3 (-3)	4 (-4)	3 (-3)
	Shore	30	30	30	27	26	27
	Offshore	0	0	0	0	0	0
Low Wave, Regular Wind	Inlet	8	15	0	6	0	0
	Shore	22	11	27	23	27	20
	Offshore	0	4	3	1	3	10
Total	Inlet	15	28	6	19 (-3)	7 (-4)	12 (-5)
	Shore	73	57	76	70	76	67
	Offshore	2	5	8	1	7	11

Table 7.1: Drogue Test Summary

When analysing the results, it was observed that the shorter groynes tend to prevent the accumulation better than the longer groynes. This may be caused by the fact that the longer groyne are slowing down the water along the shore too much. Therefore, the drogues can stay along the shore. The shorter groynes also are pushing more drogues offshore, going from 2 to 8 in the perpendicular groynes and 1 to 11 in the angled groynes. When comparing the two angles, the angled groynes as a whole have performed better than the perpendicular groynes. The total drogue accumulations in the 'inlet' area are 38 and 49 for the angled and perpendicular groynes respectively.

More specifically, the groyne that has performed the best according to the results is the short perpendicular groyne. However, it was noted that the angled groynes trapped drogues in the corner of the 'dry points' cells. In total, 3 drogues got stuck during the long angled groyne simulations, 4 during the medium angled groyne simulations and 5 during the short angled simulations. These drogues would have probably left the 'inlet' area, like the rest of the drogues in the simulations where such a phenomenon was observed. When excluding these drogues from the totals, the medium angled groyne out performs the short perpendicular groyne and the short angled groyne comes close third. Also, the total of drogues accumulating in the 'inlet' area drops

to 26 for the angled groynes. The medium perpendicular groyne has had the worst results in all the 6 with 28 drogues in the 'inlet' area.

8 Discussion

The goal of the study was to study the movement patterns of the floating debris around Bequia Island, more particularly to understand the mechanisms generating debris accumulation in the Jeff Gregg inlet. A numerical model was developed to study the existing hydrodynamics and the effect of the addition of a proposed groyne designed to mitigate the accumulation of litter. The performance of multiple groynes was tested by releasing 'drogues' in the model and by noting their location at the end of the various simulations. The main discoveries of the study are the followings:

- The JONSWAP parameter used for wind-sea condition (C_b=0.067 m^2s^{-3}) is not appropriate for the situation,
- An angled groyne is more suitable for reducing the debris accumulation,
- A longer groyne will not necessarily prevent more accumulation.

First, it was found that the JONSWAP's parameter recommended to simulate wind-sea type wave (C_b=0.067 m^2s^{-3}), also the default value in Delft3D, is too high to get accurate results for the modeling of floating debris patterns in the particular case of the Paget Farm region. This parameter is used in the formulation of the bottom friction coefficient in the SWAN model, the model used to simulate the wave action. In the validation exercise, three values for the JONSWAP parameter were evaluated: C_b=0.067 m^2s^{-3} (recommended for wind-sea conditions), C_b=0.038 m^2s^{-3} (recommended for swell conditions) and C_b=0.019 m^2s^{-3} (recommended for Caribbean sand type bottom). As shown in Figure 4.8, only the model with a JONSWAP value of C_b=0.038 m^2s^{-3} was closest to simulate the debris accumulation phenomenon. This observation reinforces the recent findings that the value of C_b=0.067 m^2s^{-3} is too high to replicate any wave conditions (Vledder, 2010). This adjustment was very important in the making of the numerical model since the waves are greatly influencing the surface velocities. Given the fact that floating debris patterns are influenced by the surface velocity, a calibration type of approach could be taken to choose the appropriate value for the JONSWAP parameter. With the sufficient field data to judge the accuracy of the model, this approach would yield better results. The

calibration of this parameter was done in a previous research by using the field measurements of wave's significant height. They found that the JONSWAP parameter would be more related to bottom friction than the type of waves (Cialone & McKee Smith, 2007). The same method could be applied to the study of surface currents.

Second, it was found that an angled groyne would be more suitable in this situation to limit the debris accumulation. In order to test the different groyne configurations' capacity to reduce debris accumulation, all the configurations were simulated with three different weather scenarios. In all the scenarios, a total of 30 drogues were released in the same tide cycle and their movements were tracked for 25 hours. Their final position was recorded and used as a point of comparison to recommend a final design. Two different angles were tested: 90 degree from shore and 50 degrees toward the inlet. Three lengths per angle were tested varying from 45m to 125m. The test results compiled in Table 7.1 indicates that the groynes that were set up with a 50 degree angle outperformed the perpendicular groynes. The total drogues accumulation in the angled groynes was 47% less than the accumulation noted in the perpendicular groynes simulation. This could be caused by two factors: (i) angled groynes create a smoother transition between the shore and the South side of the airport, (ii) the larger gap in the perpendicular groynes causes more circulation behind the groyne driving the litter at that location. Shown in Figure 8.1 are the surface velocity fields around the medium perpendicular groyne and the medium angled groyne at the 34th hour of the 'typical condition' simulation (middle of the flood tide). The patterns shown in Figure 8.1 were observed in the other groynes and in different scenarios.

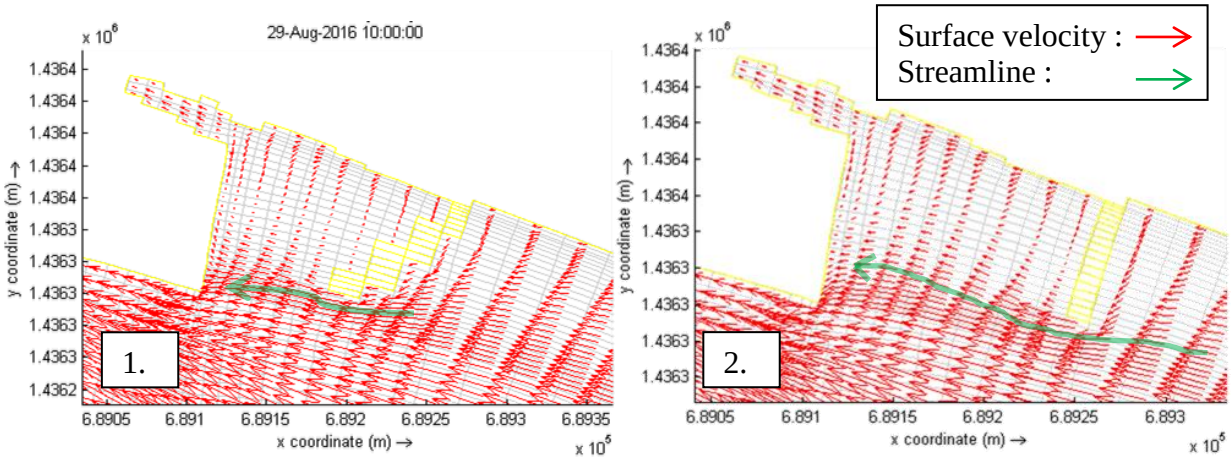

Figure 8.1: Velocity Fields around Angled Groyne vs Perpendicular Groyne

When comparing the two velocity fields, the angled groyne is more successful at reducing the velocity on its leeward side than the perpendicular groyne. A lower velocity on the leeward side is more desirable for the following factors: (i) may reduce litter accumulation behind the groyne, (ii) improve sheltering of fishing boats if docks are to be installed. Also, the direction of the point velocities South of the groyne in Figure 8.1 (1.) indicates that the surface velocity is pushing the debris toward the corner of the airport (also indicated by the streamlines). In Figure 8.1 (2.), the streamline points toward the wall of the airport behind the groyne. The velocity field observed in the perpendicular groynes will push the debris behind the groyne instead of out to sea.

Third, it was found that a longer groyne would not prevent more accumulation. In fact, the groynes that have performed the best were, in order, the medium angled groyne, short perpendicular groyne and the short angled groyne. The longer groynes have performed the second and third worst. This could be explained by the fact that the longer groynes are affecting the velocities along the shore more than the shorter ones. Therefore, accumulations in the 'inlet' area were created by this reduction in velocity. Also, the only cases of accumulations on the leeward side area were observed in the long groynes simulations. This observation means that the longer groynes are entraining floating debris on its leeward side.

In hindsight, a few modifications could have been to better the study. These modifications are divided in three parts: (i) field data collection, (ii) model development, (iii) results' analysis method. A remedy to these challenges could serve in future works of this nature to perfect the research in the field.

8.1 Field Data Collection

The field data collection activity was a crucial step in this research as virtually no hydrodynamic information is available for the region. During the field campaigns, bathymetric data and point velocities were collected in order to facilitate the making of the numerical model. Due to time constraints, the measurements were limited to these two types of data. The bathymetric data could not have been extended by collecting more points due to the availability of the towing boat. In retrospective, data should have been collected in the Jeff Gregg inlet to get the correct dimensions of the inlet. The quality of the point velocity measurements could have been increased by lengthening the measurement time. Most of the points taken close to the inlet had a

measurement time of less than 90 seconds. This measurement time could have been extended to three minutes or more to reduce the possible averaging error.

If more time had been available, a tracking of floating debris, using GPS placed on floaters released at different times and sea conditions, could have extended the information available to validate the model. This would have helped the validation process by confirming that the drogues are replicating the right movement pattern and allow a calibration of the JONSWAP parameter. The understanding of the floating debris movement would have been better. This could have helped to confirm that the floating debris are still accumulating during ebb tide or disprove it with data. Also, a time series of the depth-averaged velocity over a full tide cycle at a location where the tide-induced current creates high velocities (such as between petit Nevis and Bequia in Figure 2.7) would have been preferable to create a better numerical estimation of the tide-induced current phenomenon. Overall, the measurements were acceptable for the application, but time and equipment availability was limiting the extent of the data collected.

8.2 Model Development

When reflecting on the model development exercise, a few points could have been done differently which could have increased the precision of the model. Indeed, no debris accumulation in the Jeff Gregg inlet was successfully modeled in the full existing condition simulations. When the grid was constructed, no bathymetry data was collected in the inlet. Therefore, the inlet dimensions, along with part of the airport armoring, had to be estimated using satellite imagery. These estimations may have incorrectly assessed the size of the inlet or the angle of the airport east armoring. An underestimation of the size of the inlet and an airport armoring that is more open to the sea may reduce the debris accumulation compared to the observed mechanism. Also, the final grid has a smoothness factor over the maximum recommended by Delft3D (Deltares, 2011). This maximum value is 1.4 and some grid cells in the model have a smoothness factor of over 2. According to the FLOW user manual, instabilities might be created because of a high smoothness value. However, no error messages were signaled by the simulator that would indicate such instabilities and the latter were not observed in the post-processing exercise. Therefore, the lack of smoothness probably did not affect the results.

When modeling the different existing scenarios, it was noted that no drogues accumulated in the inlet which is contrary to the field observations. The only way that debris accumulation was

achieved in the inlet was by removing the wave action (Figure 5.2). Therefore, the waves are preventing the accumulation of debris in the model. A possible source of error is created by the way the SWAN model is simulating waves. The wave action calculated in the WAVE module is applied to the surface grid layer used by the FLOW module. Then, FLOW simulates the hydrodynamics with the momentum balance equation. As a result, the full force of the waves are applied to the surface grid and then transferred to the other layers. This might have caused an overestimation of the wave action on the surface grid. This might not have much impact when the velocities are depth-averaged, but could have an impact on the velocity profile.

Knowing that the waves have such an impact on the surface velocity, the WAVE grid could have been made with a greater resolution. This would have improved the quality of the wave field. It was also noted that the WAVE module drops the diffraction factor when the grid cells are larger than the wave length. This could have been prevented by defining more domains in the simulation.

A new grid set up that could be tried is to split the FLOW grid two sections: a 3D grid for the near inlet section with high resolution and a 2D grid that would extend passed the small island south of Bequia and contain the full island of Bequia. This would have reduced the area of the 3D grid reducing the compilation time while keeping a high resolution in the key location. By extending the grid to include the full Bequia Island and neighbouring islands, the interaction between the tide asymmetry and the island would have been simulated. The WAVE grid could have been kept the same, but with higher resolution to ensure that the diffraction is included in the SWAN simulation. Setting up the grids this way would have better render the potential of Delft3D in coastal environment while reducing the run time.

8.3 Results' Analysis Method

The original plan to analyse the groyne's performance was to count the amount of drogues that accumulated on the leeward side of the groyne, the location of the inlet, and compare the performance of each groyne configurations to the existing conditions. However, during the existing condition simulations, it was noted that no debris were collecting in the inlet. Therefore, the method of judging the groyne configurations' performance had to be changed. The new plan was to extend the 'inlet' area from the windward side of the groyne to two third of the airport landing strip. These two locations were chosen arbitrarily to cover debris accumulations that

occur close to the inlet. It is assumed that in the case of a perfectly calibrated model, these drogues would have accumulated in the Jeff Gregg inlet. Therefore, the drogue test was adapted to react to the fact that there was no drogue accumulating in the inlet during the numerical models.

During the analysis of the drogue test results, it was noted in Figure 7.10, 7.11, 7.14 and 7.17 that some drogues were getting stuck in the groyne cells. It is believed that these drogues were accumulating at that location because of the fact that the angled groynes are modeled in steps. Figure 8.2 illustrates this phenomenon. The velocity field next to the groyne is pushing those drogues toward the corner of the grid cell defined as ‘dry points’. Due to the definition of the surrounding cells and the velocity field, the drogues are blocked in X and Y at those locations. This problem was not experienced during the perpendicular groyne simulations given the drogues were never blocked in both axes. Therefore, the accumulation in scenarios where this phenomenon happened was overestimated. In the optimal groyne configuration decision, these drogues were ignored.

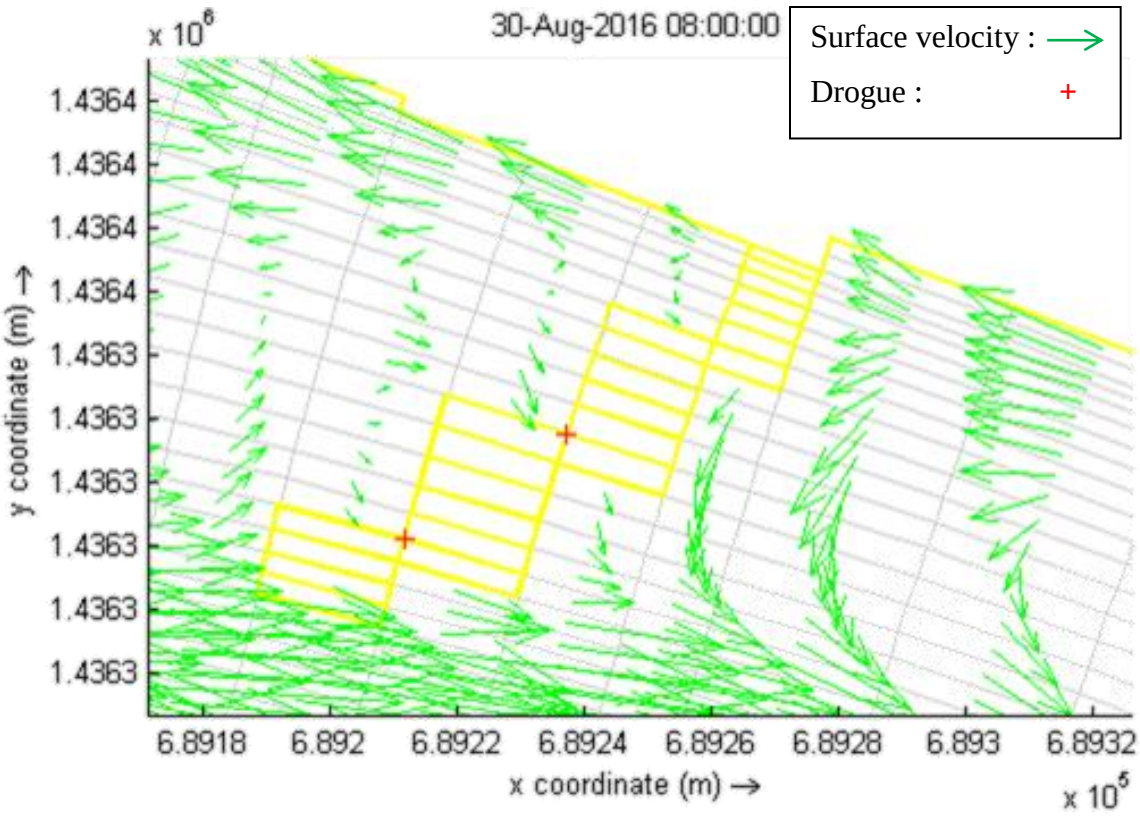

Figure 8.2: Drogues Stuck in Angled Groyne's Cell

9 Conclusions and Recommendations

The goal of this thesis was to verify if a rubble mound groyne installed east of the inlet was able to reduce the litter accumulation in the Jeff Gregg inlet. A numerical model was developed and was used to test this hypothesis. A drogue test was set up and confirmed that some groyne configurations were capable of reducing the debris accumulation. Based on the test results, the groyne that is the most suitable for this situation is a 90m long groyne angled at 50 degree toward the airport. However, the existing condition model failed to simulate precisely the accumulation patterns observed in the field. Therefore, the results give an approximation of the most suitable solution. It was concluded that this lack of exactitude is due to the surface current's sensitivity to the wave action. This is especially true due to the fact that the wave action calculated in the Delft3D model is only applied to the surface layer and then, redistributed to the other grid layers through the resolution of momentum equations.

To limit the imprecision of 3D numerical models that studies surface current dynamics, it is recommended to put great attention on the modeling of waves. This can be done by increasing the resolution of the grid used for the wave model. In a SWAN model, the size of any grid cell should never be larger than the wave length to ensure proper diffraction calculation. A calibration of the JONSWAP parameter should be done especially in the case of shallow water modeling. It is proposed to study the possibility of using field measurement collected by tracking GPS mounted floaters to perform the calibration exercise. It was also noted that the JONSWAP parameter used as default value in Delft3D (C_b= 0.067 m^2s^{-3}) is too high for this situation.

10 Future Works

As discussed in the introduction, this study is only a part of the preliminary work for the 'Enhancing community resilience to environmental and climate change impacts in the coastal zone of Paget Farm, SVG' project. This project also includes community participation projects, the renewal of Paget Farm's drainage system and a solution for the reduction of erosion. At the time of the presentation of this thesis, the documents for funding through the Community Disaster Risk Reduction Fund were submitted. The managers of the fund are in the process of deciding the most suitable project for the funds. The future steps for the completion of the engineering portion of the project are the followings:

- To design the new drainage system that will reduce the floods currently experienced in Paget Farm. A preliminary HEC-RAS model has already been developed.
- Include the secondary drain in the Delft3D model
- Study the effects of this new feature on the debris accumulation patterns and verify if the proposed groyne is still a suitable solution.
- Create a morphodynamic model that will show the erosion and accretion patterns. This will confirm that the addition of the proposed groyne is indeed preventing further erosion east of the airport.
- Do the technical drawings to submit to a contractor.

These future steps will be initiated when the fund is granted.

References

A. Heitor Reis, C. G. (2010). Sand size versus beachface slope — An explanation based on the Constructal Law. *Geomorphology 114*, pp. 276-286.

Bist LLC. (2016). Marine Navigation - Caribbean - Offline Gps Nautical Charts for Fishing, Sailing, Boating. Retrieved from https://www.microsoft.com.

California Departement of Water Resources. (1970). *Determination of the Manning Coefficient From Measured Bed Roughness in Natural Channels.* Washington: United States Government Printing Office.

C-Change Secretaria (Canada). (2010, April). *Bequia, Saint Vincent & the Grenadines*. Consulté le March 25, 2016, sur Coastal Change: http://www.coastalchange.ca/index.php/communities/caribbean-community-profiles/bequia-saint-vincent-a-the-grenadines

CDC. (2016, February 28). *Zika Virus in Saint Vincent and the Grenadines*. Consulté le July 23, 2016, sur Center for Disease Control and Prevention: http://wwwnc.cdc.gov/travel/notices/alert/zika-virus-saint-vincent-and-the-grenadines

Chatzirodou, A. &. (2014). IMPACTS OF TIDAL ENERGY EXTRACTION ON SEA BED MORPHOLOGY. *Coastal Engineering Proceedings*.

Cialone, M., & McKee Smith, J. (2007). *WAVE TRANSFORMATION MODELING WITH BOTTOM FRICTION APPLIED TO SOUTHEAST OAHU REEFS.* Vicksburg, MS: US Army Engineer Research and Development Center.

Deligny, G. (2013, January 26). *The Wings of the Web*. Consulté le May 18, 2016, sur Airliners: http://www.airliners.net/photo//2277193/L/

Deltares. (2011). *Delft3D-FLOW, User Manual.* Delft: Deltares.

Deltares. (2011, May 18). Delft3D-WAVE . *User Manual*. Delft, Netherlands: Deltares.

Elias, E. (1999). *The Egmond Model, Calibration,validation and evaluation of Delft3D-MOR with field measurements.* Delft Hydraulics.

G.Ph Van Vledder, O. J. (2009). Low-frequency wind wave penetration in a tidal inlet system during a severe winter storm. *Proc. 11th Int. Workshop on Wave Hindcasting and Forecasting.* Halifax, Canada.

Gibbs, T. (1998). *Vulnerability Assessment of Shelters in the Eastern Caribbean, Retrofitting Terms of Reference of Consultants Standards.* Consulting Engineers Partnership Ltd.

Harlow, D. (2013). *Non-Standard Rock Groynes in Poole and Christchurch Bays.* The Southern Coastal Group.

HENDRY, M. ,. (1997). *Seeking Sand Source Alternatives - An Island Case Study. In: CAMBERS, G. (ed), Managing Beach Resources in the Smaller Caribbean Islands.* Mayaguez: UNESCO.

Henson, J. (2005). *Status Report on Tide Gauges and Observing Stations in the Caribbean and Adjacent Waters.* St. Petersburg: University of South Florida.

I Coghlan, J. C. (2013). Concept designs for a groyne field on the far north NSW coast. *NSW Coastal Conference.* Port Macquarie.

J.H. Rosman, J. H. (2011, August). A framework for understanding drag parameterizations for coral reefs. *Journal of Geophysical Research*.

Koen Trouw, N. Z. (2012). NUMERICAL MODELLING OF HYDRODYNAMICS AND SEDIMENT TRANSPORT IN THE SURF ZONE : A SENSITIVITY STUDY WITH DIFFERENT TYPES OF NUMERICAL MODELS. *Coastal Engineering Proceedings*.

Matthews, E. R. (2003). *Coast Erosion and Protection - Engineering.* Watchmaker Publishing.

Meteo365. (2016, May 24). *Tide Times for Kingstown, Saint Vincent*. Consulté le May 24, 2016, sur Tide-Forecast: http://www.tide-forecast.com/locations/Kingstown-Saint-Vincent/tides/latest

Mitchell, S. J. (2016, January 28). *Bequia Airport - an essential lifeline with an even brighter future*. Consulté le March 25, 2016, sur iWitness News:

http://www.iwnsvg.com/2016/01/28/bequia-airport-an-essential-lifeline-with-an-even-brighter-future/

N. Booij, R. C. (1999, April 15). A third-generation wave model for coastal regions. *Journal of Geophysical Research, Vol. 104*, pp. 7649-7666.

NOAA. (2008, March 25). *Ocean Service Education*. Consulté le May 24, 2016, sur http://oceanservice.noaa.gov/education/kits/tides/media/supp_tide07a.html

NOAA. (2016, May 24). *Castries, St. Lucia, TEC4775 Tidal Data Daily View*. Consulté le May 24, 2016, sur Tides & Currents: https://tidesandcurrents.noaa.gov/noaatidepredictions/NOAATidesFacade.jsp?Stationid=TEC4775

Prager, E. J. (1991, December). Numerical simulation of circulation in a Caribbean-type backreef lagoon. *Coral Reefs, Volume 10, Issue 4*, pp. 177-182.

SonTek, Y. (2009). *RiverSurveryor S5/M9 System Manual Version 1.0.* San Diego.

The SWAN team. (2017). *User Manual SWAN Ctcle III version 41.10A.* Delft: Delft University of Technology.

Toy, S. M. (2015, January 31). *Speaking of Chikungunya …*. Consulté le March 10, 2016, sur Wordpress: https://islandeditions.wordpress.com/2015/01/31/speaking-of-chikungunya/

U.S. Army Corps of Engineering. (2008). *Coastal engineering manual.* Washington: Department of the army.

U.S. Geological Survey. (2009). *Measuring Discharge with Acoustic Doppler Current Profilers from a Moving Boat.* Reston, Virginia: U.S. Departement of the Interior.

UNFCCC. (2015). *St. Vincent and the Grenadines Intended Nationally Determined Contribution.* United Nations Framework Convention on Climate Change.

Visser, R. (2002). *Morphological modelling in the vicinity of groynes, an extended application of Delft3D-RAM including impact.* Delft: Delft University of Technology.

Vledder, v. G. (2010). Revisiting the JONSWAP Bottom Friction Formulation. *Coastal Engineering Proceedings No 32*, (p. waves.41). Shanghai.

Washington State Department of Transportation. (2010). *Hydraulics Manual M23-03.03.*

wisuki. (2016, March 15). *Statistics, Friendship Bay*. Consulté le March 15, 2016, sur wisuki: http://wisuki.com/statistics/925/friendship-bay?a_wi=4&wi_m=0&a_wa=4&wa_m=0&temp=monthly&rain=quantity

wisuki. (2017, March 15). *Statistics, Friendship Bay*. Consulté le March 15, 2017, sur wisuki: http://wisuki.com/statistics/925/friendship-bay?a_wi=4&wi_m=0&a_wa=4&wa_m=0&temp=monthly&rain=quantity

Appendix A: Field Investigation Schedule

Field campaign 1	
Date	Description of the day's activities
4/16/2016	Preliminary visit of the concerned area
4/17/2016	Visit of the airport and water accumulation areas
4/18/2016	
4/19/2016	Dive investigation along the airport and the possible location of the proposed groyne for bottom observation
4/20/2016	
4/21/2016	Assessment of the shore for observation of debris accumulation
4/22/2016	Dive investigation along the coast for bottom observation
4/23/2016	Visit of the quarry Sampling of the quarry rock
4/24/2016	Assessment of the shore for observation of debris accumulation Sampling of beach sand
Field campaign 2	
Date	Description of the day's activities
8/21/2016	Hydrodynamic measurements using the ADCP: - Point velocities between Petit Nevis and Bequia - Bathymetric data between Petit Nevis and Bequia Hydrodynamic data post-processing and interpretation
8/22/2016	Hydrodynamic measurements using the ADCP: - Point velocities between Petit Nevis and Bequia - Bathymetric data along Paget Farm's coast
8/23/2016	Hydrodynamic data post-processing and interpretation
8/24/2016	Hydrodynamic measurements using the ADCP: - Bathymetric data along Paget Farm's coast
8/25/2016	Arrival of Dr Ioan Nistor Visit of the village and the concerned areas
8/26/2016	First meeting with the ministries representatives, in Kingstown

8/27/2016	Hydrodynamic measurements using the ADCP: - Bathymetric data along Paget Farm's coast and between Petit Nevis and Isla a Quatre
8/28/2016	Hydrodynamic data post-processing and interpretation
8/29/2016	Hydrodynamic measurements using the ADCP - Point velocities close to the Jeff Gregg Inlet - Bathymetric data along Paget Farm's coast
8/30/2016	Dive investigation along the coast for bottom observation
8/31/2016	
9/1/2016	Meeting with the Prime minister, in Kingstown Second meeting with the ministries representatives, in Kingstown Presentation to the community, in Paget Farm

Table A.1: Field Investigation Schedule

Appendix B: Point Velocity Raw Data Example and Post-Processing

Table B1 is an example of the data produced by the Sontek post-processing program. Numerous data, such as the pitch, roll, boat speed, etc., were not included in this report for space concerns and these data weren't use by the authors.

	Latitude (deg)	Longitude (deg)	Mean Speed (m/s)	Direction (deg)	Speed in X (m/s)	Speed in Y (m/s)
7:27:31	12.9855716	-61.2534048	0.336	107.9	0.3197	-0.1033
7:27:32	12.9855721	-61.253405	0.181	78.1	0.1771	0.0373
7:27:33	12.9855729	-61.2534063	0.319	112.9	0.2939	-0.1241
7:27:34	12.9855744	-61.2534064	0.258	78.2	0.2525	0.0528
7:27:35	12.9855759	-61.2534074	0.105	102.9	0.1023	-0.0234
7:27:36	12.9855765	-61.2534086	0.215	100.8	0.2112	-0.0403
7:27:37	12.9855759	-61.2534107	0.165	96.2	0.1640	-0.0178
7:27:38	12.9855764	-61.2534103	0.318	107.3	0.3036	-0.0946
7:27:39	12.9855782	-61.2534114	0.124	284.4	-0.1201	0.0308
7:27:40	12.9855789	-61.2534114	0.173	137.7	0.1164	-0.1280
7:27:41	12.9855798	-61.2534116	0.132	92.7	0.1319	-0.0062
7:27:42	12.9855808	-61.2534113	0.22	156.5	0.0877	-0.2018
7:27:43	12.9855816	-61.2534117	0.127	153.5	0.0567	-0.1137
7:27:44	12.9855809	-61.2534108	0.237	173.5	0.0268	-0.2355
7:27:45	12.9855826	-61.2534104	0.204	72.1	0.1941	0.0627
7:27:46	12.9855821	-61.2534093	0.103	102.9	0.1004	-0.0230
7:27:47	12.9855828	-61.2534098	0.17	104	0.1650	-0.0411
7:27:48	12.9855833	-61.2534092	0.027	159.8	0.0093	-0.0253
7:27:49	12.9855837	-61.2534097	0.354	116.3	0.3174	-0.1568
7:27:50	12.9855838	-61.2534079	0.272	78.2	0.2663	0.0556
7:27:51	12.9855842	-61.2534082	0.098	127.6	0.0776	-0.0598
7:27:52	12.9855848	-61.2534087	0.173	141.5	0.1077	-0.1354
7:27:53	12.9855842	-61.2534079	0.29	126.6	0.2328	-0.1729
7:27:54	12.985584	-61.2534079	0.22	84	0.2188	0.0230
7:27:55	12.9855852	-61.2534087	0.183	119.1	0.1599	-0.0890
7:27:56	12.9855865	-61.2534093	0.146	65.7	0.1331	0.0601
7:27:57	12.9855875	-61.2534098	0.246	123.7	0.2047	-0.1365
7:27:58	12.9855893	-61.2534092	0.117	93	0.1168	-0.0061
7:27:59	12.9855895	-61.2534099	0.219	125.1	0.1792	-0.1259
7:28:00	12.9855914	-61.2534097	0.246	78.9	0.2414	0.0474
7:28:01	12.9855931	-61.253411	0.074	101.9	0.0724	-0.0153
7:28:02	12.9855922	-61.2534093	0.412	122.4	0.3479	-0.2208

7:28:03	12.985592	-61.2534094	0.075	154.1	0.0328	-0.0675
7:28:04	12.9855938	-61.2534119	0.112	311.5	-0.0839	0.0742
7:28:05	12.9855952	-61.2534113	0.197	100	0.1940	-0.0342
7:28:06	12.9855949	-61.2534089	0.236	123.9	0.1959	-0.1316
7:28:07	12.9855946	-61.2534083	0.384	133.1	0.2804	-0.2624
7:28:08	12.9855938	-61.2534079	0.365	109.6	0.3439	-0.1224
7:28:09	12.9855944	-61.253407	0.227	125.3	0.1853	-0.1312
7:28:10	12.9855947	-61.2534096	0.057	356.9	-0.0031	0.0569
7:28:11	12.9855957	-61.2534099	0.203	125.7	0.1649	-0.1185
7:28:12	12.9855955	-61.2534097	0.313	126.4	0.2519	-0.1857
7:28:13	12.9855951	-61.2534099	0.148	65.8	0.1350	0.0607
7:28:14	12.9855954	-61.2534111	0.2	113.7	0.1831	-0.0804
7:28:15	12.9855965	-61.2534116	0.147	94.2	0.1466	-0.0108
7:28:16	12.9855961	-61.2534137	0.291	120.3	0.2512	-0.1468
7:28:17	12.9855953	-61.2534155	0.104	154.6	0.0446	-0.0939
7:28:18	12.9855954	-61.2534145	0.153	83.7	0.1521	0.0168
7:28:19	12.9855958	-61.2534148	0.12	64.4	0.1082	0.0519
7:28:20	12.9855963	-61.2534152	0.194	87.5	0.1938	0.0085
7:28:21	12.9855964	-61.2534147	0.139	103.5	0.1352	-0.0324
7:28:22	12.9855963	-61.2534144	0.195	107.2	0.1863	-0.0577
7:28:23	12.9855976	-61.2534142	0.258	90.4	0.2580	-0.0018
7:28:24	12.9855975	-61.2534136	0.204	100.3	0.2007	-0.0365
7:28:25	12.9855994	-61.2534144	0.189	104.2	0.1832	-0.0464
7:28:26	12.9855996	-61.2534153	0.162	138.8	0.1067	-0.1219
7:28:27	12.9855991	-61.2534159	0.276	118.9	0.2416	-0.1334
7:28:28	12.9855986	-61.2534168	0.335	82	0.3317	0.0466
7:28:29	12.9855981	-61.2534162	0.131	113.5	0.1201	-0.0522
7:28:30	12.9855989	-61.2534154	0.179	64.6	0.1617	0.0768
7:28:31	12.9855988	-61.2534161	0.067	144.7	0.0387	-0.0547
7:28:32	12.9855986	-61.2534165	0.162	169.3	0.0301	-0.1592
7:28:33	12.9855977	-61.2534163	0.193	151.5	0.0921	-0.1696
7:28:34	12.9855985	-61.2534173	0.104	112.2	0.0963	-0.0393
7:28:35	12.9855984	-61.2534181	0.146	145.6	0.0825	-0.1205
7:28:36	12.9856002	-61.2534193	0.148	108.1	0.1407	-0.0460
7:28:37	12.9855996	-61.253419	0.279	120.5	0.2404	-0.1416
7:28:38	12.9855991	-61.2534189	0.147	166.4	0.0346	-0.1429
7:28:39	12.9855985	-61.2534192	0.161	90.7	0.1610	-0.0020
7:28:40	12.9855994	-61.2534191	0.167	91.3	0.1670	-0.0038
7:28:41	12.9856008	-61.2534207	0.221	108.2	0.2099	-0.0690
7:28:42	12.9855999	-61.2534216	0.059	72.2	0.0562	0.0180
7:28:43	12.9855987	-61.2534213	0.338	120.6	0.2909	-0.1721
7:28:44	12.9855982	-61.2534224	0.198	150.5	0.0975	-0.1723
7:28:45	12.9855994	-61.2534225	0.203	63	0.1809	0.0922

7:28:46	12.9856026	-61.2534215	0.139	86.1	0.1387	0.0095
7:28:47	12.9856015	-61.25342	0.255	128.8	0.1987	-0.1598
7:28:48	12.9856011	-61.2534211	0.252	134.5	0.1797	-0.1766
7:28:49	12.9856011	-61.2534179	0.289	63.6	0.2589	0.1285
7:28:50	12.9856012	-61.2534195	0.142	82.3	0.1407	0.0190
7:28:51	12.9856003	-61.2534192	0.22	111.1	0.2052	-0.0792
7:28:52	12.9856016	-61.2534199	0.087	113.7	0.0797	-0.0350
7:28:53	12.9856025	-61.25342	0.231	75.9	0.2240	0.0563
7:28:54	12.9856027	-61.2534203	0.288	135.7	0.2011	-0.2061
7:28:55	12.9856027	-61.2534194	0.249	102.6	0.2430	-0.0543
7:28:56	12.9856027	-61.2534198	0.138	95.7	0.1373	-0.0137

Table B.1: Point Velocity Raw Data Example

The columns 'Speed in X' (V_x) and Speed in Y' (V_y) were calculated from the 'Mean Speed' (V_M) and 'Direction' (θ) columns using equations (6) and (7):

$$V_x = V_M * sin\theta \qquad (6)$$

$$V_y = V_M * cos\theta \qquad (7)$$

The depth averaged velocity was split in X and Y to easily compare it to the results of Delft3D which gives results in X and Y components. The velocities were averaged over the whole sampling period and the averaging error for each of the point velocities used is shown in Table B.1. The 'Longitude' and 'Latitude' were converted in UTM at the start location of the measurement using the default conversion of Sontek post-processor. The start location is assumed to be the location of the point velocity.

The velocity had a lot of variation through the sampling time because of wave-generated velocity:

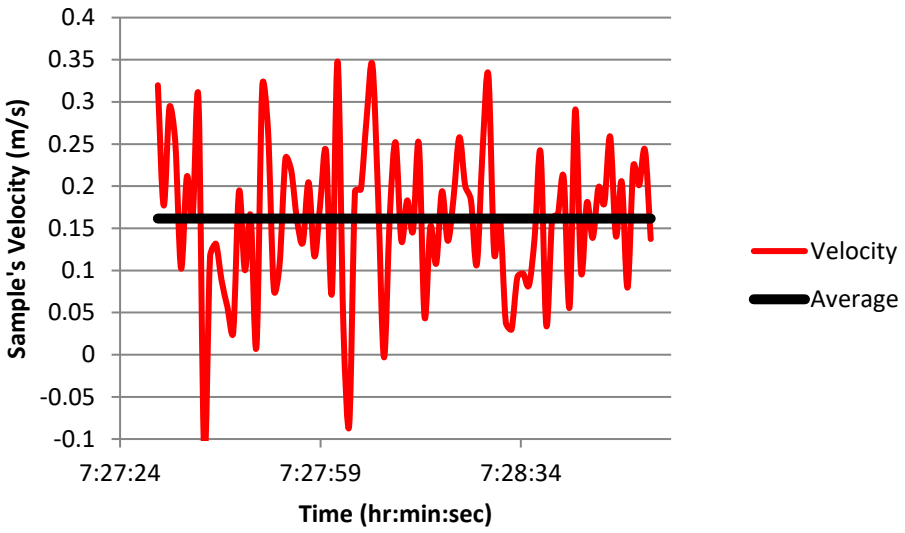

Figure B.1: Example of Velocity Variation over Time

This variation induced a possible averaging error. That limits the precision of the results that the calibration is based on.

Bottom Roughness Calibration				
Points	**Date**	**Time**	**Error in X (m/s)**	**Error in Y (m/s)**
1	8/29/2016	7:03:02	0.020	0.034
2	8/29/2016	7:05:11	0.042	0.041
3	8/29/2016	7:10:53	0.066	0.060
4	8/29/2016	7:15:16	0.071	0.046
5	8/29/2016	7:19:13	0.059	0.051
6	8/29/2016	7:23:15	0.054	0.043
7	8/29/2016	7:27:31	0.037	0.044
8	8/29/2016	7:31:56	0.044	0.044
9	8/29/2016	7:35:46	0.050	0.064
10	8/29/2016	7:39:44	0.043	0.055
		Average:	0.049	0.048
Tide-Induced Calibration				
Points	**Date**	**Time**	**Error in X (m/s)**	**Error in Y (m/s)**
11	8/21/2016	8:50:27	0.017	0.013
12	8/21/2016	8:58:49	0.018	0.023
11	8/22/2016	12:54:54	0.029	0.040
12	8/22/2016	13:04:31	0.067	0.085
		Average:	0.033	0.040

Table B.2: Point Velocities Averaging Error

Table B.3 and B.4 compile the point velocities that were used for the calibration of the tide-induced current and the bottom friction respectively. The point velocities were calculated using the method described below.

Time	Depth (m)	Velocity X (m/s)	Velocity Y (m/s)	Time of Measurement (s)	UTM(m)	UTM(m)
8:50:27	20.42	-0.592	-0.066	237	690486.63	1435900.71
8:58:49	22.61	-0.587	-0.055	210	690575.49	1435452.29
12:54:54	21.49	0.722	-0.010	147	690899.82	1435865.63
13:04:31	25.26	0.767	-0.004	125	690879.19	1435413.47

Table B.3: Point Velocities Used for the Tide-Induced Current Calibration

Time	Depth (m)	Velocity X (m/s)	Velocity Y (m/s)	Time of Measurement (s)	UTM(m)	UTM(m)
7:03:02	2.16	-0.055	-0.002	80	689243.04	1436328.50
7:05:11	2.66	-0.038	0.017	64	689238.87	1436322.48
7:10:53	2.08	-0.068	-0.036	77	689319.94	1436308.85
7:15:16	3.28	-0.118	-0.038	79	689397.92	1436262.99
7:19:13	3.29	-0.120	-0.034	74	689477.33	1436238.94
7:23:15	5.00	-0.170	-0.057	103	689485.18	1436189.92
7:27:31	5.67	-0.162	-0.059	85	689438.65	1436193.31
7:31:56	5.53	-0.144	-0.051	88	689351.88	1436223.49
7:35:46	5.70	-0.154	-0.038	75	689286.46	1436243.29
7:39:44	5.96	-0.127	0.004	83	689182.92	1436269.85

Table B.4: Point Velocities Used for the Bottom Friction Calibration

Appendix C: Sieve Analysis Full Results

Sieve Analysis - Lab Results

Project Information			
Client:	North Grenadines Community Developpement Inc.	Sample No.:	First Groyne
Project:	Reclaiming Paget Farm	Date Sampled:	4/24/2016
Project No.:		Date tested:	5/27/2016

Sieve Test Results						
Large Sieve Analysis				Small Sieve Analysis		
Mass of Dry Soil (g):	100.00			Mass of Soil Before Wash:	498.54	
Mass of Soil Recovered (g):	100.00			Mass of Dry Soil after Wash(g):	498.54	
				Mass of Soil Recovered (g):	497.85	
% of soil lost	0.000			% of Soil Lost	0.138	
Sieve #	Sieve size (mm)	Mass of soil retained (g)	cumulative mass of soil (g)	Percentage on each sieve (%)	Cumulative percent retained (%)	percent finer (%)
Large Sieve Test						
	150.00	0.00	0.00	0.00	0.00	100.00
	106.00	0.00	0.00	0.00	0.00	100.00
	37.50	0.00	0.00	0.00	0.00	100.00
	26.50	0.00	0.00	0.00	0.00	100.00
	19.00	0.00	0.00	0.00	0.00	100.00
	13.20	0.00	0.00	0.00	0.00	100.00
	9.50	0.00	0.00	0.00	0.00	100.00
4	4.75	0.00	0.00	0.00	0.00	100.00
Pan		100.00	100.00	100.00	100.00	0.00
Small Sieve Test						
10	2	0.27	0.27	0.05	0.05	99.95
16	1.19	4.10	4.37	0.82	0.88	99.12
40	0.425	153.13	157.50	30.76	31.64	68.36
60	0.25	175.05	332.55	35.16	66.80	33.20
80	0.18	72.28	404.83	14.52	81.32	18.68
100	0.15	68.22	473.05	13.70	95.02	4.98
200	0.075	24.23	497.28	4.87	99.89	0.11
Pan		0.57	497.85	0.11	100.00	0.00
			497.85	0.00	100.00	0.00
			497.85	0.00	100.00	0.00

Comments/Observations			
By:	Philippe April Le Quéré	Signature:	
Date:	5/27/2016	Approved by:	

Table C.1: Sieve Analysis on First Fishermen's Groyne Sand – Lab Results

Sieve Analysis - Distribution Graph

Project Information

Client: North Grenadines Co North Grenadines Community Deve
Project: Reclaiming Paget Fan Reclaiming Paget Farm
Project No.:
Sample No.: First Groyne
Date Sampled: 4/24/2016
Date tested: 5/27/2016

Sieve Test Results

Coarse Grains					Fine Grain				
Sieve size (mm)	Percent finer (%)				Sieve No.	Sieve Size (mm)	Percent finer (%)		
150.00	100.00				10	2	99.95		
106.00	100.00				16	1.19	99.12		
37.50	100.00				40	0.425	68.36		
26.50	100.00				60	0.25	33.20		
19.00	100.00				80	0.18	18.68		
13.20	100.00				100	0.15	4.98		
9.50	100.00				200	0.075	0.11		

Grain Size Distribution

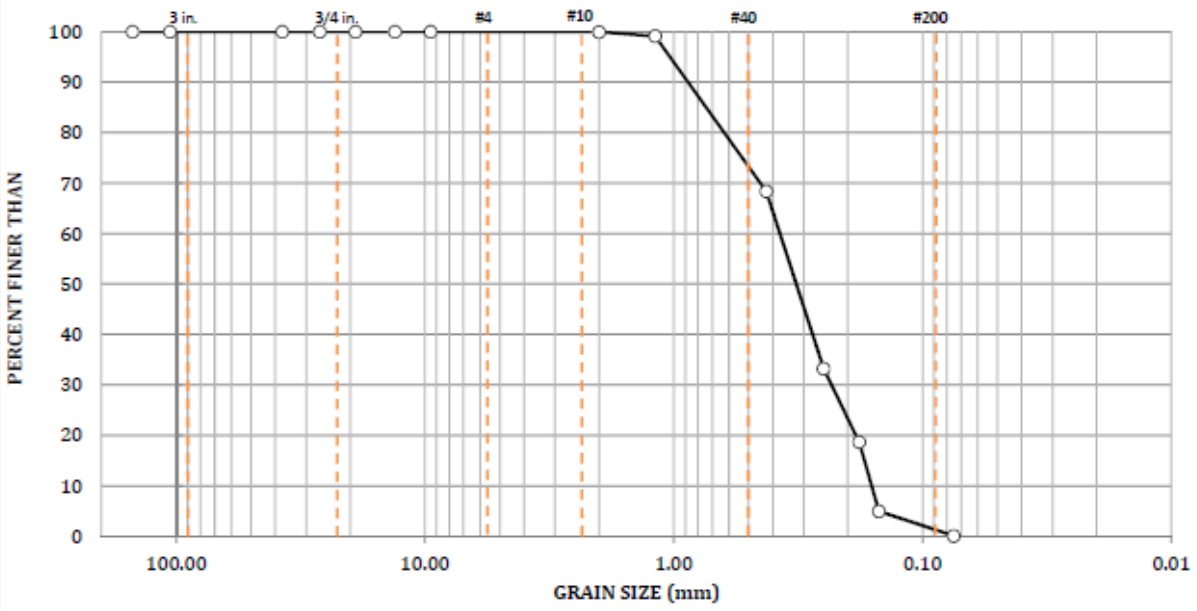

% +3"	% Gravel		% Sand			% Fines
	Coarse	Fine	Coarse	Medium	Fine	Silt & Clay
0.00	0.00	0.05	0.82	65.92	33.09	0.11

Comments/Observations

Test Completed by: Philippe April Le Quéré
Test Approved By:

Figure C.1: Sieve Analysis on First Fishermen's Groyne Sand – Distribution Graph

Sieve Analysis - Lab Results

Project Information			
Client:	North Grenadines Community Developpement Inc.	Sample No.:	Fishery Groyne
Project:	Reclaiming Paget Farm	Date Sampled:	4/24/2016
Project No.:		Date tested:	5/27/2016

Sieve Test Results						
Large Sieve Analysis				Small Sieve Analysis		
Mass of Dry Soil (g):	100.00			Mass of Soil Before Wash:	453.13	
Mass of Soil Recovered (g):	100.00			Mass of Dry Soil after Wash(g):	453.13	
				Mass of Soil Recovered (g):	452.91	
% of soil lost	0.000			% of Soil Lost	0.049	
Sieve #	Sieve size (mm)	Mass of soil retained (g)	cumulative mass of soil (g)	Percentage on each sieve (%)	Cumulative percent retained (%)	percent finer (%)
Large Sieve Test						
	150.00	0.00	0.00	0.00	0.00	100.00
	106.00	0.00	0.00	0.00	0.00	100.00
	37.50	0.00	0.00	0.00	0.00	100.00
	26.50	0.00	0.00	0.00	0.00	100.00
	19.00	0.00	0.00	0.00	0.00	100.00
	13.20	0.00	0.00	0.00	0.00	100.00
	9.50	0.00	0.00	0.00	0.00	100.00
4	4.75	0.00	0.00	0.00	0.00	100.00
Pan		100.00	100.00	100.00	100.00	0.00
Small Sieve Test						
10	2	0.00	0.00	0.00	0.00	100.00
16	1.19	0.17	0.17	0.04	0.04	99.96
40	0.425	10.27	10.44	2.27	2.31	97.69
60	0.25	235.18	245.62	51.93	54.23	45.77
80	0.18	100.97	346.59	22.29	76.53	23.47
100	0.15	79.79	426.38	17.62	94.14	5.86
200	0.075	26.09	452.47	5.76	99.90	0.10
Pan		0.44	452.91	0.10	100.00	0.00
			452.91	0.00	100.00	0.00
			452.91	0.00	100.00	0.00

Comments/Obeservations			
By:	Philippe April Le Quéré	Signature:	
Date:	5/27/2016	Approved by:	

Table C.2: Sieve Analysis on Fishery Groyne Sand – Lab Results

Sieve Analysis - Distribution Graph

Project Information

Client: North Grenadines Co North Grenadines Community Deve
Project: Reclaiming Paget Fan Reclaiming Paget Farm
Project No.:

Sample No.: Fishery Groyne
Date Sampled: 4/24/2016
Date tested: 5/27/2016

Sieve Test Results

Coarse Grains					Fine Grain				
Sieve size (mm)	Percent finer (%)				Sieve No.	Sieve Size (mm)	Percent finer (%)		
150.00	100.00				10	2	100.00		
106.00	100.00				16	1.19	99.96		
37.50	100.00				40	0.425	97.69		
26.50	100.00				60	0.25	45.77		
19.00	100.00				80	0.18	23.47		
13.20	100.00				100	0.15	5.86		
9.50	100.00				200	0.075	0.10		

Grain Size Distribution

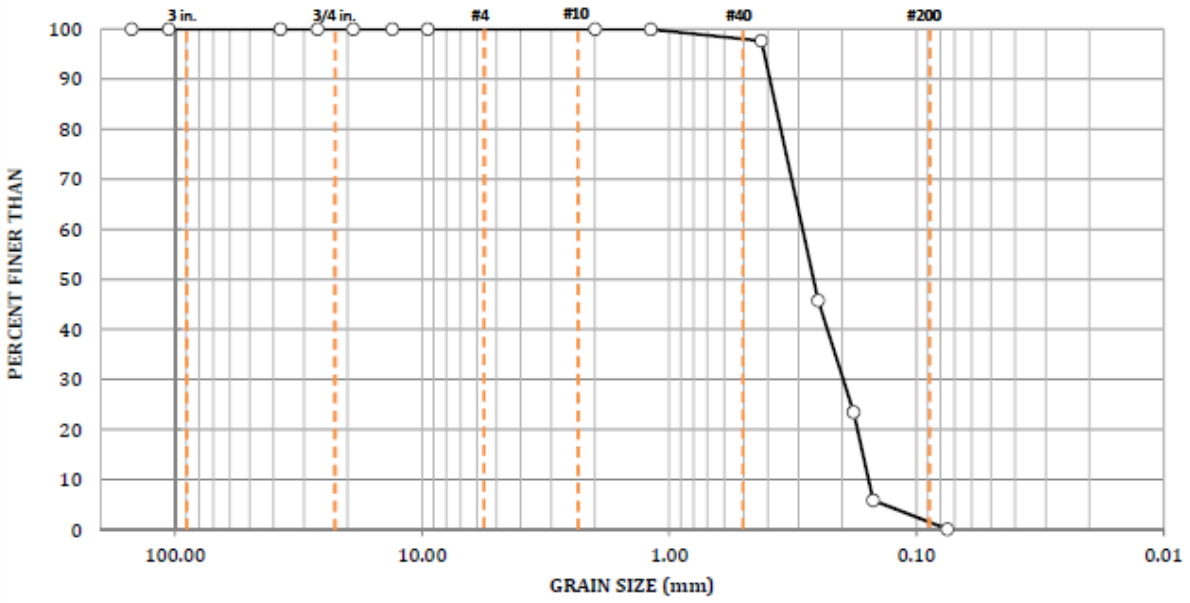

% +3"	% Gravel		% Sand			% Fines
	Coarse	Fine	Coarse	Medium	Fine	Silt & Clay
0.00	0.00	0.00	0.04	54.19	45.67	0.10

Comments/Observations

Test Completed by: Philippe April Le Quéré
Test Approved By:

Figure C.2: Sieve Analysis on Fishery Groyne Sand – Distribution Graph

Sieve Analysis - Lab Results

Project Information			
Client:	North Grenadines Community Developpement Inc.	Sample No.:	Inlet Sand
Project:	Reclaiming Paget Farm	Date Sampled:	4/24/2016
Project No.:		Date tested:	5/27/2016

Sieve Test Results						
Large Sieve Analysis				Small Sieve Analysis		
Mass of Dry Soil (g):	100.00			Mass of Soil Before Wash:	370.60	
Mass of Soil Recovered (g):	100.00			Mass of Dry Soil after Wash(g):	370.6	
				Mass of Soil Recovered (g):	371.03	
% of soil lost	0.000			% of Soil Lost	-0.116	
Sieve #	Sieve size (mm)	Mass of soil retained (g)	cumulative mass of soil (g)	Percentage on each sieve (%)	Cumulative percent retained (%)	percent finer (%)
Large Sieve Test						
	150.00	0.00	0.00	0.00	0.00	100.00
	106.00	0.00	0.00	0.00	0.00	100.00
	37.50	0.00	0.00	0.00	0.00	100.00
	26.50	0.00	0.00	0.00	0.00	100.00
	19.00	0.00	0.00	0.00	0.00	100.00
	13.20	0.00	0.00	0.00	0.00	100.00
	9.50	0.00	0.00	0.00	0.00	100.00
4	4.75	0.00	0.00	0.00	0.00	100.00
Pan		100.00	100.00	100.00	100.00	0.00
Small Sieve Test						
10	2	0.97	0.97	0.26	0.26	99.74
16	1.19	0.27	1.24	0.07	0.33	99.67
40	0.425	8.61	9.85	2.32	2.65	97.35
60	0.25	130.63	140.48	35.21	37.86	62.14
80	0.18	101.95	242.43	27.48	65.34	34.66
100	0.15	71.57	314.00	19.29	84.63	15.37
200	0.075	53.80	367.80	14.50	99.13	0.87
Pan		3.23	371.03	0.87	100.00	0.00
		0.00	371.03	0.00	100.00	0.00
		0.00	371.03	0.00	100.00	0.00

Comments/Obeservations			
By:	Philippe April Le Quéré	Signature:	
Date:	5/27/2016	Approved by:	

Table C.3: Sieve Analysis on Inlet Sand – Lab Results

Sieve Analysis - Distribution Graph

Project Information

Client: North Grenadines Community Developpement Inc.
Project: Reclaiming Paget Farm
Project No.:

Sample No.: Inlet Sand
Date Sampled: 4/24/2016
Date tested: 5/27/2016

Sieve Test Results

Coarse Grains					Fine Grain				
Sieve size (mm)	Percent finer (%)				Sieve No.	Sieve Size (mm)	Percent finer (%)		
150.00	100.00				10	2	99.74		
106.00	100.00				16	1.19	99.67		
37.50	100.00				40	0.425	97.35		
26.50	100.00				60	0.25	62.14		
19.00	100.00				80	0.18	34.66		
13.20	100.00				100	0.15	15.37		
9.50	100.00				200	0.075	0.87		

Grain Size Distribution

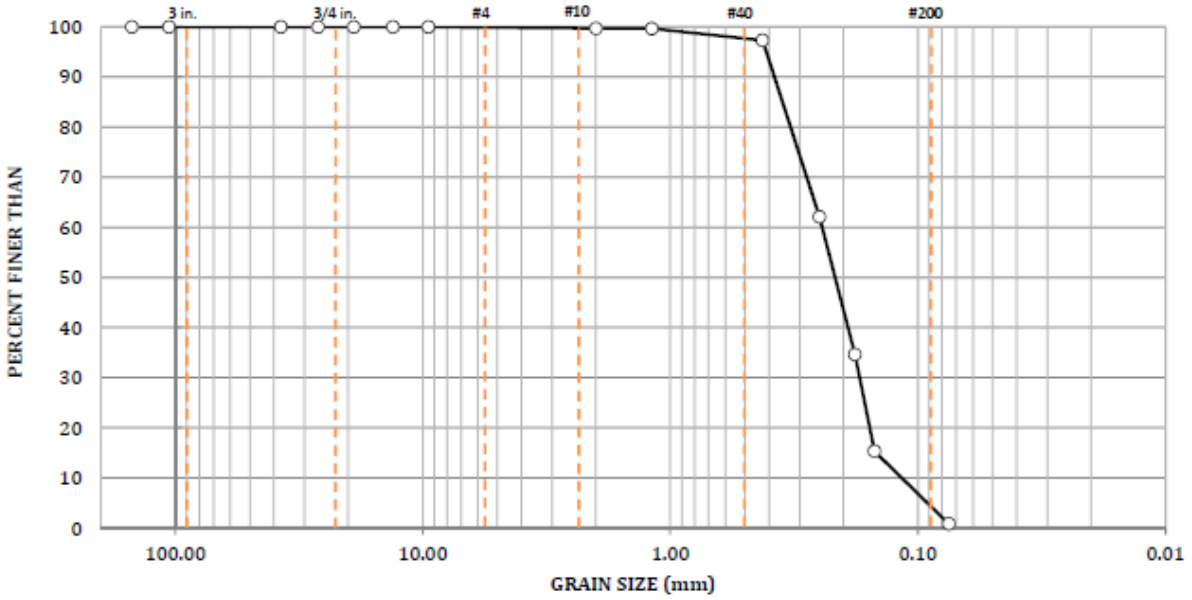

% +3"	% Gravel		% Sand			% Fines
	Coarse	Fine	Coarse	Medium	Fine	Silt & Clay
0.00	0.00	0.26	0.07	37.53	61.27	0.87

Comments/Observations

Test Completed by: Philippe April Le Quéré
Test Approved By:

Figure C.3: Sieve Analysis on Inlet Sand – Distribution Curve

Appendix D: Dry Points/Obstacles Grid Coordinates

The way that groynes are defined in Delft3D is through the functions 'dry points' and 'obstacles'. Cells were defined as such where groynes were observed and where the proposed groyne is tested. Table D.1 summarizes the cells that were defined as groynes:

		Starting Location		End Location	
		X1	Y1	X2	Y2
Existing Groynes	Fisherman Groyne 1	57	151	57	148
	Fisherman Groyne 2	60	151	60	148
	Fishery Groyne	78	151	78	142
Proposed Groynes	Small Straight Groyne	52	149	52	136
	Medium Straight Groyne	52	149	52	132
	Long Straight Groyne	52	149	52	125
	Short Angled Groyne	52	149	52	143
		51	143	51	139
		50	139	50	136
	Medium Angled Groyne	52	149	52	143
		51	143	51	138
		50	138	50	133
		49	133	49	130
	Long Angled Groyne	52	149	52	143
		51	143	51	137
		50	137	50	133
		49	133	49	130
		48	130	48	125

Table D.1: Dry Points/Obstacles Grid Coordinates

Appendix E: FLOW and WAVE Grids Superposed in Front of Paget Farm's Map

The following figure represents the area covered by the grids.

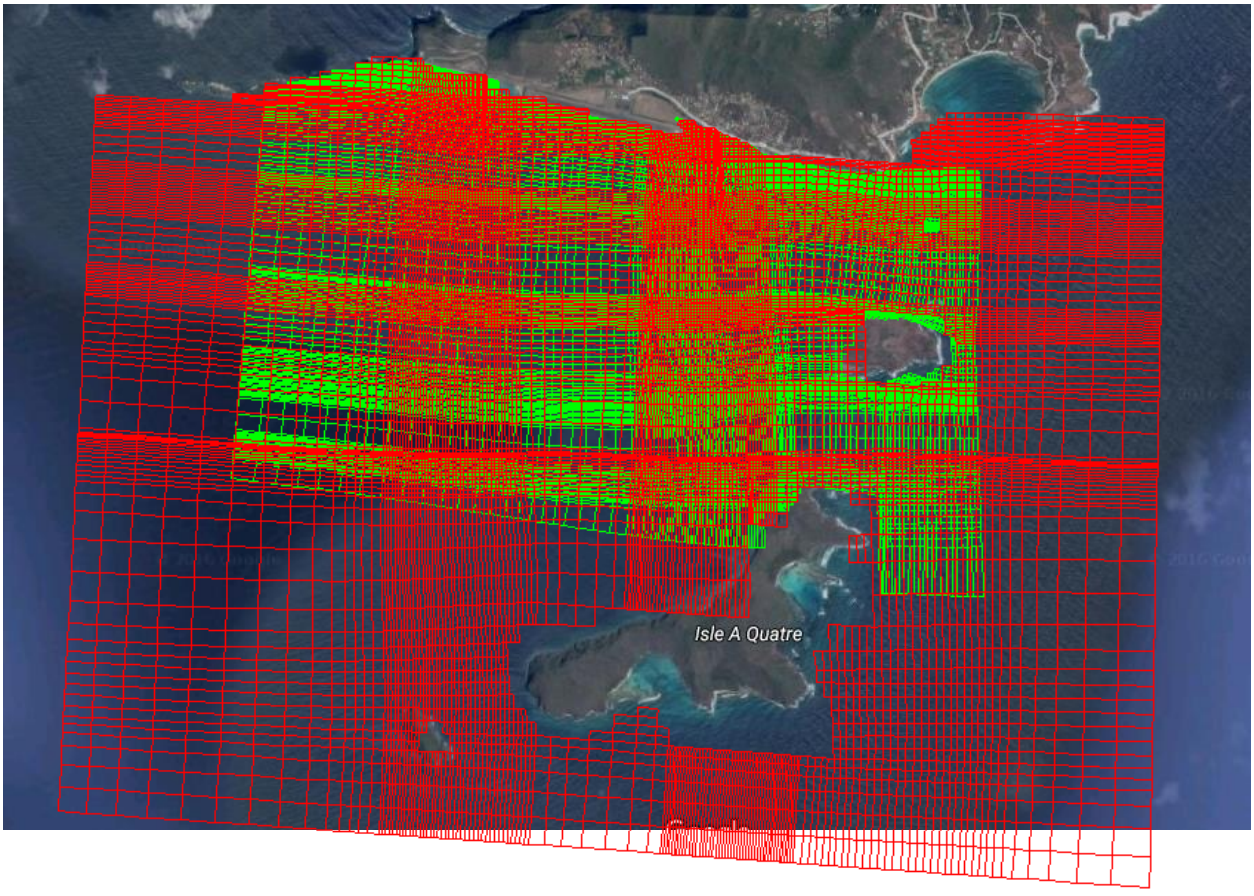

Figure E.1: FLOW and WAVE Grids Superposed in Front of Paget Farm's Map

Appendix F: Calibration Results in a Table Format

Table F.1 compiles some of the results from the calibration of the tide-induced current through the boundary definition. The set up that had the best agreement was by defining the West boundary's total discharge as 60000 times the tide amplitude, the South boundary's total discharge as 5000 times the tide amplitude and with a lag between the discharges and the tide cycle of 120 degree.

Date	**8/21/2016**				**8/22/2016**				
Time	8:50:27	8:58:49	8:50:27	8:58:49	12:54:54	1:04:31	12:54:54	13:04:31	
	Vx at Point 11 (m/s)	**Vx at Point 12 (m/s)**	**Vy Point 11 (m/s)**	**Vy at Point 12 (m/s)**	**Vx at Point 11 (m/s)**	**Vx at Point 12 (m/s)**	**Vy at Point 11 (m/s)**	**Vy at Point (m/s)**	**RMSE (m/s)**
Field Data	-0.592	-0.587	-0.066	-0.055	0.722	0.768	-0.010	-0.004	
40000A, 5000A +90d	-0.03	-0.05	-0.01	0.02	0.65	0.82	0.08	-0.11	0.283
40000A, 5000A +110d	-0.28	-0.29	-0.05	0.03	0.65	0.71	0.08	-0.12	0.169
40000A, 5000A +130d	-0.56	-0.52	-0.09	0.04	0.44	0.27	0.05	0.03	0.208
60000A, 5000A +110d	-0.35	-0.38	-0.06	0.03	0.93	0.96	0.12	-0.15	0.169
60000A, 5000A +120d	-0.48	-0.62	-0.08	0.04	0.65	0.82	0.08	-0.13	0.082

Table F.1: Calibration Results for the Tide-Induced Current Calibration

Table F.2 compiles the results from the calibration of the bottom roughness. This calibration was done by defining two regions to vary their respective roughness: (i) Ocean and (ii) Shore.

	Points	**1**	**2**	**3**	**4**	**5**	**6**	**7**	**8**	**9**	**10**	
	Time	7:03:02	7:05:11	7:10:53	7:15:16	7:19:13	7:23:15	7:27:31	7:31:56	7:35:46	7:39:44	RMSE (m/s)
Field Data	Vx (m/s)	0.04	0.05	0.07	0.12	0.12	0.17	0.16	0.14	0.16	0.13	0.092
	Vy (m/s)	0.01	0.01	-0.03	-0.04	-0.04	-0.06	-0.06	-0.05	-0.04	0.00	
n=0.018, Cb=0.067	Vx (m/s)	0.01	0.01	-0.02	-0.03	-0.12	0.03	0.09	0.11	0.14	0.12	0.078
	Vy (m/s)	-0.02	0	-0.03	-0.03	0	-0.05	-0.09	-0.07	-0.05	-0.03	
No Waves	Vx (m/s)	0.08	0.07	0.13	0.19	0.19	0.24	0.25	0.22	0.21	0.18	0.046
	Vy (m/s)	0.01	0.02	-0.01	-0.06	-0.07	-0.08	-0.07	-0.05	-0.03	0	
n=0.018, Cb=0.038	Vx (m/s)	0.01	0.01	-0.03	-0.03	-0.12	0.02	0.08	0.12	0.15	0.12	0.080
	Vy (m/s)	-0.01	0.00	-0.02	-0.03	0.01	-0.04	-0.09	-0.06	-0.05	-0.03	
Ocean n=0.018 Shore n=0.05	Vx (m/s)	0.02	0.03	0.04	0.07	0.06	0.12	0.13	0.13	0.13	0.11	0.026
	Vy (m/s)	-0.01	-0.01	-0.02	-0.03	-0.04	-0.06	-0.06	-0.04	-0.03	-0.01	
Ocean n=0.018 Shore n=0.10	Vx (m/s)	0.01	0.01	0.00	0.03	0.02	0.06	0.08	0.08	0.07	0.06	0.059
	Vy (m/s)	-0.02	-0.02	-0.02	-0.02	-0.01	-0.03	-0.04	-0.02	-0.02	-0.02	

Table F.2: Calibration Results for the Bottom Roughness Calibration

The end results proved that a manning's of n=0.018 in the ocean area and n=0.05 in the shore area makes a model that has the most agreement with the field measurements. It was also observed that the change of the JONSWAP coefficient (C_b) had little effect on the depth-averaged velocity. The change of JONSWAP coefficient only increased the RMSE by 0.002 m/s.

Appendix G: Detailed Drogue Test Result Tables

Figures G.1 to G.3 summarize in detail the location of the drogues at the end of the different simulations.

Drogues final position			Red	Blue	Green	Total
Angled Groyne	Long	Inlet	3	2	5	10
		Shore	7	8	5	20
		Offshore	0	0	0	0
	Medium	Inlet	1	0	2	3
		Shore	8	7	8	23
		Offshore	1	3	0	4
	Short	Inlet	3	3	3	9
		Shore	7	6	7	20
		Offshore	0	1	0	1
Perpendicular Groyne	Long	Inlet	1	3	3	7
		Shore	9	6	6	21
		Offshore	0	1	1	2
	Medium	Inlet	5	1	7	13
		Shore	5	9	2	16
		Offshore	0	0	1	1
	Short	Inlet	3	0	3	6
		Shore	6	8	5	19
		Offshore	1	2	2	5

Table G.1: Summary of the Drogue Tracking Test For Typical Condition

Drogues final position			Red	Blue	Green	Total
Angled Groyne	Long	Inlet	3	0	0	3
		Shore	7	10	10	27
		Offshore	0	0	0	0
	Medium	Inlet	4	0	0	4
		Shore	6	10	10	26
		Offshore	0	0	0	0
	Short	Inlet	3	0	0	3
		Shore	7	10	10	27
		Offshore	0	0	0	0
Perpendicular Groyne	Long	Inlet	0	0	0	0
		Shore	10	10	10	30
		Offshore	0	0	0	0
	Medium	Inlet	0	0	0	0
		Shore	10	10	10	30
		Offshore	0	0	0	0
	Short	Inlet	0	0	0	0
		Shore	10	10	10	30
		Offshore	0	0	0	0

Table G.2: Summary of the Drogue Tracking Test For High Wind, High Wave Condition

Drogues final position			Red	Blue	Green	Total
Angled Groyne	Long	Inlet	3	1	2	6
		Shore	7	9	7	23
		Offshore	0	0	1	1
	Medium	Inlet	0	0	0	0
		Shore	10	9	8	27
		Offshore	0	1	2	3
	Short	Inlet	0	0	0	0
		Shore	7	7	6	20
		Offshore	3	3	4	10
Perpendicular Groyne	Long	Inlet	4	1	3	8
		Shore	6	9	7	22
		Offshore	0	0	0	0
	Medium	Inlet	7	3	5	15
		Shore	2	5	4	11
		Offshore	1	2	1	4
	Short	Inlet	0	0	0	0
		Shore	9	8	10	27
		Offshore	1	2	0	3

Table G.3: Summary of the Drogue Tracking Test For Low Wave, Regular Wind Condition